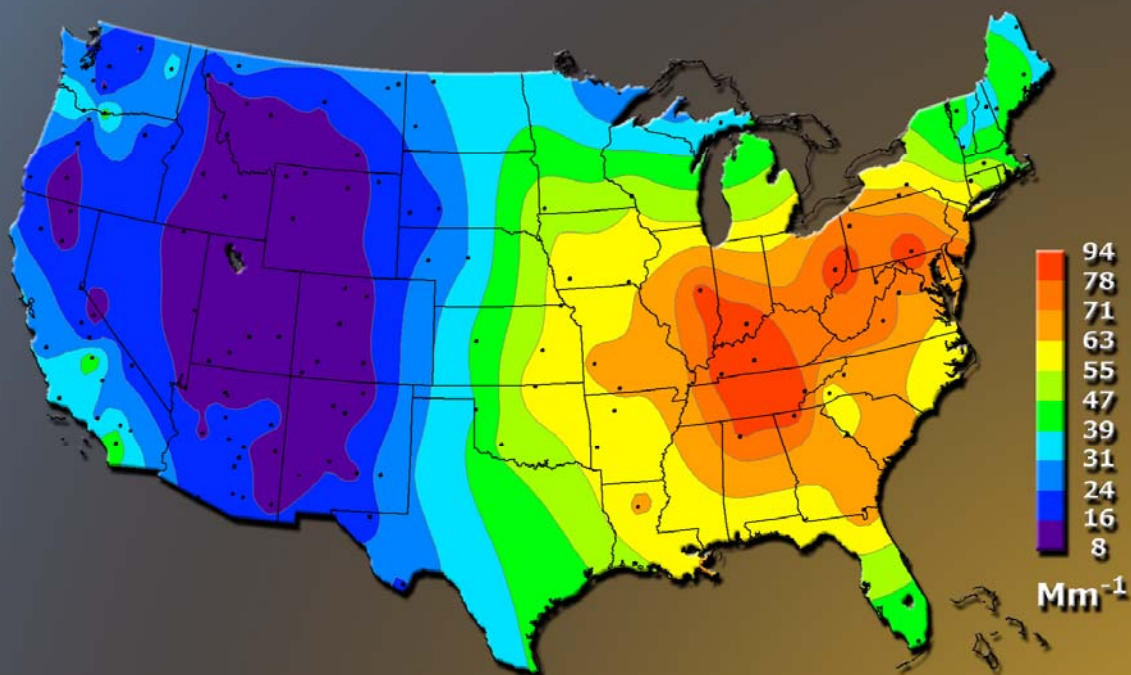# Review of the IMPROVE Equation for Estimating Ambient Light Extinction Coefficients

J. L. Hand and W. C. Malm

Spatial Variability of Atmospheric Particulate Extinction

	Mm^{-1}
	94
	78
	71
	63
	55
	47
	39
	31
	24
	16
	8

National Park Service

Colorado State University CIRA

Review of the IMPROVE Equation
for
Estimating Ambient Light Extinction Coefficients

J. L. Hand and W. C. Malm

TABLE OF CONTENTS

LIST OF FIGURES

LIST OF TABLES

Disclaimer

The assumptions, findings, conclusions, judgments, and views presented herein are those of the authors and should not be interpreted as necessarily representing the National Park Service policies.

ABSTRACT

The Interagency Monitoring of Protected Visual Environments (IMPROVE) protocols for reconstructing ambient light extinction from measured aerosol species are the basis for evaluating compliance under the Regional Haze Rule. We review the assumptions involved in computing reconstructed light extinction using the IMPROVE protocol. This review includes examining the biases in the measurements of aerosol composition, the assumed chemical forms of aerosol species, particle hygroscopicity, and assumed mass scattering efficiencies. We present a thorough survey of estimates of mass scattering efficiencies from recent peer-reviewed literature. Furthermore, we use IMPROVE nephelometry and composition data to estimate mass scattering efficiencies using a variety of methods. The current mass scattering efficiencies applied in the IMPROVE equation are then interpreted in the context of this survey and results derived from the IMPROVE data analyses. Finally, a summary of provisional recommendations for refinements to the IMPROVE equation and a discussion of important uncertainties to consider in the assumptions are presented. Although tentative recommendations of refinements to the IMPROVE equation are presented, final refinements to the IMPROVE equation await future discussions of the results presented here.

1. Introduction

The role of aerosols in visibility degradation has been the subject of research for several decades, but recently interest has intensified with attempts to quantify the optical properties of aerosols, especially because of the uncertainties surrounding the role of aerosols in climate change and because of the need for compliance under the Regional Haze Rule. In most instances, visibility reduction is primarily due to scattering and absorption by particles. Particle scattering and absorption properties can, with a number of limiting assumptions, be calculated using Mie theory (Mie, 1908; van de Hulst, 1981).

Compliance under the Regional Haze Rule is based on protocols for reconstructing aerosol mass and light extinction (b_{ext}) from speciated mass concentrations. Reconstruction equations are used to estimate $PM_{2.5}$ mass concentrations (for particles with aerodynamic diameters less than 2.5 μm) as well as light extinction coefficients. Dry $PM_{2.5}$ fine mass is computed using equations 1 and 2

$$PM_{2.5} = (NH_4)_2SO_4 + NH_4NO_3 + POM + LAC + Soil \tag{1}$$

$$Soil = 2.2Al + 2.49Si + 1.94Ti + 1.63Ca + 2.42Fe \tag{2}$$

where sulfate is assumed to be fully neutralized ammonium sulfate ($(NH_4)_2SO_4$), nitrate is assumed to be in the form of ammonium nitrate (NH_4NO_3), and organic carbon is included as particulate organic material (POM), computed by multiplying organic carbon (OC) concentrations by a molecular weight per carbon weight ratio (POM = R_{oc}·OC). Light-absorbing carbon is referred to as LAC. We use the term LAC because it is more representative of the optical properties of light-absorbing carbon rather than elemental (EC) or black carbon (BC), although these terms are often used interchangeably in the literature. Fine soil concentrations include the contributions from assumed forms of elemental species (equation 2) (Malm et al., 1994b). Mass concentrations are given in units of μg m^{-3}.

The light extinction coefficient (b_{ext}) includes the contributions from light scattering by particles (b_{sp}) and gases (b_{sg}), and light absorption by particles (b_{ap}) and gases (b_{ag}).

$$b_{ext} = b_{sp} + b_{ap} + b_{sg} + b_{ag} \tag{3}$$

The only gas in the atmosphere that absorbs visible light is nitrogen dioxide, NO_2. Absorption by NO_2 at a wavelength of 550 nm is computed as $b_{ag} = 330[NO_2]$, where the units of b_{ag} are Mm^{-1} (Mm^{-1} = 10^{-6} meters^{-1}) and the units of $[NO_2]$ are ppm (Dixon, 1940; Hodkinson, 1966). Light scattering by gases (b_{sg}) is described by Rayleigh scattering theory (van de Hulst, 1981).

Rayleigh scattering is isotropic and is nearly completely polarized for light scattering at 90° to incoming radiation. Rayleigh scattering is proportional to molecular number density and has a strong spectral dependence (λ^{-4}, where λ is the wavelength of light). Correspondingly, $b_{sg} = 12$ Mm^{-1} at sea level and $\lambda = 550$ nm.

Reconstructed scattering and absorption by particles as formulated in the IMPROVE (Interagency Monitoring of Protected Visual Environments) protocol are given by equations 4 and 5, respectively, assuming an externally mixed aerosol.

$$b_{sp} = 3.0 \, f(RH)_{AS}[AS] + 3.0 \, f(RH)_{AN}[AN] + 4.0 \, R_{OC}[OC] + 1.0 \, [Soil] + 0.6 \, [CM] \tag{4}$$

$$b_{ap} = 10.0 \, [LAC] \tag{5}$$

Estimates of total ambient b_{sp} in this formulation are in units of Mm^{-1} and correspond to visible wavelengths ($\lambda \sim 550$ nm). This formulation assumes that contributions to total ambient light scattering are from ammonium sulfate (AS), ammonium nitrate (AN), organic carbon (OC), soil, and coarse mass (CM). Each species has a corresponding dry mass scattering or absorption efficiency (α) in m^2 g^{-1}. The terms in the brackets correspond to mass concentrations in µg m^{-3}. Organic carbon mass is multiplied by an organic aerosol mass to organic carbon ratio, $R_{oc} = 1.4$, to estimate particulate organic matter. The effects of the uptake of water as a function of relative humidity (RH) by hygroscopic species are estimated by the f(RH) factor.

The formulation of the equations used in the IMPROVE reconstructions (equations 1–5) requires a number of assumptions. Each assumption has associated uncertainties that obviously will have consequences for reconstructed extinction, albeit to varying degrees. The purpose of this report is to evaluate or comment on each assumption, and when possible, suggest refinements. Refinements of many of the assumptions are not suggested at this time because data do not currently exist to support modifications, or they would require further measurements to

characterize. Suggested refinements do include increasing the R_{oc} factor used to compute particulate organic matter and modifying the f(RH) factor to reflect some water associated with particles below a relative humidity of 40%. Mass scattering efficiencies for ammonium sulfate and POM may also be adjusted to reflect current data. The assumptions and some related questions are listed below, along with the section in which they are discussed. Although estimating uncertainties and their combined effects on extinction from the assumptions described in the following sections is important, it is beyond the scope of this report.

- Section 2. Sampling biases: definitions and descriptions of their effects on nitrate (2.1), ammonium (2.2), carbonaceous aerosols (2.3), and elemental and coarse mass (2.4).

- Section 3. Chemical and physical forms of species: multiplier used to compute particulate organic matter from organic carbon (3.1), nitrate as ammonium nitrate (3.2), sulfate as ammonium sulfate (3.3), soil composition (3.4), coarse mass speciation (3.5), sea salt (3.6), and size distributions (3.7).

- Section 4. Hygroscopic growth curves and scattering enhancement curves (f(RH)): hygroscopicity of species, assumed growth curves, and relative humidity ranges.

- Section 5. Mass scattering efficiencies: theoretical discussion of mass scattering efficiencies (5.1), review of methods used for deriving efficiencies (5.2), survey of reported efficiencies (5.3), and derived values using IMPROVE data (5.4).

- Section 6. Evaluation of methods for computing mass scattering efficiencies using the combined IMPROVE data set.

- Section 7. Discussion of computed biases between measured and reconstructed scattering for various methods of calculating mass scattering efficiencies.

- Section 8. Suggested refinements of IMPROVE equation.

4

2. Sampling Biases

Before investigating the assumptions involved for each species included in the IMPROVE equation, it is of interest to review any sampling issues or uncertainties related to the measurements of these species. The IMPROVE network utilizes four separate sampling modules to characterize the $PM_{2.5}$ aerosol composition and total mass. Module A is equipped with Teflon® filters used for analysis of $PM_{2.5}$ mass by gravimetry and elemental composition by X-ray fluorescence (XRF). In module B, nylon filters are used to collect particles for ion analysis using ion chromatography (IC). The module is preceded by a denuder designed to capture acidic gases. Module C incorporates quartz filters for use in quantifying organic and light-absorbing carbon by thermal optical reflectance (Chow et al., 1993), and module D uses Teflon® filters to collect particles for gravimetric PM_{10} total mass measurements.

Sampling artifacts, or biases, are not uncommon with filter sampling. An artifact is defined as any increase or decrease in the material being sampled that results in a positive or negative bias in the ambient concentration measured. Artifacts can occur due to contamination issues (contamination of the filter medium or of the cassettes during transport) or adsorption of gases on the filter medium during sampling or transportation and handling. These types of artifacts are considered positive. Negative sampling artifacts arise from volatilization of gases from disassociated particles on the filter or during handling after collection (McDade et al., 2004). Sampling biases affect aerosol species differently, depending on the volatility of the particles being measured and the sampling technique being used; therefore applying corrections for sampling biases is not always straightforward.

Corrections of IMPROVE data due to sampling artifacts have been applied as part of the routine IMPROVE methodology since the beginning of the network. We will briefly review the methodology IMPROVE applies for artifact correction and then discuss recent research about

artifacts that are associated with specific species, such as nitrate, ammonium, and carbonaceous aerosols.

Dynamic field blanks for both Teflon® and nylon filters are collected at all of the sites. These filters are treated like network filters in that they are placed in the sampler, but no sample air is drawn through them. Concentrations on Teflon® field blanks are statistically insignificant, so no corrections are made for measurements on Teflon® filters. The concentrations measured on the nylon filter field blanks are subtracted from the measured filters. Monthly median artifact corrections have been applied to the data since the change in IMPROVE data processing from seasonal to monthly in June 2002. These corrections are applied separately for each ion. Analysis of artifacts on the nylon filter suggests that sulfate ion artifacts are typically less than 10% of the ambient concentration, and nitrate artifacts range between 10 and 20% (McDade et al., 2004). Further discussion of nitrate artifacts, including discussions on denuder efficiency will be presented in the next section.

Quartz field blanks are also collected at all of the sites, but quartz after-filters are collected at six sites only. The after-filters are placed behind the primary quartz filter and are designed to capture organic gases (positive artifact). Negative artifacts for carbonaceous aerosols are assumed to be insignificant compared to positive artifacts, although other studies suggest negative artifacts (volatilization) can be important (Turpin et al., 2000). Concentrations from the after-filters from the subset of sites are used to correct for positive artifacts from data at all of the sites. Monthly median values are also used for quartz filters, and each fraction of organic carbon has a separate artifact correction. Typical artifacts for organic carbon can correspond to half of the reported ambient concentration (McDade et al., 2004). A more in-depth discussion of carbonaceous aerosol artifacts will be presented in section 2.3.

2.1. *Nitrate Sampling Issues*

The nylon filters in module B are used for analysis of particulate nitrate because the nitrate ion is retained by the filter when ammonium nitrate dissociates under conditions of high temperature and low relative humidity. Preceding the filter is an annular denuder coated with Na_2CO_3 and glycerin to remove gaseous nitric acid that would otherwise be retained by the nylon filter. The denuders are serviced once per year during annual maintenance. A positive artifact could occur due to degradation of efficiency of the denuder with time, allowing nitric acid to be collected on the nylon filter. Therefore characterizing the efficiency of the denuders has been a topic of recent study (Ashbaugh et al., 2004; Yu et al., 2005a). Daily samples were collected for four consecutive weeks during different times of the year at IMPROVE sites, representing areas with significant seasonal nitrate contributions to fine mass (Brigantine National Wildlife Refuge NJ, Grand Canyon National Park AZ, San Gorgonio Wilderness CA, and Bondville IL). At each site a combination of IMPROVE ion modules with different denuder configurations were operated. The denuder configurations were designed to compare freshly coated denuders to denuders that had been previously exposed to high levels of nitric acid. The combination also represented different coating options, from the typical IMPROVE coating to no coating. One module was operated with no denuder at all. For all the sites, no differences in nitrate concentrations due to the different denuder configurations were observed. The denuder configuration used regularly as a part of the IMPROVE network was found to be efficiently removing HNO_3 (Ashbaugh et al., 2004).

As part of the same study, the extraction efficiency of nitrate from the nylon filter was investigated (Yu et al., 2005a). Typically, basic solutions (e.g., sodium bicarbonate) are used to extract nitrate on nylon filters; however, this leads to interference from Na^+ ions during ion chromatography (IC). Instead, the use of deionized water for extraction of nylon filters has been

investigated. Data from this study suggest that deionized water extraction with ultrasonification efficiently extracts nitrate and sulfate ions from nylon filters (Yu et al., 2005a) and successfully avoids issues of Na^+ and NH_4^+ interference during IC analysis.

While the previous discussions suggest that nitrate measurements and artifacts from denuder-nylon filter configurations are fairly well understood, the effects of nitrate loss on Teflon® filters remain a sampling issue and have important implications for measurements of fine mass concentrations by gravimetry. Hering and Cass (1999) investigated the effects of nitrate loss from the Federal Reference Method (FRM) measurements of $PM_{2.5}$ mass on Teflon® filters. They found that nitrate concentrations were 28% lower on Teflon® filters compared to nylon filters. Ammonium nitrate particles are volatile and disassociate to form nitric acid gas and ammonia gas, and this reaction is very sensitive to temperature, pressure, and relative humidity. Changes in these parameters during sampling can cause significant losses of nitrate and ammonium from the sampling media, as Teflon® filters do not retain nitric acid as nylon filters do. Correcting mass concentrations for lost nitrate is difficult because knowledge of the history of the equilibrium of ammonium nitrate/nitric acid and ammonia gases at the temperature, pressure, and relative humidity that the filter substrate experienced during the sampling period is required. Recent work by Frank (2005) suggests that applying a thermodynamic model can assist in reducing the uncertainties in fine mass due to nitrate volatilization. Diurnal and seasonal trends in nitrate loss were observed by Hering and Cass (1999), as well as Ashbaugh and Eldred (2004) who performed a similar study. The implications for the negative artifact of sampling volatile particles on Teflon® filters are obvious. Underreporting nitrate concentrations results in an overemphasis of nonvolatile species such as dust and sulfate when computing mass concentrations. Comparisons of reconstructed fine mass using the IMPROVE equation and

gravimetric fine mass could be highly affected by significant underestimations of nitrate due to the volatilization of ammonium nitrate from the Teflon® filter used for gravimetric analysis.

2.2. *Ammonium Sampling Issues*

Although ammonium is not routinely analyzed as part of the IMPROVE procedures, it is important to review the sampling issues related to ammonium to understand measurements made during special studies and by other researchers. The effects of ammonium loss from filter media were studied as part of the nitrate loss study described in the previous section (Yu et al., 2005b). Losses of ammonium are affected by sample location (urban versus rural), meteorological sampling conditions (e.g., relative humidity, temperature), chemical composition of the sampled aerosol, and gas-to-particle partitioning. Volatilization of ammonium nitrate can lead to ammonium loss from filter media, as can reaction of ammonium nitrate with strong acids. Also, when ammonium nitrate is captured by the nylon filter, nitrate is bound by the filter but ammonium can volatilize. Two filter pack configurations were designed to study ammonium loss: denuded nylon-nylon (N-N) and denuded Teflon®-nylon (T-N). Ammonium loss from nylon filters was observed at the four sites where measurements were performed (ranging from ~ 10 to 52%), suggesting a single nylon filter is not sufficient for capturing ammonium nitrate. Results from the N-N and T-N filter pack systems suggest that the T-N configuration is as good as, or better than, the N-N configuration for ammonium retention (Yu et al., 2005b). Applying a correction factor for the negative bias in ammonium would require estimates of ammonium loss at each site, which is a difficult task. Understanding the sampling biases for ammonium is very important, especially during special studies when NH_4^+ is measured, because its concentrations are required in predicting the chemical form of aerosol species, which reduces the uncertainty in reconstructed fine mass and light extinction.

2.3.   *Carbonaceous Aerosol Sampling Issues*

Understanding sampling biases for carbonaceous aerosols is important for accurately quantifying the concentrations of organic and light-absorbing carbon and has been the focus of several studies. Before we discuss the sampling issues related to quantifying the concentrations of carbonaceous aerosols, we provide a brief review of the analytical technique used by the IMPROVE network. The Desert Research Institute (DRI) thermal/optical reflectance (TOR) technique used for IMPROVE (Chow et al., 1993) is one of the thermal methods available to analyze carbonaceous aerosols (also referred to as evolved gas analysis). Typically, for thermal methods the sample filter is heated in a step-wise manner in different atmospheres (e.g., oxygen or helium) and the volatilized carbon from the filter is detected. For each temperature regime a carbon concentration is determined, with the lower temperature concentrations summed for organic carbon (O1, O2, O3, O4, and OP) and the highest temperature regime corresponding to what is typically referred to as elemental or light-absorbing carbon (E1, E2, and E3). A more representative nomenclature would refer to this high temperature carbon as refractory carbon; because of its low volatility it does not evolve without oxidants at lower temperatures. The pyrolysis of organic carbon on the filter as the temperature is increased can contribute to the concentrations of refractory carbon. To account for this effect, the filter is monitored by the reflectance (or transmittance, as is used in thermal optical transmittance methods) of laser light, which decreases when the filter darkens due to pyrolysis. Once oxygen is introduced into the chamber, the pyrolized carbon combusts, the filter lightens, and the laser light returns to its original intensity. After this point, the amount of carbon measured is associated with refractory (light-absorbing) carbon. The split between organic and light-absorbing carbon is based on the conditions for which this process occurs and is dependent on refractory properties of both pyrolyzed and light-absorbing carbon. Huebert and Charlson (2000) discuss several of the

uncertainties associated with measurements of thermally defined carbonaceous aerosols, especially pointing out that these methods differ from one laboratory to another (e.g., temperatures regimes, rate of temperature changes, carrier gases in the chamber), making it very difficult to compare results. In section 5.3 we will discuss in more detail the issues related to the definitions of OC and LAC by this method.

Turpin et al. (2000) review the difficulties inherent in measuring particulate organic carbon. Interference from gaseous and condensable organics can result in sampling errors due to interactions with the filter media. Positive artifacts arise from adsorption of organic gases onto the filter, and negative artifacts occur due to volatilization of particulate organics. They report artifact contributions to organic carbon mass ranging from -80 to +50%. Positive and negative artifacts occur simultaneously, which makes correcting for them difficult. Subramanian et al. (2004) utilized several sampling approaches in an attempt to estimate these artifacts. Depending on the types of denuders and filter configurations, they found that positive artifacts could be eliminated, or that artifacts may depend on sampling duration and probably also depend on sampling location. Huebert and Charlson (2000) state that systematic errors on the order of ±80% are possible using thermal methods.

The IMPROVE network assumes negative artifacts are insignificant and only corrects for positive artifacts that are estimated from quartz after-filters collected at six sites (Chiricahua AZ, Grand Canyon AZ, Yosemite CA, Okefenokee GA, Shenandoah VA, and Mount Rainier WA) (McDade et al., 2004). The after-filters are placed directly behind the primary quartz filter. Quartz filter field blanks are collected at every site and are only used for identification of problems. Field blank filters and the after-filters have similar concentrations; however, the after-filters are used because they are exposed to the same air sample as the primary filter. Artifacts

are determined separately for each fraction of organic and light-absorbing carbon from TOR analyses. McDade et al. (2004) evaluate the artifacts for O3 and E2, the more prominent fractions of OC and LAC. The O3 artifact represents nearly half of the reported ambient concentration (higher for cleaner conditions), and the E2 artifact decreased to less than 10% of ambient concentrations after the IMPROVE sampler switched to version 2 in 2000. Although some spatial and seasonal differences are observed in the artifact estimates (the Okefenokee site has higher artifacts than the other sites, and summer appears to have higher O3 and E2 artifacts than winter), the same monthly median artifact value is applied to the entire network. Based on studies performed at the University of California, Davis, it appears that the positive artifact is due to saturation of the quartz filter from exposure to ambient organic acids in the atmosphere and would probably affect all filters sent to the field similarly. These results are substantiated by Subramanian et al. (2004), who found that quartz after-filters provided a robust estimate of positive artifacts for sampling durations of 24 hours, long enough for equilibrium to be achieved. However, if some volatile organic compounds are being lost from the primary filter to the after-filter, this correction could be too large.

2.4.   *Issues Related to Elemental Species and Coarse Mass*

An X-ray fluorescence (XRF) technique is used to determine concentrations of trace elements with atomic mass number (Z) from 11 to 82 (Na-Pb). White et al. (2004) report on the uncertainties and detection limits for trace elements. Lower Z elements (e.g., Na, Mg) have much higher minimum detection limits (White, personal communication, 2004), and therefore detectable amounts of those elements can be much more difficult to obtain. Other uncertainties in trace elements, especially those corresponding to coarse mode aerosols, arise due to uncertainties in the flow rates of the samplers. The size cut of the cyclone used to collect and separate $PM_{2.5}$ aerosols is very sensitive to the flow rate of the sampler. Variations in the flow rate (e.g., due to

clogged inlets) can have significant impacts on the size range of aerosols being collected and termed "fine". This issue can be important when interpreting fine mass versus coarse mass because the soil contribution in the IMPROVE equation typically corresponds to the tail of coarse mode mineral aerosols. The size distribution of the coarse mode aerosols can vary significantly, as shown by Hand et al. (2002). Over a four-month study in Big Bend National Park, the volume mean diameter of the coarse mode ranged from ~ 2 μm to 5 μm. The tail of this mode that is measured as part of the $PM_{2.5}$ mass is obviously sensitive to the size distribution statistics of the coarse mode aerosols, which complicates any correction that may be applied to data with flow rate issues. The interpretation of coarse soil as fine soil has important consequences for reconstructed mass as well as reconstructed light extinction because the applied optical properties are significantly different for each mode (as will be seen in section 5).

3. Chemical and Physical Forms of Species in the IMPROVE Equation

Aerosol species included in the reconstructed mass and IMPROVE reconstructed extinction equation are assumed to be in specific chemical forms and size ranges. In this section we investigate whether these assumptions are appropriate. In particular we investigate the speciation of POM, sulfate, soil, nitrate, coarse mass, and sea salt.

3.1. Particulate Organic Material (POM)

Accurate estimates of particulate organic material (POM) are required in order to compute $PM_{2.5}$ mass closure and to estimate optical properties such as light scattering. Estimating the contributions of organic carbon aerosol to mass or scattering requires an estimate of the total mass associated with organic carbon. The organic carbon multiplier (R_{oc}) used to estimate particulate organic material (POM) is an estimate of the average molecular weight per carbon weight for organic carbon aerosol and takes into account contributions from other elements associated with the organic matter, such as N, O, and H. It is highly spatially and

temporally variable. It is impossible to determine which and how many elements are associated with POM without knowing the chemical formula of the organic compound, and it is common for ~ 20–40 % of organic aerosol mass to remain unidentified (Turpin and Lim, 2001).

Because the organic compounds that compose POM are largely unknown, the approach for taking into account other elements in POM mass has been to apply an average multiplier. As Turpin and Lim (2001) review, the often-used value of 1.4 dates back to samples collected in Pasadena CA in the early 1970s and 1980s (Grosjean and Friedlander, 1975; White and Roberts, 1977; Van Vaeck and Van Cauwenberghe, 1978; Countess et al., 1980; Japar et al., 1984). More recently, Turpin and Lim (2001) have reviewed several estimates of R_{oc} in terms of the types of compounds known to compose POM, and that review will not be repeated here. However, to summarize their findings, they recommend a factor of 1.6 ± 0.2 for urban organic aerosols, a factor of 2.1 ± 0.2 for nonurban organic aerosols, and values ranging from 2.2 to 2.6 for samples with impacts from biomass burning. Russell (2003) used Fourier Transform Infrared (FTIR) spectroscopy to estimate POM from the number of carbon bonds present and the molecular mass of each functional group associated with the carbon bonds. Over 90% of R_{oc} from estimates from samples in northeastern Asia and the Caribbean were between 1.2 and 1.6, with mean values below 1.4. Values of R_{oc} like those reported by Turpin and Lim (2001) and Russell (2003) are derived using techniques that depend on the functional groups and molecular compounds of organic carbon aerosols. El-Zanan et al. (2005) used solvent extractions from archived IMPROVE filters at five sites to directly measure POM mass and carbon content and derive an average R_{oc} of 1.92 (range of 1.58–2.58). They also used a mass balance approach to estimate the R_{oc} ratio using the IMPROVE data that resulted in an average value of 2.07 across the IMPROVE network. Other types of methods result in similar findings. Reconstruction of fine

mass and light scattering coefficients allow estimates of R_{oc} to be derived, as was done in a two-month study in Yosemite National Park by Malm et al. (2005a) where POM dominated the fine mass. They found that an R_{oc} factor of approximately 1.8 allowed for closure in fine mass and light scattering coefficients for periods that encompassed both pristine conditions as well as the impacts of biomass burning and regional haze. Poirot and Husar (2004) found better agreement between measured and reconstructed fine mass by applying an R_{oc} factor of 1.8 during a biomass burning event in the New England and mid-Atlantic state regions.

Previous investigators have attempted to estimate R_{oc} from comparisons of gravimetric and reconstructed mass; however, a number of issues arise with this type of analysis. These issues originate from the uncertainties in the assumptions involved in the formulation of reconstructed mass and have been discussed in the literature (Andrews et al., 2000; Rees et al., 2004; Tanner et al., 2004; El-Zanan et al., 2005); therefore they will be mentioned only briefly here. Some of the uncertainties inherent in reconstructed mass equations include the assumed form of aerosol species. For example, sulfate is typically assumed to be in the form of fully neutralized ammonium sulfate, although in reality the form of sulfate could be different (more acidic). Nitrate is assumed to be in the form of ammonium nitrate, and as we will show later, this assumption may be inappropriate under certain conditions. Water may be retained by hygroscopic species on the filters used to determine gravimetric $PM_{2.5}$ mass. Soil mass requires an assumption of soil composition as defined by equation 2, and OC concentrations may be affected by sampling artifacts and analytical issues regarding the method-dependent definitions of organic and light-absorbing carbon. El-Zanan et al. (2005) performed sensitivity studies related to these issues and found that values of R_{oc} varied between 1.74 and 2.2, although they

believe the lower values are not realistic. They also found higher values of R_{oc} determined from

mass balance methods in the summer (2.33) compared to the winter (1.87).

The approach implemented here for estimating R_{oc} from IMPROVE data applies an

ordinary least square (OLS) multiple-linear regression (MLR) analysis using

$$PM_{2.5,i} = a_1[(NH_4)_2SO_4]_i + a_2[NH_4NO_3]_i + a_3[OC]_i + a_4[LAC]_i + a_5[soil]_i + a_6[sea\ salt]_i \qquad (6)$$

The results of the regression analysis for each site are presented in Appendix 1, including

a statistical summary of gravimetric mass and aerosol species mass concentrations (minimum,

maximum, mean, and standard deviation). Also presented for each site is the fractional

contribution of each species to gravimetric mass and a comparison between reconstructed and

gravimetric mass. The statistically significant (95% level) regression coefficients for each site

are reported in Table 1, with the mean and standard deviation of the coefficients listed in the

final two rows. If the mass for each species (other than POM) is accurately estimated and the

regression is unbiased, then the regression coefficient for a given species should equal 1. The

regression coefficient for POM corresponds to the R_{oc} factor. Scatter plots of gravimetric and

reconstructed mass are presented in Appendix 1. Reconstructed mass has been computed using

equation 1 and using the regression coefficients derived from equation 6.

Table 1. Statistically significant (95%) regression coefficients using the ordinary least square multiple-linear regression analysis (equation 6). Site code is in the first column. The remaining columns correspond to coefficients associated with ammonium sulfate (AS), ammonium nitrate (AN), particulate organic matter (POM), light-absorbing carbon (LAC), soil, and sea salt, respectively. Insignificant coefficients are replaced with ".".

Site	AS	AN	POM	LAC	Soil	Sea Salt
ACAD	1.23	.	1.85	.	1.40	1.02
ADPI	1.23	0.49	1.67	.	1.68	.
AGTI	1.05	0.67	1.63	.	1.09	.
AREN	1.08	0.80	1.70	2.36	0.50	.
BADL	1.14	0.65	1.98	.	1.06	.
BALD	1.29	0.75	1.76	.	1.18	.
BAND	1.21	0.54	1.52	.	1.12	.
BIBE	1.08	0.74	1.84	.	1.02	.
BLIS	1.25	0.54	1.74	.	1.06	.

BLMO	1.00	1.09	1.27	.	1.09	.
BOAP	1.18	0.68	1.71	0.65	1.30	.
BOND	0.98	1.01	1.28	.	1.17	.
BOWA	1.18	0.84	1.88	.	1.32	.
BRCA	1.25	0.50	1.40	1.16	1.41	.
BRET	1.16	0.70	1.53	.	1.51	.
BRID	1.31	.	1.73	.	1.22	.
BRIG	1.08	0.54	1.99	.	1.18	0.95
BRLA	0.97	.	1.91	.	1.52	.
BRMA	1.04	.	1.42	.	1.10	.
CABA	1.17	0.56	1.16	2.52	1.10	1.19
CABI	1.46	.	2.05	.	1.19	.
CACO	1.25	0.51	1.62	.	1.31	0.82
CACR	1.11	0.50	1.67	.	1.06	.
CADI	1.22	0.63	1.40	2.77	1.05	.
CANY	1.10	0.55	1.74	.	1.21	.
CAPI	1.04	0.50	2.07	.	1.21	.
CEBL	1.11	1.14	2.07	.	1.11	.
CHAS	1.17	.	1.44	0.90	0.99	0.59
CHER	1.11	0.98	1.43	.	1.57	.
CHIR	1.28	0.79	1.36	1.59	1.15	0.88
CLPE	1.25	.	1.71	.	1.38	.
COGO	1.10	0.57	1.63	.	1.10	.
COHI	1.21	0.63	1.92	.	1.68	.
COHU	1.01	0.33	1.71	.	1.16	.
CORI	1.33	0.60	1.59	.	1.14	0.95
CRES	1.00	0.98	2.16	.	1.14	.
CRLA	1.68	.	1.68	0.48	1.10	1.10
CRMO	1.40	0.71	1.96	.	1.25	.
DENA	1.39	.	1.89	.	0.85	1.13
DEVA	1.05	0.70	1.65	.	1.25	.
DOME	0.95	0.81	1.77	.	1.36	.
DOSO	1.16	.	1.58	.	1.00	.
ELDO	1.13	0.82	1.44	.	1.05	.
ELLI	1.07	0.97	2.07	.	1.10	.
EVER	1.00	.	1.44	4.40	1.20	.
FLAT	1.33	.	1.74	.	1.23	.
FOPE	1.10	0.49	2.06	.	1.27	.
GAMO	1.20	.	1.66	.	1.29	.
GICL	1.22	1.79	1.54	.	1.09	.
GLAC	1.16	0.93	1.58	1.43	1.17	.
GRBA	1.45	0.58	1.70	.	1.35	.
GRCA	1.29	.	1.36	4.66	1.27	.
GRGU	1.10	.	1.65	3.90	0.99	.
GRRI	1.04	0.96	1.73	.	1.34	.
GRSA	1.34	.	1.98	.	1.16	.
GRSM	1.23	.	1.71	.	1.02	.

GUMO	1.14	.	1.66	.	1.02	1.96
HALE	1.01	2.05	1.45	.	0.97	.
HAVO	1.61	.	1.45	.	1.15	.
HECA	1.01	0.69	1.52	.	1.29	.
HEGL	1.09	0.69	1.75	.	1.19	.
HILL	1.36	.	2.04	.	1.42	.
HOOV	1.37	.	2.08	.	1.59	.
IKBA	1.12	0.33	1.86	.	1.61	.
INGA	1.12	.	1.36	.	1.27	.
ISLE	1.00	0.82	1.67	.	0.72	0.51
JARB	1.23	0.99	1.49	.	1.29	.
JARI	1.22	0.52	1.66	1.39	0.73	.
JOSH	1.25	0.74	2.00	.	1.03	.
KAIS	1.11	1.03	1.81	.	1.27	.
KALM	2.25	.	2.16	.	1.64	.
LABE	0.86	1.48	1.72	.	1.41	0.85
LASU	1.10	1.01	1.54	.	1.03	.
LAVO	1.52	0.43	1.41	1.42	1.17	.
LIGO	1.24	.	1.75	.	1.07	.
LIVO	1.26	0.73	1.79	.	1.17	.
LOST	1.16	0.93	1.80	.	1.37	.
LYBR	1.10	0.37	1.63	.	1.02	.
MACA	1.01	0.22	1.81	.	1.08	.
MELA	1.08	0.80	1.84	.	1.16	.
MEVE	1.32	1.27	1.45	.	1.00	.
MING	1.27	0.85	1.45	.	1.14	.
MKGO	1.39	0.66	1.38	.	0.40	.
MOHO	1.36	.	1.77	.	1.11	1.23
MOMO	1.08	.	2.04	.	1.35	.
MONT	1.48	.	1.74	11.08	2.21	.
MOOS	1.13	0.62	1.66	0.68	1.50	1.04
MORA	1.30	0.76	1.59	1.55	0.90	1.14
MOZI	1.25	.	1.70	.	1.11	.
NEBR	1.21	0.66	2.06	.	1.20	.
NOAB	0.82	.	1.26	4.98	1.30	.
NOCA	1.62	.	1.48	.	1.09	1.60
NOCH	.	.	1.71	.	2.64	.
OKEF	1.12	.	1.44	2.51	1.01	0.62
OLTO	1.15	0.97	1.29	0.97	1.01	0.66
OLYM	1.15	0.96	1.73	.	1.36	0.80
PASA	1.54	.	1.53	.	1.21	2.85
PEFO	1.35	0.77	1.76	2.13	1.18	.
PHOE	1.28	0.68	1.29	0.78	1.13	.
PINN	1.32	0.64	1.66	0.89	1.28	1.15
PMRF	1.22	0.54	1.36	.	1.02	.
PORE	1.28	0.74	1.93	.	1.26	1.04
PRIS	0.93	1.00	1.30	.	1.19	0.62

PUSO	1.23	0.76	1.35	0.82	1.07	1.21
QUCI	1.30	0.64	1.95	.	0.40	.
QURE	1.05	0.28	1.63	2.12	0.87	.
QUVA	1.17	0.79	2.00	.	1.37	.
RAFA	1.39	0.95	1.57	.	0.96	1.20
REDW	1.23	1.59	2.16	.	1.25	0.92
ROMA	1.19	.	1.60	.	1.20	0.91
ROMO	1.27	.	1.71	.	1.34	.
SACR	1.30	0.97	1.45	.	1.55	2.80
SAFO	1.08	0.99	1.63	.	0.80	.
SAGA	1.12	0.60	1.57	.	0.91	.
SAGO	1.00	0.91	1.27	.	1.07	1.46
SAGU	1.25	0.26	1.50	1.29	1.26	.
SAMA	1.17	.	1.58	.	1.42	.
SAPE	1.08	.	1.57	.	1.23	.
SAWE	1.30	.	1.50	.	1.29	.
SAWT	1.84	.	1.74	.	1.20	.
SENE	1.16	0.70	1.81	.	0.72	.
SEQU	1.29	0.91	1.35	2.93	0.98	.
SHEN	1.11	.	1.97	.	0.87	.
SHRO	1.22	.	1.74	.	1.10	.
SIAN	1.10	0.38	1.37	2.25	1.37	.
SIKE	1.18	.	1.53	.	1.15	.
SIME	1.43	.	1.28	.	1.32	1.16
SIPS	1.04	.	1.69	.	1.04	.
SNPA	1.33	0.64	1.71	.	1.23	1.23
SPOK	1.24	0.71	1.66	.	1.28	.
STAR	1.61	.	1.11	.	1.70	.
SULA	1.58	.	1.63	.	1.15	.
SWAN	1.13	.	1.75	.	1.33	.
SYCA	1.43	0.44	1.59	.	1.10	.
TALL	1.05	0.84	1.12	3.34	1.51	.
THBA	1.00	0.77	1.84	.	1.04	.
THRO	1.13	0.81	1.85	.	1.01	.
THSI	1.75	.	1.28	.	1.52	.
TONT	1.17	0.67	1.92	.	1.09	.
TRCR	1.59	.	1.91	.	0.62	.
TRIN	2.08	.	1.16	.	1.15	1.03
TUXE	2.20	.	1.91	3.09	0.62	1.05
ULBE	0.98	0.91	1.99	.	1.17	.
UPBU	1.10	0.67	1.94	.	0.88	.
VIIS	0.75	2.34	1.44	.	1.31	.
VILA	1.07	1.02	1.27	.	0.80	.
VOYA	1.22	1.01	1.83	.	1.32	0.89
WASH	1.16	0.82	1.70	0.87	1.04	0.82
WEMI	1.41	.	1.68	.	1.21	.
WHIT	1.23	1.04	2.19	.	1.23	.

WHPA	1.13	0.96	1.57	.	1.09	.
WHPE	1.05	.	1.66	0.87	1.31	.
WHRI	1.32	.	1.74	.	1.27	.
WICA	1.06	0.55	1.93	.	1.17	.
WIMO	1.23	0.80	1.55	.	1.18	.
YELL	1.12	0.62	1.54	2.57	1.30	.
YOSE	1.15	0.74	1.68	.	1.26	0.99
ZION	1.34	0.64	1.63	.	1.28	.
Avg	1.22	0.78	1.66	2.28	1.18	1.12
Std Dev	0.22	0.32	0.24	2.00	0.26	0.51

The mean values of R_{oc} derived from equation 6 (see Table 1) are shown as a summary in Figure 1. There are clear spatial trends in the R_{oc} factor. The highest coefficients of 1.8–2.0+ are just east of the Rocky Mountain range and may be reflective of wild and prescribed fire activity to the west of this region. Both Malm et al. (2005a) and Poirot and Husar (2004) derived R_{oc} factors near 1.8 at sites with air masses influenced by aged biomass smoke, and higher R_{oc} values corresponding to biomass burning were reported by Turpin and Lim (2001). Three of the four sites in Alaska (not shown) also have coefficients near 1.9, with the exception of Simeonof National Wildlife Refuge on the Alaskan peninsula. Other remote locations have R_{oc} values near 1.8. Coefficients ranging from 1.6 to 1.8 are found around most of the United States, with distinct regions having coefficients less than 1.6. Regions in the Northwest, interior Midwest, and Northeast are in this category.

Figure 1. Mean values of R_{oc} multiplier derived from an ordinary least square multi-linear regression analysis (equation 6).
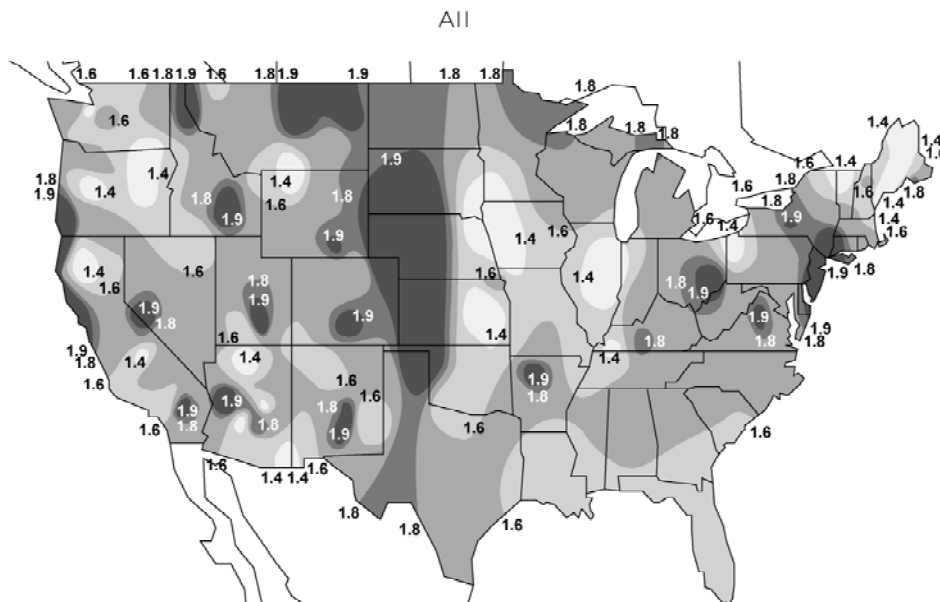
The average coefficient over all sites is R_{oc} = 1.66 ± 0.24, with all 158 sites having significantly valid coefficients. On a seasonal basis the coefficients do not vary significantly, as seen by the mean and standard deviation values presented in Figure 2. The mean summer value (R_{oc} ~ 1.7) is near the average value of 1.66, while the lowest values were derived during winter (R_{oc} ~ 1.5). Some seasonality in R_{oc} is expected, with higher values in summer due to photochemical reactions from warmer temperatures and higher solar insolation. Results from these analyses suggest that the existing R_{oc} value of 1.4 in the IMPROVE equation is probably too low. Based on estimates reported from other studies and the analysis performed here, we recommend an R_{oc} value in the range of 1.7–1.8.

Figure 2. Mean seasonal values of R_{oc} for all sites. Standard deviations are also shown as upper and lower error bars.
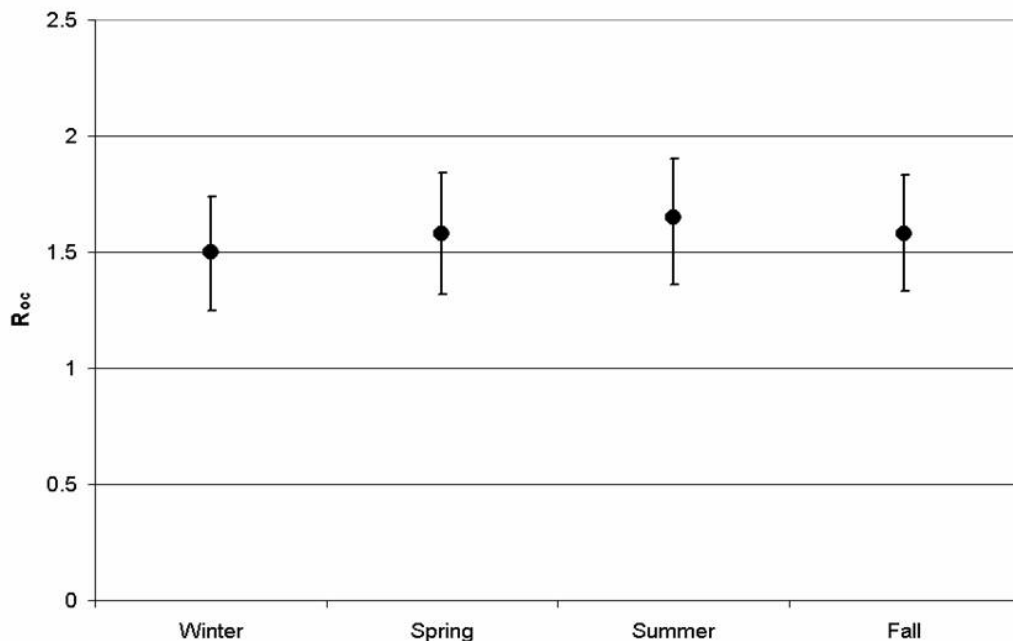
As will be discussed in section 5, the particle density is often needed to compute optical properties. Inorganic particle densities for species such as ammoniated sulfate are well known; however, the density of organic aerosols can range from 1 to 2 g cm^{-3} or higher, depending on the organic composition. Because the composition of organic aerosol is largely unknown, the value of organic density has large uncertainties. Turpin and Lim (2001) review densities of particle-phase organic compounds and summarize them by compound class. The values they report range from 0.77 to 1.64 g cm^{-3}. Values near 1.2 g cm^{-3} were found for the urban areas of the Los Angeles Basin, West Los Angeles, downtown Los Angeles, Pasadena, and Roubidoux CA (Rogge et al., 1993). However, higher values of organic aerosol density would be expected with increased concentrations of carboxylic acids and/or polycyclic aromatic hydrocarbons, or in the presence of significant concentrations of amines and amino acids (Turpin and Lim, 2001). Investigating mass closure studies can assist in understanding if a particular organic density is appropriate, particularly when organic mass fractions are significant.

22

During the Aerosols99 campaign, Quinn et al. (2001) performed closure studies of mass and light extinction from cruise-based measurements from Virginia to South Africa. Organic carbon was collected using a three-stage impactor and analyzed with thermographic methods. Particulate organic material (POM) was computed by assuming an R_{oc} factor for North American air masses and a value of 2.1 for all other air masses (Turpin and Lim, 2001). POM was assumed to be nonhygroscopic and distributed as non-sea-salt sulfate and the organic density was 1.4 g cm^{-3}. The highest submicron POM mass fractions were measured off the coast of North America (~ 15%) and for biomass burning air masses off the coast of Africa (15–20 %). For both of these regions the submicron mass closure was within experimental uncertainty, as was the measured and computed light scattering coefficient.

During INDOEX (Indian Ocean Experiment), Quinn et al. (2002b) used a similar method to the Aerosols99 campaign, but collected three samples with a seven-stage impactor to obtain OC size distributions. An R_{oc} value of 1.6 was applied to all samples. Organics were assumed to be nonhygroscopic and an organic aerosol density of 1.4 g cm^{-3} was applied. The highest submicron POM mass fractions were obtained for Arabian air masses (~ 15%). Both calculated mass and light scattering coefficients agreed with measured values within experimental uncertainty.

During the ACE-Asia (Aerosol Characterization Experiment in Asia) study, Quinn et al. (2004) used a seven-stage impactor to collect organic carbon and computed POM assuming an R_{oc} of 2.1 in marine regions and 1.6 elsewhere. POM was assumed to be nonhygroscopic and a density of 1.4 g cm^{-3} was applied. At most, the POM submicron mass fractions were approximately 20% and calculated and measured mass and light scattering coefficients agreed within experimental uncertainty.

Hand and Kreidenweis (2002) used differential mobility analyzer (DMA), optical particle counter (OPC), and aerodynamic particle sizer (APS) volume distributions to compute mass concentration during the Big Bend Regional Aerosol and Visibility Observational (BRAVO) study. Closure between measured and reconstructed total mass was found between these data, assuming an R_{oc} of 1.4 and an organic density of 1.4 g cm^{-3}. On average, POM was 22% of the PM$_{2.5}$ mass. Good agreement between micro-orifice uniform deposit impactor (MOUDI) size distributions and DMA volume distributions converted to mass distributions (as a function of aerodynamic diameter) was also found.

Ames et al. (2000) computed mass concentrations from OPC volume distributions during the Southeastern Aerosol and Visibility Study (SEAVS) in the Great Smoky Mountains National Park and found good agreement with measured mass concentrations when assuming $R_{oc} = 1.4$ and an organic density of 1.4 g cm^{-3}. Dick et al. (2000) also applied an organic density of 1.4 g cm^{-3} during SEAVS.

Although the above studies did achieve closure with the assumptions made about organic aerosols, it is difficult to glean too much information about organics from closure studies when they are not the dominant aerosol type, because the integrated mass or optical properties will be less sensitive to what is assumed for organic properties. Very few ground-based closure studies exist with a carbon-dominated aerosol, except during extreme smoke events. During a field study in Yosemite National Park, the submicron organic mass fraction was 69% on average (Malm et al., 2005a). McMeeking et al. (2005) used DMA and OPC size distributions in successful closure studies of mass concentrations and light scattering coefficients assuming an R_{oc} of 1.8 and organic density of 1.4 g cm^{-3}. Similar agreement was found by Malm et al. (2005a) during the

same study, suggesting these estimates were reasonable for organic aerosol properties at this location.

Organic aerosol densities typically applied by researchers tend to vary from 1 to 2 g cm^{-3}, depending on the application and type of organics (e.g., urban, rural, smoke). Since there are large uncertainties on organic compounds themselves (20–40% of organic mass is unidentified, Turpin and Lim, 2001), there is also high uncertainty in its density. Furthermore, direct measurements of aerosol density do not exist, so these values have to be inferred from other measurements. Because this number is not well known, investigators often apply a reasonable number. A value of $\rho = 1$ g cm^{-3} previously has been used (e.g., Sloane et al., 1991; Zhang et al., 1993; Neusüß et al., 2002; Adam et al., 2004), as well as $\rho = 1.4$ g cm^{-3} (e.g., Ames et al., 2000; Dick et al., 2000; Hand, 2001; Quinn et al., 2001, 2002b, 2004; Hand et al., 2002; 2004; Gao et al., 2004; McMeeking et al., 2005). Currently a value of $\rho = 1.2$ g cm^{-3} often is being applied that corresponds to a value recommended by Turpin and Lim (2001) for urban organic aerosol measurements in Los Angeles (e.g., Lowenthal et al., 2000; McMurry et al., 2002; Wang et al., 2002; Fridlind and Jacobson, 2003; Gasparini et al., 2004; Stanier et al., 2004; Zhang et al., 2005). Reid et al. (2005) report higher densities for specific organic aerosol types, such as smoke, from various investigators in a review of biomass burning properties. Values between 0.79 and 1.35 g cm^{-3} were reported by Stith et al. (1981) for two temperate fires. Densities of 1 g cm^{-3} and 1.53 g cm^{-3} were reported by Radke et al. (1988, 1991) and Martins et al. (1996), respectively, for temperate forest fires, and Reid and Hobbs (1998) report a value of 1.35 g cm^{-3} for fires in the Amazon. From these estimates, Reid et al. (2005) suggest the average density of dry smoke particles range from 1.2 to 1.4 g cm^{-3}.

3.2.   *Nitrate*

Nitrate is an important seasonal contributor to particulate matter at many locations in the United States. Nitrate is assumed to be present in the fine mode as ammonium nitrate; however, it can be present in the coarse mode also. Field studies at several IMPROVE monitoring sites investigated the speciation and size of aerosol nitrate using a size-resolved impactor (MOUDI) and have shown that nitrate is often present as coarse mode nitrate. Lee et al. (2004a) computed the speciation of nitrate by first calculating leftover ammonium from $(NH_4)_2SO_4$. Excess ammonium is then associated with nitrate as NH_4NO_3, and any excess nitrate not associated with ammonium is determined. Sodium is first combined with Cl^- as sea salt, and any excess sodium is combined with excess nitrate $(NaNO_3)$. If additional nitrate is left over, it is associated with crustal compounds such as Ca^{+2} or Mg^{+2} $(Ca(NO_3)_2$ or $Mg(NO_3)_2)$.

NH_4NO_3 forms from the reaction of gas phase ammonia and nitric acid and is more favorable in regions with high ammonia and nitric acid concentrations and low sulfate concentrations. The equilibrium reaction producing aerosol-phase NH_4NO_3 is sensitive to small changes in temperature and relative humidity that can shift the equilibrium to the gas phase. However, the reaction of gas phase nitric acid with sea salt or calcium carbonate is not an equilibrium reaction and results in nitrate being transferred to the aerosol phase and associated with coarse mode particles.

Two estimates of fine mode nitrate for the three forms discussed above have been computed by summing the nitrate in the MOUDI size bins corresponding to $D_p < 1$ and $D_p < 3.2$ μm (although the MOUDI does not have a 2.5 μm size bin, we assume that the fine mode corresponding to $D_p < 3.2$ μm most closely represents the IMPROVE $PM_{2.5}$ measurement). Fine mode nitrate estimates are presented in Figures 3a and 3b for $D_p < 1$ and $D_p < 3.2$ μm, respectively. Coarse mode nitrate is computed in a similar manner for $D_p > 1$ μm and is

presented in Figure 3c. The size of the pie charts in Figure 3 represents the total nitrate concentration in that size range (in these figures, a doubling of the pie size corresponds to 8 times the concentration), and the total nitrate concentration in that size mode is listed beside its chart.

Figure 3. **(a) Fine mode (D_p < 1 µm) nitrate speciation of NH_4NO_3, $NaNO_3$ and $Ca(NO_3)_2$ at several IMPROVE sites. The size of the pie chart reflects the magnitude of the concentration of total nitrate in this size mode, which is listed under each chart. (b) Same as (a) but for D_p < 3.2 µm. (c) Same as (a) but for coarse mode (D_p > 1 µm).**

Yosemite
(summer-fall)
711 ng/m^3

2%
35%
63%

San Gorgonio
(April)
2993 ng/m^3

7%
6%
87%

Grand
Canyon
(spring)
606 ng/m^3

26%
43%
31%

Bondville
(winter)
3930 ng/m^3

26%
3%
71%

Brigantine
(fall)
953 ng/m^3

2%
35%
63%

Great Smoky Moutains
(summer)
102 ng/m

14%
86%

Big Bend
(summer)
640 ng/m^3

1%
38%
61%

500 ng/m^3

NH_4NO_3
$NaNO_3$
$Ca(NO_3)_2$

28
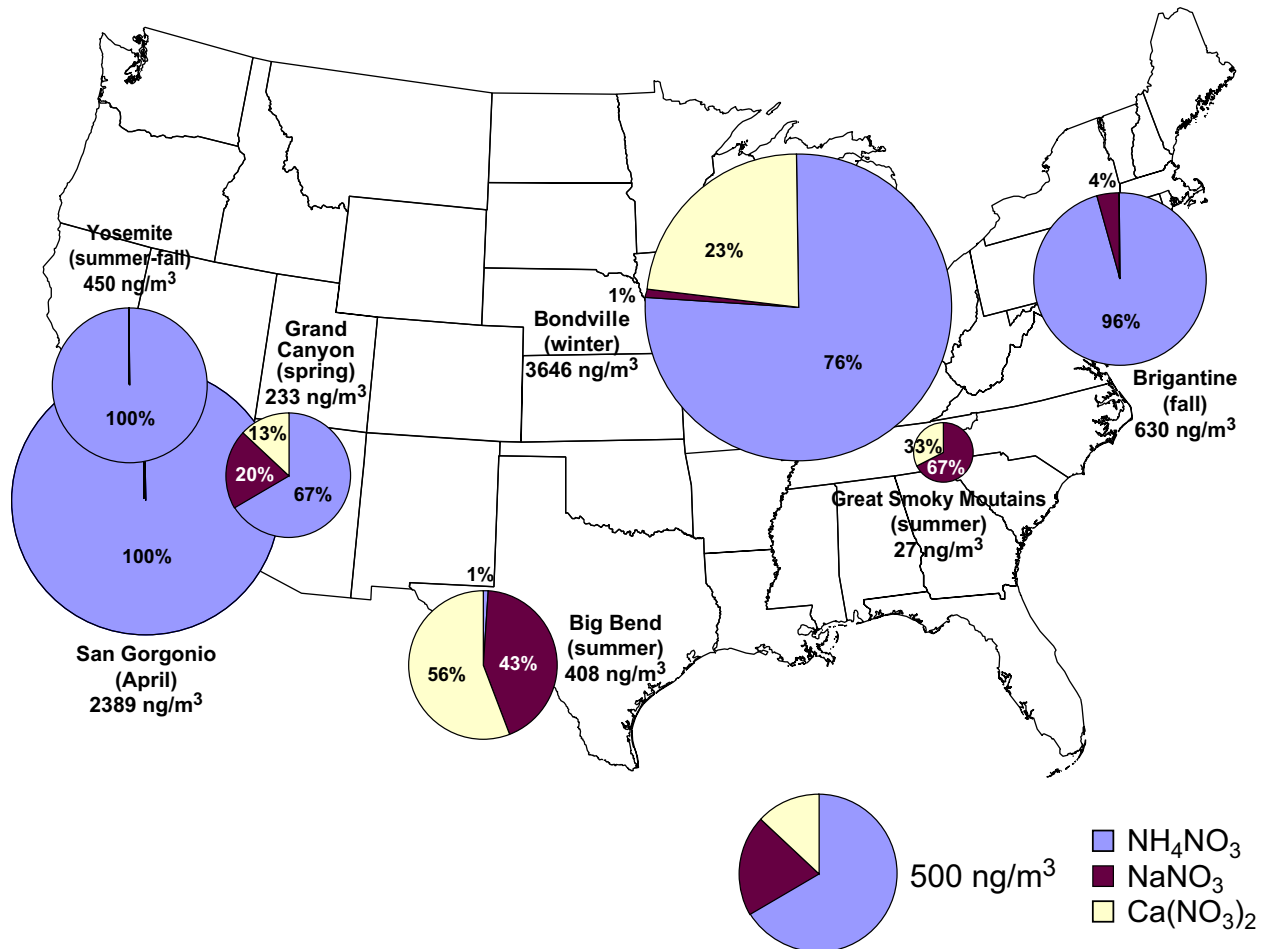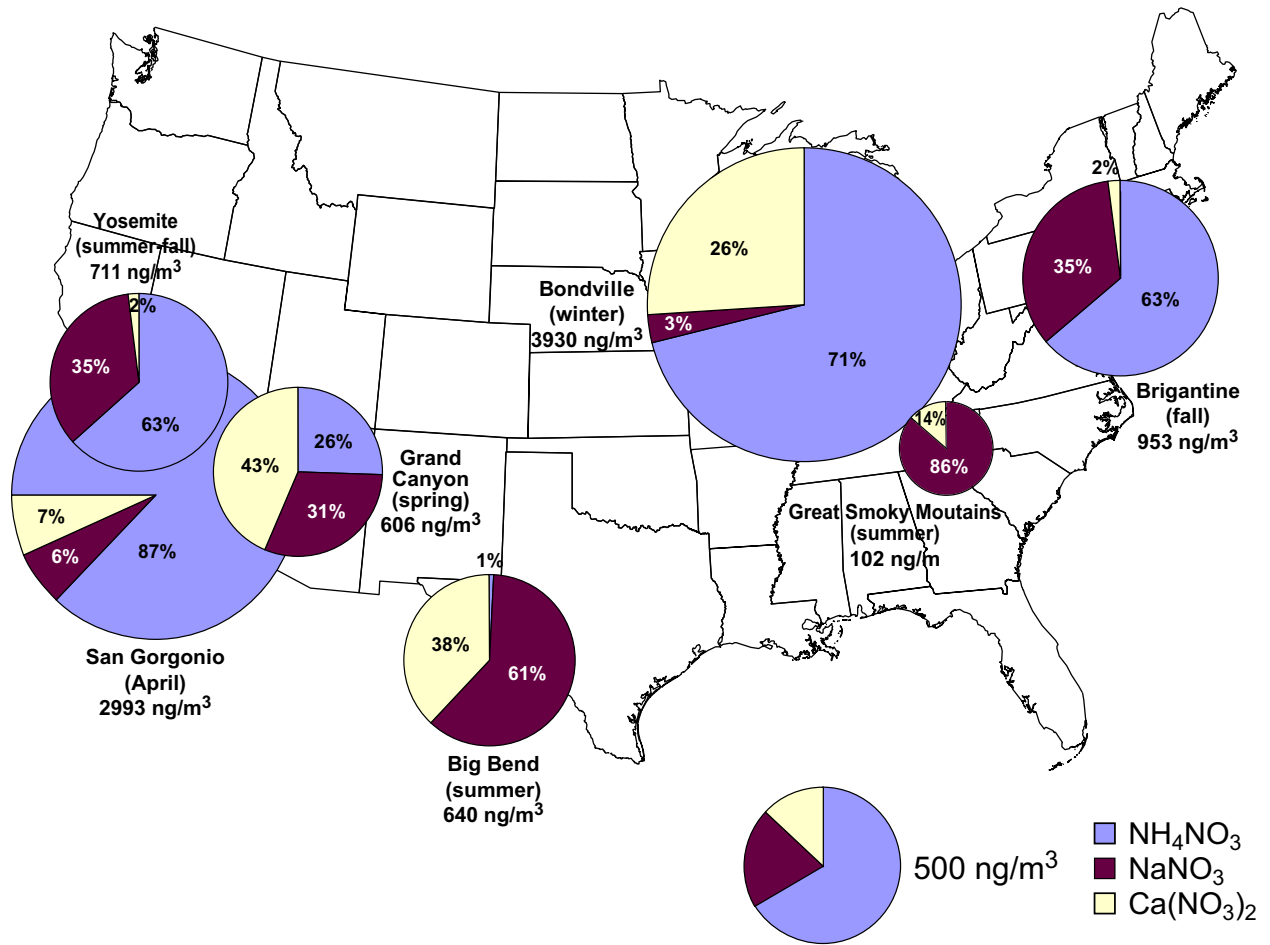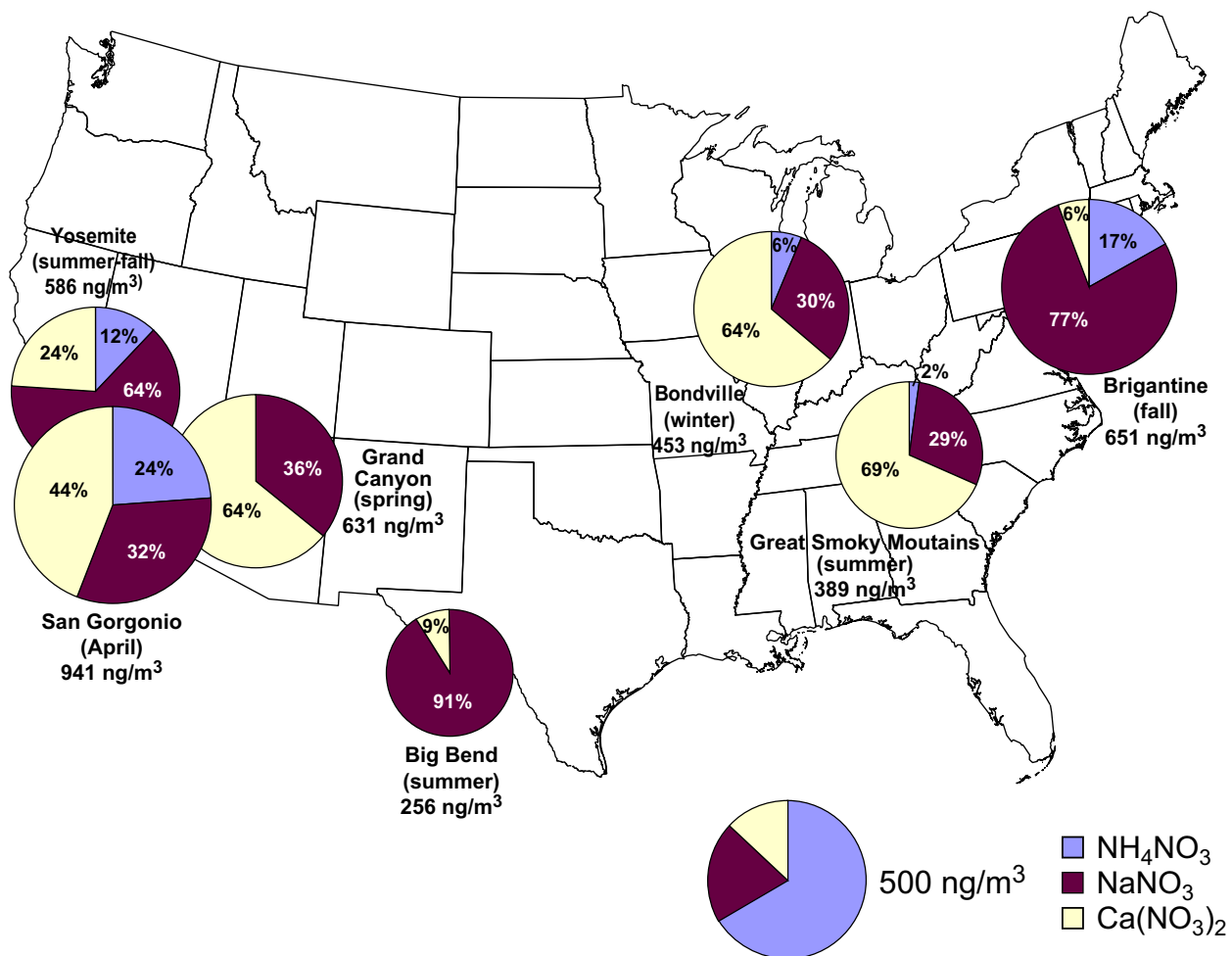
The data presented in Figure 3a demonstrate that fine mode ($D_p < 1$ μm) nitrate is not always speciated as ammonium nitrate. For example, during summer in Big Bend National Park TX, only 1% of fine mode nitrate was in the form of ammonium nitrate, and during winter in Bondville IL, ammonium nitrate accounted for 76% of the nitrate species in the fine mode while $Ca(NO_3)_2$ accounted for 24%, even though the fine mode total nitrate concentrations in Bondville are considerably higher than the other sites. During spring in Grand Canyon National Park AZ, NH_4NO_3 was 67% of fine mode nitrate, and during summer at Great Smoky Mountains National Park TN, it was only 33%. However, in both San Gorgonio National Park CA (spring) and Yosemite National Park CA (summer), the fine mode nitrate was completely speciated as ammonium nitrate, and in Brigantine NJ (autumn), it was nearly all ammonium nitrate (96%).

For the sites where ammonium nitrate was not the dominant form of nitrate in the fine mode, the contribution of nitrate ion to $PM_{2.5}$ mass concentration was less than ~ 20%.

Coarse mode speciation of nitrate at these sites (see Figure 3c) reflects the reaction pathways of nitric acid with mineral aerosols discussed earlier. For example, at several of the sites (Brigantine NJ, Yosemite National Park CA, and Big Bend National Park TX), coarse mode nitrate was associated with sea salt as $NaNO_3$. At Big Bend National Park TX, nitrate had replaced Cl^- in sea salt ($NaNO_3$) (Lee et al., 2004a), and MOUDI data showed that nitrate and sodium had similar size distributions. However, at other sites nitrate was associated with crustal material ($Ca(NO_3)_2$) (Bondville IL, Great Smoky Mountains National Park TN, and Grand Canyon National Park AZ).

At many of the sites, the nitrate concentrations in the coarse mode were higher than in the fine mode. For example, data from Grand Canyon National Park (spring) indicate that concentrations of nitrate in the coarse mode were almost three times higher than nitrate in the fine mode, and roughly 14 times higher in Great Smoky Mountains National Park. Nitrate concentrations at Yosemite National Park were comparable for both modes, similarly for Brigantine NJ. The only sites where fine mode nitrate mass was considerably higher than coarse mode nitrate mass were Bondville IL and San Gorgonio CA.

The two estimates of fine mode nitrate for $D_p < 1$ μm and $D_p < 3.2$ μm in Figures 3a and 3b, respectively, were computed to demonstrate the importance of the size cut of the impactor on the interpretation of nitrate speciation. For example, shifting the fine mode cutpoint from 1 to 3.2 μm for data from the Brigantine NJ site results in the speciation of nitrate changing from predominantly NH_4NO_3 (96%) to 63% NH_4NO_3 and 35% $NaNO_3$ because more of the coarse mode tail is being included (see Figures 3a–c). Similar behaviors are observed at Grand Canyon

National Park AZ, Big Bend National Park TX, and Great Smoky Mountains National Park TN, where the speciation of fine mode nitrate changes significantly because of the inclusion of coarse mode nitrate mass.

Determining or predicting the form of nitrate is not straightforward; it depends on meteorological parameters such as temperature and relative humidity, as well as the presence and acidity of other species such as sulfate. Also, the amount of coarse mode nitrate being attributed to the fine mode also depends on the cutpoint of the impactor, which depends on the accuracy of the flow rate. However, for data gathered at the sites shown in Figures 3a–c, when fine mode total nitrate concentrations were roughly greater than 0.5 μg m^{-3}, ammonium nitrate contributed over 70% of the observed total nitrate in the fine mode. Obviously, the form of nitrate is very important in accurately accounting for contributions of nitrate to fine mass and to light extinction—optical properties of fine mode ammonium nitrate (as well as hygroscopic properties) are quite different from coarse mode sodium nitrate or calcium nitrate. Accurately estimating the speciation of nitrate would require measurements of fine mode ammonium and speciation of coarse mass. Because these measurements are not currently available at all sites, and based on the previous discussion that suggests higher levels of nitrate in the fine mode are probably associated with NH_4NO_3, we recommend that nitrate remains in the form of ammonium nitrate in the IMPROVE formulation.

3.3.   *Sulfate*

Elemental sulfur and the sulfate ion are measured as part of the IMPROVE network. To assess the contributions of sulfate to fine mass or light extinction, the molecular form of sulfate must be known. The IMPROVE algorithm assumes that sulfate is in the form of fully ammoniated sulfate (($NH_4)_2SO_4$). The molecular form of sulfate depends on its degree of neutralization, for which routine measurements of the ammonium ion are required. The

IMPROVE network does not measure the NH_4^+ ion, and as discussed in section 2.2, there are inherent sampling issues with respect to ammonium measurements. The molar ratio of ammonium to sulfate ranges from 2 for fully neutralized ammonium sulfate to 0 for sulfuric acid. Many authors have shown that aerosol sulfate acidity can vary temporally and spatially. More acidic aerosols have been measured at many locations around the United States (e.g., Gebhart et al., 1994; Liu et al., 1996; Day et al., 1997; Lowenthal et al., 2000; Lefer and Talbot, 2001; Quinn et al., 2002a; Chu, 2004; Hogrefe et al., 2004; Schwab et al., 2004; Tanner et al., 2004; Zhang et al., 2005). Special studies at IMPROVE sites have also demonstrated variability. At Great Smoky Mountains National Park during the summer of 1995 (SEAVS), ammonium to sulfate molar ratios of 1.1 were observed (Hand et al., 2000). During the BRAVO study at Big Bend National Park, Lee et al. (2004a) found ammonium to sulfate molar ratios of 1.54 on average. Also, on average, fully neutralized ammonium sulfate was observed at Yosemite National Park during the summer of 2002 (Malm et al., 2005a). Seasonal and spatial variations in aerosol acidity complicate recommendations of a single form of ammoniated sulfate, and regular measurements of the NH_4^+ ion at IMPROVE sites do not exist.

The coefficient (a_1) multiplying ammonium sulfate in the regression model described in section 3.1 provides some indication of the role of sulfate in reconstructed fine mass. A coefficient greater than 1 suggests that water mass retained on the gravimetric filter is associated with sulfate, because ammonium sulfate is assumed in the regression and it has the highest molecular weight of any ammoniated sulfate species. Gravimetric fine mass is measured from Teflon® filters that are weighed at a relative humidity of ~ 40%; therefore an acidic sulfate (or other) species could be responsible for retained water on the filter. The amount of residual water on the filter is a function of the relative humidity at which the filter is weighed and the RH

history to which the aerosol is exposed. Issues related to water on the filter cannot be avoided because acidic sulfate species retain water to very low relative humidity. On average, the MLR coefficient associated with sulfate was greater than 1 at almost all of the IMPROVE sites (see Table 1). Others have found similar results; for example, Andrews et al. (2000) suggested that up to half of the discrepancy between measured and reconstructed fine mass could be accounted for by water uptake on the Teflon® filter by sulfate species during the SEAVS study in Great Smoky Mountains National Park. As previously stated, it is impossible to know the form of sulfate to assume in the IMPROVE equation because ammonium is not measured; therefore we recommend that ammonium sulfate remain as the form of sulfate in the IMPROVE equation.

3.4.   *Soil Composition*

The composition of soil varies as a function of soil taxonomy at a given location. Soil taxonomy charts show variability across the United States with soil type, with the southwestern United States differing from the eastern United States, and many finer differentiations beyond that. Soil composition can also vary due to long-range intercontinental and transcontinental transport. Several studies have shown that contributions of Asian dust to U.S. fine soil concentrations can be significant episodically, affecting aerosol concentrations and mineralogy across the United States (e.g., VanCuren and Cahill, 2002; Jaffe et al., 2003; VanCuren, 2003). Transport of North African dust to the United States occurs regularly, affecting aerosol concentrations in the Virgin Islands, the eastern and southeastern United States (Perry et al., 1997), and even as far west as Big Bend National Park (Hand et al., 2002). Due to the spatial and temporal variability in dust sources, it is very difficult to characterize an appropriate aerosol soil composition for each measurement site. Soil mass concentrations are therefore estimated by a general method that sums the oxides of elements that are typically associated with soil (Al_2O_3,

SiO_2, CaO, K_2O, FeO, Fe_2O_3, TiO_2), with a correction for other compounds such as MgO, Na_2O, H_2O and carbonates (Malm et al., 1994b).

Elemental concentrations are multiplied by factors that represent the mass concentrations of the oxide forms. Several corrections are also made. Molar concentrations of iron are assumed to be equally abundant in the forms of FeO and Fe_2O_3. Potassium has a nonsoil contribution from biomass smoke, so the soil potassium is estimated by using Fe as a surrogate, or *[K] = 0.6[Fe]*. The formula for computing soil concentration is given in equation 2 and has been divided by 0.86 to take into account missing compounds. Results from the multiple linear regression technique described in section 3.1 (see Table 1 and Figure 4) suggest that, on average for all the IMPROVE sites, the soil composition is being underestimated by roughly 20%. Spatial variability is observed in the soil coefficient from the MLR method, with soil concentrations in the western United States being underestimated more than in the Midwest and eastern United States. An area of the country from Michigan south through the Ohio River valley appears to have overestimated soil concentrations by 10–30%. Although the results from the MLR method suggest an underestimation of soil mass on average, the lack of measurements of soil composition around the United States and the additional complication of contributions of long-range (Mexico, Asia, and Africa) soil at many U.S. sites do not allow for suggestions for refinements to the soil formula at this time.

Figure 4. Mean values of the soil coefficient from an ordinary least square multi-linear regression analysis (equation 6).

Soil multiplier
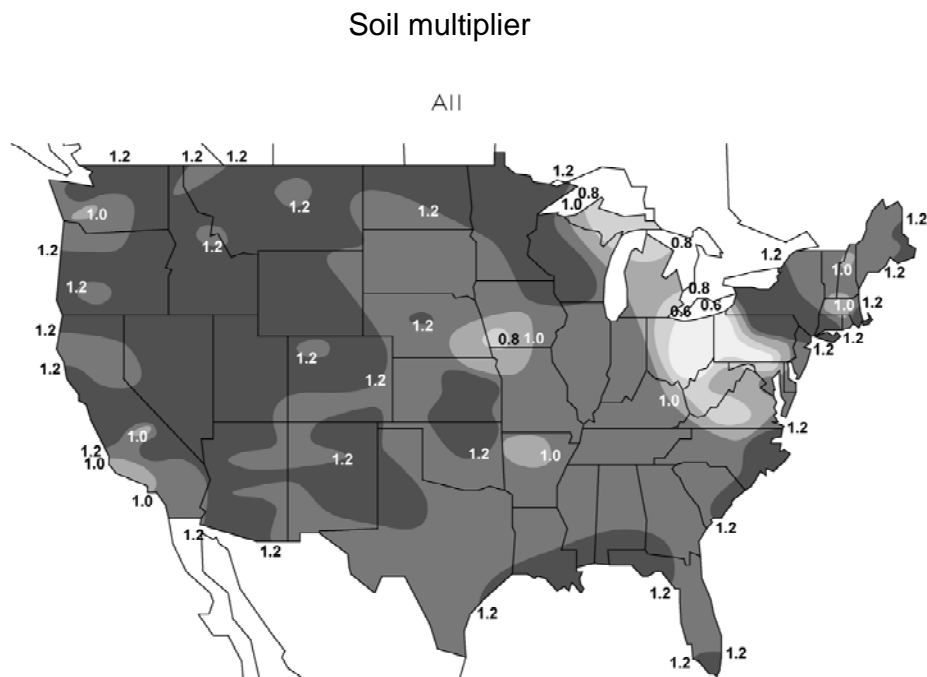
3.5. *Coarse Mass*

Coarse mass is the difference between PM_{10} and $PM_{2.5}$ mass concentrations measured gravimetrically and is not routinely analyzed for speciation; therefore the IMPROVE equation treats all of coarse material as nonhygroscopic dust. A few short-term special studies at national parks during which coarse mass speciation and aerosol mass size distributions were measured have shown that coarse mass consists of a substantial amount (~ 40–50%) of carbonaceous material and inorganic salts such as calcium and sodium nitrate (Malm and Day, 2000; Hand, 2001; Lee et al., 2004a,b). To investigate the speciation of coarse mass, a coarse particle speciation network was initiated at nine IMPROVE sites in 2003. Sites were selected to be representative of the continental United States and were operated according to IMPROVE

protocol analytic procedures for a period of one year, with additional A, B, and C modules operating with PM_{10} inlets. Preliminary results from one year of data from the sites suggest that over 50% of coarse mass is soil (as defined by the IMPROVE soil equation), with soil contributions higher in the western than eastern half of the country. Particulate organic material is the next highest contributor (15–35%) with fairly homogeneous spatial distribution. Nitrate is next highest contributor (5–15%), probably associated with sea salt on the coast and dust in the inner and western areas of the country. Sulfate is a minor contributor to coarse mass, although at coastal regions in the Northeast it averaged up to 10%, probably related to sea salt. The optical, physical, chemical, and hygroscopic properties of coarse mode aerosols can vary significantly, depending on the composition and size distribution of coarse mass, and could have important implications to total scattering, because in some remote areas contributions to total scattering from the coarse mode scattering could be comparable to fine mode contributions. For example, there were several periods during the BRAVO study in Big Bend National Park when up to 80% of total scattering was attributable to the coarse mode (Hand, 2001; Hand et al., 2002).

Several special studies at IMPROVE sites have suggested that the coarse mode aerosol composition can affect the fine mode mass because often the tail of the coarse mode is measured as part of the fine mode. For example, during the BRAVO study at Big Bend National Park, size-segregated MOUDI impactor measurements (Lee et al., 2004a), as well as particle size distribution measurements (Hand et al., 2002), suggested that a 1 μm aerodynamic diameter was a much more realistic separation between the fine and coarse mode. Similar results were found in Yosemite National Park, San Gorgonio CA, Grand Canyon AZ, Brigantine NJ, and Great Smoky Mountains National Park (Lee et al., 2004b). The use of a $PM_{2.5}$ size cut for IMPROVE samplers results in a substantial fraction of the tail of the coarse mode distribution in fine mode samples,

and this can vary significantly with a variable sampler flow rate that affects the size cut of the cyclone. The implications can be important for understanding the hygroscopicity, optical properties, mixing, and trends of fine mode aerosols.

3.6.   Sea Salt

Although contributions from sea salt to coarse mass (and indirectly to fine mass) are not included in the IMPROVE reconstruction equation, sea salt can be a significant fraction of the fine mass at many coastal locations, (e.g., the Virgin Islands), as well as contribute significantly to light scattering (e.g., Quinn et al., 2001, 2002b, 2004). Sea salt concentrations are typically computed from sea salt markers like the sodium ion, chloride ion, or combination of ions (Quinn et al., 2001). Difficulties in computing sea salt from data from the IMPROVE network arise because positive ions are not analyzed; therefore sodium ion (the strongest indicator of sea salt) data are not available. Elemental sodium data are available from XRF analyses; however sensitivity issues regarding poor detection of Na result in large uncertainties corresponding to Na from XRF (White et al., 2004). Issues also arise when using the chloride ion or chlorine to estimate sea salt because reaction of gaseous nitric acid with sea salt produces sodium nitrate particles and the release of gaseous HCl. The depletion of chloride during this reaction results in an underestimation of sea salt when using chloride to compute it.

For noncoastal sites, the inclusion of sea salt is not expected to have a considerable impact on reconstructed light scattering, so underestimating the contribution at those sites is not significant. However, Lowenthal and Kumar (2003) found that including sea salt (computed using Na and Cl) in reconstructed fine mass at Point Reyes CA increased reconstructed fine mass by 30% on average. Because sea salt is hygroscopic, the added effects of water mass to light scattering in coastal higher RH environments could be important also. Recent work by Lowenthal and Kumar (2005) suggests the possibility of using strontium as a surrogate for sea

salt. Investigations into this possibility are ongoing. The elemental abundance of strontium varies depending on the type of soil (Siefert et al., 1999) and estimates of Sr-derived sea salt depend on accurate estimates of its crustal abundance in relation to other elements. Because many IMPROVE sites have been shown to be influenced by long-range transport of Asian and North African dust (e.g., Perry et al., 1997; VanCuren and Cahill, 2002; Jaffe et al., 2003, 2005; VanCuren, 2003; Hand et al., 2004) as well as local dust sources, it is very important that the contributions to Sr from dust sources versus sea salt be accurately characterized, as both can be very important contributors to light scattering. For example, in Barbados (near the Virgin Islands), Li et al. (1996) found that for a 10-year mean, dust contributed 56% to light scattering, compared to 33% by sea salt.

The MLR analysis in section 3.1 and summarized in Table 1 included sea salt as 1.6·Cl⁻ (NaCl). This analysis suggests that east and west coastal sites underestimate sea salt mass by about 10% on average, even with some chloride depletion. We recommend that sea salt be included in the reconstructed fine mass equation as 1.8·Cl (sea salt is 55% Cl by weight as defined by the composition of sea water by Seinfeld and Pandis, 1998) because of the uncertainties related to sodium measurements. Interestingly, the ratio of the 1.8 and 1.6 factors is 1.12, similar to the average regression coefficient for sea salt, so perhaps some of the underestimate was related to the sea salt multiplication factor. The contributions of sea salt to the light extinction equation (including its hygroscopic properties) should also be included.

3.7.   Size Distributions

Atmospheric aerosols are typically described by a trimodal size distribution. The three modes are commonly referred to as the nucleation mode ($0.01 < D_p < 0.1$ μm), accumulation mode ($0.1 < D_p < 1$ μm), and the coarse mode ($D_p > 1$ μm), and each mode is typically

associated with different formation mechanisms. However, several observations have shown that bimodal structure can exist in the accumulation mode.

The existence of a bimodal size distribution was documented by Hering and Friedlander (1982) in the urban Los Angeles area. Their measurements of sulfur size distributions using a low pressure impactor demonstrated two types of distributions. Type I distributions had mass mean aerodynamic diameters (D_{ae}) ranging from 0.42 to 0.65 μm and were observed over a wide range of sulfur concentrations (5–52 μg m^{-3}), but typically on days with heavy sulfate loadings. Type II distributions were associated with smaller mass median diameters (D_{ae} ranging from 0.17 to 0.22 μm) and occurred on days with low sulfate loadings and lower relative humidity. Their calculations suggested that Type I sulfate distributions formed from aerosol phase reactions, while Type II distributions formed from gas phase reactions. Later measurements by Hering et al. (1997) in southern California during the Southern California Air Quality Study (SCAQS) campaign in 1987 suggested that that the total size distribution (in contrast to a single species) was bimodal in the accumulation mode with peaks around 0.25 and 0.65 μm in the summer, while size distributions measured in the fall were more monomodal.

Other mass size distribution measurements performed during SCAQS by John et al. (1990) suggested that typical sulfate size distributions were bimodal with aerodynamic mass mean diameters around 0.2 and 0.7 μm. The average mode concentration increased with mode diameter, with the larger size mode corresponding to the highest sulfate concentrations on average. The transition observed between the modes suggested that the larger size mode was a continuation of the smaller mode.

The formation of the two modes observed by Hering and Friedlander (1982), Hering et al. (1997), and John et al. (1990) was investigated by Meng and Seinfeld (1994) using modeling. The first mode is referred to as the condensation mode (D_{ae} ~ -0.2 µm) and is believed to be formed from nucleation and/or condensation processes. The larger size mode is referred to as the droplet mode (D_{ae} ~ 0.7 µm). Hering and Friedlander (1982) demonstrated that for ambient concentrations, coagulation of submicrometer particles to form the droplet mode is too slow to account for the droplet mode within normal residence times, as is growth of the condensation mode by accretion of water vapor or by gas-phase or aerosol-phase production. Meng and Seinfeld (1994) demonstrated that activation of condensation mode particles into fog or cloud drops, followed by aqueous phase sulfate formation and then evaporation, is a realistic mechanism for formation of the droplet mode. This mechanism demonstrates the importance of heterogeneous aerosol processing in the formation of the droplet mode.

The early evidence for the bimodality of the accumulation mode and several of the following examples that will be discussed are from impactor measurements that typically have fairly coarse size resolutions. Inversions of impactor measurements using techniques such as the Twomey inversion may provide further size-resolved information, but interpretation of Twomey-inverted size distributions should also be cautioned, as artifacts can result using this method, possibly producing spurious modes. Ideally, size distributions measured with finer size resolution techniques (e.g., differential mobility analyzer, DMA, and optical particle counter, OPC) can be quite useful in observing multi-modes; however, these instruments measure the total aerosol and cannot be easily assigned to a single species. Both types of measurements are included in the following discussion of examples of bimodal accumulation mode size

distributions. It should be pointed out that the type of diameter reported may be different depending on the type of measurement, e.g., aerodynamic (D_{ae}) versus geometric size (D_g).

Although the early observations of bimodality in the accumulation mode were made in urban regions, John et al. (1990) state that the presence of bimodality in the accumulation mode is a general feature of atmospheric aerosols and not just a feature of urban aerosols. The following examples are by no means exhaustive, but are provided to demonstrate that these types of size distributions are not necessarily assigned to one type of location or aerosol.

Urban Observations

Zhuang et al. (1999) performed MOUDI measurements for 22 days in Hong Kong in the winter of 1996 and early 1997. These impactor data were analyzed for sulfate, ammonium, and nitrate, and fit with lognormals. Sulfate and ammonium size distributions were bimodal with aerodynamic mode diameters around 0.2 ± 0.15 µm and 0.58 ± 0.11 µm. The droplet mode dominated and was associated with high relative humidity and low clouds. During the 2002 Baltimore field campaign (4–12 July 2002), Adam et al. (2004) observed a haze event that was due to smoke originating from Canadian forest fires. Size distributions were measured with an SMPS (scanning mobility particle sizer) and an APS (aerodynamic particle sizer), and volume size distributions showed multiple modes in the accumulation mode range.

MOUDI aerosol size distributions were measured during the Pittsburgh Air Quality Study (PAQS) for one year during summer of 2001 through summer 2002. Cabada et al. (2004) showed that in summer sulfate size distributions peaked around 0.7 µm, with another peak around 0.2 µm revealed by the Twomey inverted data. Winter sulfate size distributions were more bimodal (D_{ae} around 0.2 and 0.7 µm), corresponding to lower sulfate concentrations overall.

Rural Observations

Aircraft measurements performed by Hegg et al. (1993) in remote regions over the North Atlantic Ocean suggested that measurements in clouds show different types of sulfur size distribution compared to those in clear air, probably due to heterogeneous aerosol processing by clouds. In Point Reyes National Seashore, Rivera-Carpio et al. (1996) measured MOUDI and DMPS (differential mobility particle sizer) size distributions in October 1993 and summer 1994. Low mass sulfate concentrations corresponded to bimodal peaks in the accumulation mode ($D_g \sim$ 0.1, 0.4 μm), medium mass concentrations corresponded to a monomodal peak ($D_g \sim 0.25$ μm), and high sulfate concentrations corresponded to a mostly monomodal peak around $D_g \sim 35$ μm. In October, bimodal sulfate distributions were observed for both low and high mass days, with peak diameters around 0.15 and 0.35 μm. Similar measurements were performed at El Yunque in Puerto Rico in spring 1992 that indicated two types of sulfate size distributions. Most of the samples were bimodal with peaks around 0.1 and 0.3 μm, and monomodal size distributions peaked around 0.3 μm.

Several size distribution measurements have been performed in the Grand Canyon region. Zhang et al. (1994) report sulfate size distributions measured with a low-pressure impactor corresponding to D_{ae} around 0.1–0.3 μm and 0.5-1.0 μm, and in some cases bimodal size distribution. Malm and Pitchford (1997) report DRUM (Davis rotating universal size-cut monitor) size distributions measured at the Grand Canyon in winter 1988 and in summer in Shenandoah. Larger geometric mass mean diameters were observed at Shenandoah (0.32 μm) than at the Grand Canyon (0.21 μm). Relationships between size parameters and mass concentrations suggest larger sulfate masses correspond to larger mass mean diameters, especially at Shenandoah. At both locations sulfate higher mass concentrations were also associated with narrower size distributions.

Recent Observations of Size Distributions Using DMA and OPC Data at National Park Service Special Studies

Southeastern Aerosol and Visibility Study (SEAVS)

During the SEAVS study at Great Smoky Mountains National Park TN in 1995, ASASP-X size distributions were measured in the size range from 0.1 to 3 µm (Ames et al., 2000; Hand et al., 2000). Because of the multi-valued response of the instrument in the 0.4–0.6 µm range, determining bimodality of these distributions is difficult, although there were several periods where the presence of multi-modes was indicated.

Grand Canyon Visibility Study (GRAVS)

Size distribution measurements were made using a DMA and OPC (active scattering aerosol spectrometer probe, ASASP-X) during the GRAVS study in Grand Canyon National Park AZ in summer 1998 (Hand, unpublished data). These size distributions are not ideal for investigating bimodality of the accumulation mode because an impactor was used with the DMA to remove large particles that contribute to multiple-charged particles. The ASASP-X data are aligned with the DMA data for sizes greater than 0.5 µm, but the ASASP-X data have considerable uncertainty due to calibration issues. However, there are some size distributions that do appear to be bimodal in the accumulation mode.

Big Bend Regional Aerosol and Visibility Observational Study (BRAVO)

Size distribution data were obtained using a DMA, OPC (LASAIR), and APS during the BRAVO study at Big Bend National Park in 1999 (Hand and Kreidenweis, 2002; Hand et al. 2002). Bimodal accumulation mode volume size distributions were often observed. Out of 117 days of hourly size distributions, bimodal structure in the accumulation mode was observed for some part or all of the day for 62 days.

During the Yosemite Aerosol Characterization Study (YACS) of 2002, DMA, and OPC size distribution measurements were performed during summer and early fall (McMeeking et al., 2005). Although less frequently than at BRAVO, bimodal accumulation mode size distributions were observed for some portion of eight days during the study.

4. Hygroscopic Growth

The hygroscopicity of atmospheric aerosols is an important characteristic that determines how a particle will behave in a changing relative humidity (RH) environment. Soluble particles will uptake water, resulting in increased mass and particle size, both of which determine how efficiently particles scatter light, as well as their atmospheric lifetimes. A pure salt particle (e.g., ammonium sulfate) exposed to increasing RH will undergo an abrupt change from a solid particle to a droplet at a particular relative humidity (referred to as deliquescence) that is specific to its chemical composition. Above this point the particle continues to grow exponentially. As the RH decreases, the solution droplet will lose water by evaporation and remain in a metastable supersaturated state until it effloresces and returns to a solid particle at a lower RH than that at which it deliquesced. The metastable state can exist for indefinite periods of time. This behavior is also referred to as hysteresis because the particle follows a different path of growth and evaporation.

Although extensive laboratory studies have been performed to characterize the hysteresis behavior of hygroscopic aerosols of known composition (e.g., Tang and Munkelwitz, 1994; Tang, 1996), many field studies have also been performed to understand the relationship between the hygroscopic, optical, and chemical properties of ambient aerosols. These types of measurements are typically performed by a few different methods. Tandem differential mobility analyzers (TDMA) arranged in series allow for the selection of a single particle size in the first

DMA (typically a dry size). The particle size is measured in the second DMA after it has been

exposed to increased (or decreased) relative humidity in a conditioner that separates the two

DMAs. Growth factors (D/D_o) are derived from these measurements as a ratio of a humidified

particle diameter (D) to the initial dry particle diameter (D_o) as a function of relative humidity.

This technique has been employed in many field studies, several of which are reviewed by

Cocker et al. (2001). The results of most of these studies suggest the presence of particle modes

with varying degrees of solubility and hygroscopic characteristics ("more" or "less" hygroscopic

modes), reflecting the varying chemical composition and mixing properties of the aerosols.

Bimodal growth of urban aerosols has been shown to have a less hygroscopic mode with D/D_o

ranging from 1.0 to 1.4 (for RH ~ 80–90%) and a more hygroscopic mode with D/D_o = 1.1–1.8

(e.g., Zhang et al., 1993; Busch et al., 1999; Ferron et al., 1999). Carrico et al. (2005) observed

monomodal, bimodal, and trimodal growth profiles at Yosemite National Park. They found an

inverse relationship between the mass fraction of POM and hygroscopicity and found that the

growth factors were significantly lower than expected for ionic components of the aerosol

composition, especially during periods dominated by biomass smoke.

Another technique for characterizing particle growth utilizes optical particle counters that

measure aerosol size distributions at changing relative humidities. During SEAVS, Kreisberg et

al. (2001) used a relative-humidity-moderated differential mobility optical particle size

spectrometer to measure dry and humidified particle size distributions. Hand et al. (2000) used a

relative-humidity-controlled optical particle counter to obtain both dry and humidified size

distributions. Size distributions statistics (such as geometric mean diameter and integrated

volume concentrations) for both the wet and dry distributions are used to construct diameter

growth curves (D/D_o). This method differs from the TDMA method in that D/D_o curves are

determined for an integrated aerosol size distribution, rather than for individual sizes, so information regarding mixing and "more" and "less" hygroscopic modes is not available.

Both of the above mentioned techniques to measure growth curves rely on measurements of particle size in a changing relative humidity environment. Another method for estimating particle growth is to condition the aerosol sample in a nephelometry system. Day et al. (2000) describe an experimental technique used to measure dry and humidified light scattering coefficients from which light scattering growth curves ($f(RH) = b_{sp}(RH)/b_{sp}(dry)$) have been derived for several special studies in national parks (e.g., Day and Malm, 2001; Malm et al., 2003; Malm et al., 2005b). Several investigators have used a variation on this technique of measuring a dry and humidified b_{sp} to compute f(RH) (e.g., Sheridan et al., 2001; Eldering et al., 2002; Carrico et al., 2003). Growth curves derived from nephelometry systems (f(RH)) and from TDMA systems (D/D_o) are not directly comparable because, besides being a function of aerosol composition and mixing characteristics (similar to D/D_o), f(RH) curves are also a function of aerosol size distributions that could be changing independently of RH effects during a measurement cycle and correspond to an average of scattering due to aerosol types growing at different rates.

Laboratory studies suggest that mixed salt particles have a complicated growth behavior with multiple deliquescence points (Tang, 1997), but the behavior is fairly well understood and can be predicted by several equilibrium models (Kim et al., 1993; Clegg et al., 1998a,b; Nenes et al., 1998). Less is understood about the hygroscopic properties of organic aerosols or inorganic/organic aerosol mixtures. Laboratory and some field studies have investigated the role that organic species have in the hygroscopic growth of inorganic salts or minerals and indicate that organics can change the deliquescence point of the pure inorganic species (e.g., Andrews

and Larson, 1993; Lightstone et al., 2000) and, depending on the properties and mass fractions of the organic compounds, can enhance, reduce, or not effect the rate of growth of the inorganic species (Andrews and Larson, 1993; Saxena et al., 1995; Hansson, et al., 1998; Lightstone et al., 2000; Chan and Chan, 2003; Prenni et al., 2003; Brooks et al., 2004; Gysel et al., 2004; Mikhilov et al., 2004; Carrico et al., 2005; Malm et al., 2005b). Many organic compounds have been shown to have no deliquescent or efflorescent behavior at all (e.g., Peng et al., 2001). Virkkula et al. (1999) found during a field study in Spain that internally mixed particles of ammonium sulfate and organic compounds take up water independently of one another.

In the atmosphere, the aerosols are a complicated mixture of inorganic and organic species with complex growth behaviors that may not be well represented by laboratory studies. It is likely that a large fraction of hygroscopic particles exist in supersaturated equilibrium as aqueous droplets below their deliquescence RH, based on the numerous studies that report a smooth function of particle growth with relative humidity rather than step-wise growth behavior. This behavior has been observed for D/D_o growth curves in southeast Texas (Santarpia et al., 2004, 2005), Great Smoky Mountains National Park (Hand et al., 2000), and Yosemite National Park (Carrico et al., 2005). Smooth f(RH) curves have also been observed in the Netherlands (ten Brink et al., 1996), Great Smoky Mountains, Grand Canyon, Big Bend, and Yosemite national parks (e.g., Malm and Day, 2001; Malm et al., 2003, 2005b), Portugal (Carrico et al., 2000), China (Xu et al., 2002), North Carolina (Im et al., 2001), the Maldives (Eldering et al., 2002), and during ACE-Asia (Carrico et al., 2003). Although a variety of aerosol types likely exist at these locations, their smooth growth curves suggest these particles exist either in a equilibrium state, lacking growth characteristics like deliquescence points due to their nonsoluble/soluble

mixture, or in a supersaturated equilibrium state with a very low efflorescence RH (i.e., acidic aerosols). In either case, water appears to be associated with these aerosols at low values of RH.

The difference between f(RH) for ammoniated sulfate states between fully neutralized ammonium sulfate and more acidic sulfate is summarized in Figures 5a–c. Figure 5a shows the f(RH) "no solids" curves (Clegg et al., 1998b) for ammonium sulfate, bisulfate, and sulfuric acid for a mass size distribution with $D_g = 0.4$ μm and $\sigma_g = 1.9$. Notice there is little difference between the ammonium sulfate and bisulfate f(RH) curves up to ~ 70% RH, while for RH > 70% the bisulfate f(RH) curve is about 1.2 times the ammonium sulfate curve. The sulfuric acid f(RH) curve is about twice the ammonium sulfate curve for most RH values. However, the dry mass scattering efficiencies for ammonium sulfate, bisulfate, and sulfuric acid are 3.72, 3.35, and 2.66 m^2 g^{-1}, respectively, offsetting the differences in f(RH) curves at high humidity. The mass scattering efficiencies for ammonium sulfate, bisulfate, and sulfuric acid are plotted as a function of RH in Figure 5b to assess the effective scattering of a fixed amount of sulfate ion interpreted as any of these three forms of sulfate. Notice that at low RH the mass scattering efficiency for bisulfate is lower than the ammonium sulfate mass scattering efficiency and about equal at higher RH. Sulfuric acid mass scattering efficiency is about the same as ammonium sulfate mass scattering efficiency at low RH but greater at high RH. Figure 5c summarizes these differences. The ratio of the sulfate ion mass scattering efficiency interpreted as ammonium bisulfate and as sulfuric acid to the ammonium sulfate efficiency curve is shown as a function of RH. Notice that at low RH (10–70%) the bisulfate efficiency is about 20% lower than the ammonium sulfate mass scattering efficiency, and at high RH they are about equal. Sulfuric acid mass scattering efficiencies are 10–20% greater than ammonium sulfate efficiencies over most of the RH range and 40% greater at very high RH values (95–98%).

In the IMPROVE formulation, the form of sulfate is assumed to be ammonium sulfate. From Figure 5c it is evident that this choice of ammonium sulfate can either be an over- or underestimate of true sulfate scattering, depending on the ratio of the ammonium to sulfate ion. However, the current f(RH) growth curve used in the IMPROVE equation is based on an interpolated D/D_o curve between the ascending and descending branches of growth for ammonium sulfate and reaches a value of 1 at 40% RH (no water is associated with the particles below 40% RH) (Sisler and Malm, 1994). This curve was derived to approximate smooth growth curves observed in field studies. We propose applying an f(RH) growth curve corresponding to equilibrium calculations for ammonium sulfate below the deliquescence point to 0% RH using the Aerosol Inorganics Model (AIM) with the "no solids" option (Clegg et al., 1998b). This smooth curve also approximates the behavior observed for mixtures of aerosols as those observed in the studies cited above; however, it differs from the current curve in that it allows water to be associated with the aerosol for RH values below 40%. Organics are assumed to be nonhygroscopic because of the lack of conclusive evidence; however, laboratory and field results suggest they are weakly to nonhygroscopic, (Malm et al., 2003; Carrico et al., 2005; Malm et al. 2005b). Sea salt f(RH) curves are computed using NaCl growth factors derived from the AIM model (Clegg et al., 1998b). No water is associated with sea salt below its crystallization point (RH = 47%).

Figure 5. (a) f(RH) curves using the "no solids" method for ammonium sulfate, ammonium bisulfate, and sulfuric acid (assuming a size distribution with $D_g = 0.4$ μm and $\sigma_g = 1.9$). (b) Sulfate mass scattering efficiencies for ammonium sulfate, ammonium bisulfate, and sulfuric acid using the curves in part (a). (c) Ratios of ammonium bisulfate and sulfuric acid mass scattering efficiencies to the ammonium sulfate mass scattering efficiency shown in (b).

5a

f(RH) curves d_g=0.4 sig=1.9
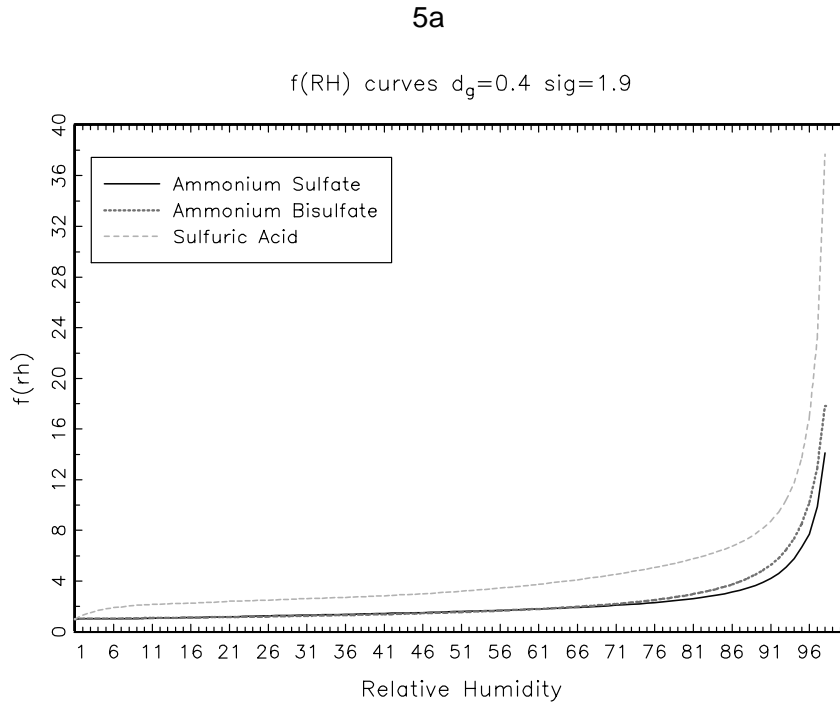
5b

Sulfate mass scattering efficiency
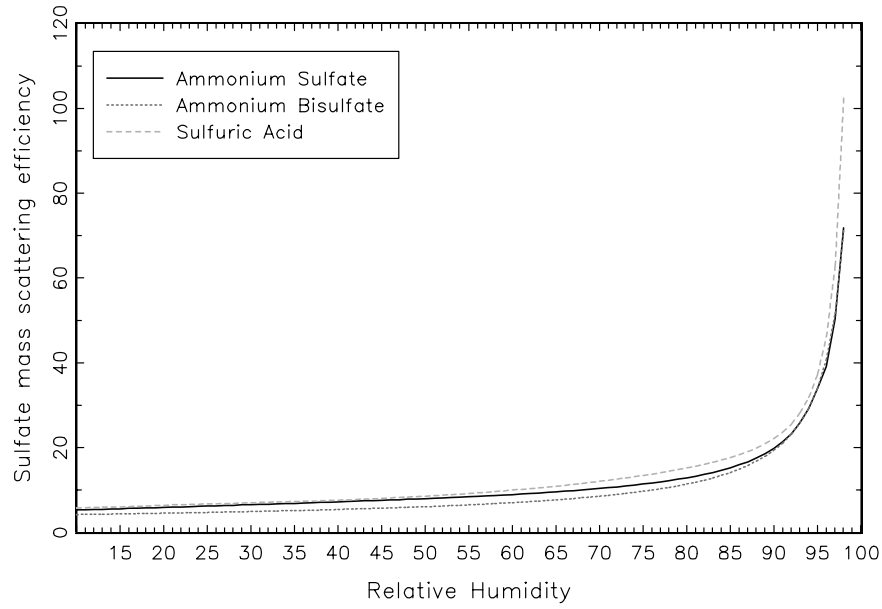
5c

Normalized to Ammonium Sulfate

51
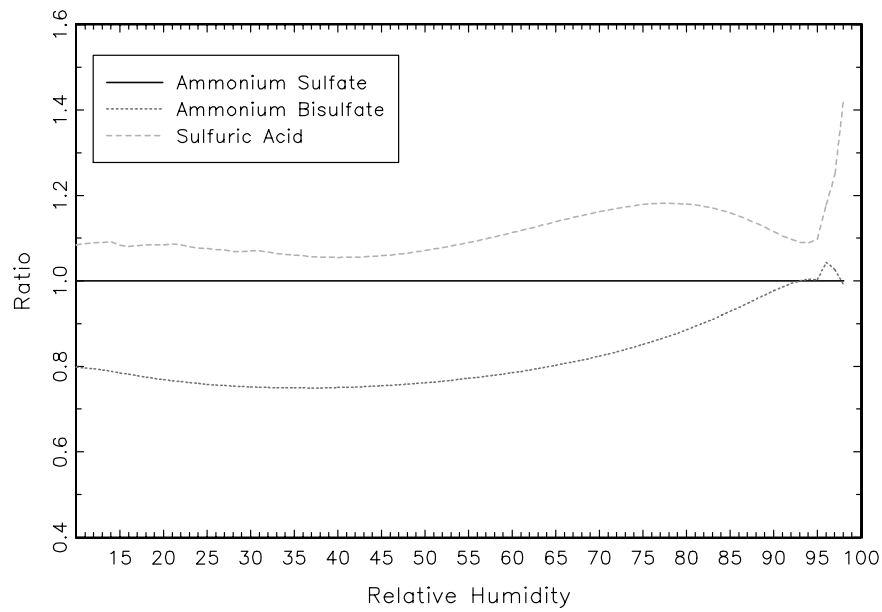
5. Mass Scattering Efficiencies

In order to review mass scattering efficiencies, it is important to understand the terminology used and the impact of assumed aerosol models upon the resulting estimates. We motivate this section by a theoretical discussion of mass scattering efficiencies, including derivations and effects of the assumed model on derived estimates. Later we review other empirical methods used for estimating mass scattering efficiencies from measurements and how the assumptions applied in these methods may result in estimates that, although they may be referred to as mass scattering efficiencies, in fact may actually differ in their physical meaning. The final subsections provide a survey of reported measured mass scattering efficiencies using different methods and estimates derived from IMPROVE data.

5.1. *Theoretical Discussion*

The role of aerosols in visibility degradation or climate forcing has motivated efforts to quantify the optical properties of specific aerosol species. The terminology used and the impact of assumed models on the amount of change in extinction apportioned to individual aerosol species have been subjects of debate. For example, ranges in estimates of mass scattering efficiency of sulfate aerosol applied in climate forcing models (Penner et al., 1993) arose due to the assumptions regarding the presence of other chemical species (e.g., ammonium and/or water) or assumptions concerning shifts in the size distribution with changes in aerosol mass in the calculation of mass scattering efficiency (Zhang et al., 1993; Anderson et al., 1994; McMurry et al., 1996). White (1986) presents a thorough discussion of the definitions of extinction efficiency and the consequences of various assumptions of the assumed aerosol microstructure upon the apportionment of extinction to its chemical components.

Mass extinction (or scattering) efficiencies are defined as the total aerosol extinction (or scattering) divided by the total aerosol mass and can be calculated theoretically for spherical

particles of known composition and size using Mie theory (van de Hulst, 1981). Aerosol models typically assume that aerosol species are mixed externally; the simplest example is a particle composed of a single chemical species such as ammonium sulfate, and for this case the extinction efficiency is referred to as a "mass extinction efficiency". However, realistically, particles in the atmosphere comprise a variety of inorganic and organic species. These types of particles are referred to as internal mixtures, and their extinction efficiencies are termed "specific mass extinction efficiencies". Internally mixed particles can also be externally mixed from other particle populations; the most obvious case would be internally mixed fine mode aerosols externally mixed from coarse mode aerosols.

For the following discussion, the aerosol size distribution refers to an externally mixed aerosol of a single chemical component, j. For a corresponding aerosol number distribution $f_{N,j}(D_p)$ and complex refractive index $n_j = m + ik$, the light extinction coefficient ($b_{ext,j}$) is computed with equation 7 and has units of inverse length.

$$b_{ext,j} = \int_0^\infty \frac{\pi}{4} D_p^2 Q_{ext}(n_j, D_p, \lambda) f_{N,j}(D_p) dD_p \qquad (7)$$

The Mie extinction efficiency is given by $Q_{ext}(n_j, D_p, \lambda)$ and is a function of refractive index, particle diameter (D_p), and wavelength (λ). Equation 7 can be reformulated in terms of aerosol mass size distribution $f_{M,j}(D_p)$ by making the following substitution for the number distribution (equation 8), with species particle density given by ρ_j:

$$f_{N,j}(D_p) = \frac{6}{\rho_j \pi D_p^3} f_{M,j}(D_p) \qquad (8)$$

Substituting equation 8 into equation 7 gives

$$b_{ext,j} = \int_0^\infty \alpha_{ext,j}(n_j, D_p, \lambda) f_{M,j}(D_p) dD_p \tag{9}$$

where the single particle mass extinction efficiency ($\alpha_{ext,j}$) has units of m^2 g^{-1} and is given by

$$\alpha_{ext,j} = \frac{3}{2} \frac{Q_{ext}(n_j, D_p, \lambda)}{\rho_j D_p} \tag{10}$$

Normalizing equation 9 by the total mass concentration of species j (M_j) allows the extinction efficiency to be written as

$$\alpha_{M_j} = \int_0^\infty \alpha_{ext,j} f'_{M,j}(D_p) d(D_p) \tag{11}$$

where $f'_{M,j}(D_p)$ is the normalized mass distribution. If $f'_{M,j}(D_p)$ does not vary with total mass concentration, then the average mass scattering efficiency for species j can be considered a constant and the light extinction coefficient corresponding to species j can be written as

$$b_{ext,j} = \alpha_{M_j} M_j \tag{12}$$

The total extinction is then a linear combination of the species mass concentrations.

$$b_{ext} = \Sigma \alpha_{M_j} M_j \tag{13}$$

Equation 13 also holds for an internally mixed aerosol where the chemical species are mixed in fixed proportions to each other, the index of refraction is not a function of composition or size, and the aerosol density is independent of volume.

When computing total extinction using Mie theory, the microscopic structure of the aerosol (that is, the extent of internal or external mixing) is found to be relatively unimportant, so that the assumption of internally versus externally mixed particles does not have much impact on the predicted results. This insensitivity of total scattering or extinction to the aerosol mixture has

been demonstrated by a number of authors, including Hasan and Dzubay (1983), Sloane (1983),

Pilinis et al. (1995), and McMurry et al. (1996).

The mass extinction (or scattering) efficiency is a stronger function of density and size

than optical properties such as refractive index (see equation 10). Several investigators have

reported on the size dependence of mass scattering efficiencies (Malm and Pitchford, 1997; Li et

al., 2000; Hand, 2001; Malm et al., 2003). Other authors report the dependence of mass

scattering on mass concentrations (Malm et al., 2003) or on light scattering coefficients

(Lowenthal and Kumar, 2004); however, these relationships arise due to the dependence of b_{sp}

and mass on particle size.

Estimating the change in extinction due to the removal or addition of a single species is

different from assigning a fraction of extinction to a chemical species or mixture of species, and

is referred to as a "partial mass extinction efficiency" ($\alpha_{ext,part}$).
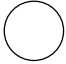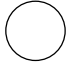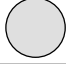
$$\alpha_{ext,part} = \left(\frac{\partial b_{ext}}{\partial M_j} \right) \tag{14}$$

The partial extinction efficiency is dependent on change in composition as well as change in

aerosol size as species are added or removed. For example, McMurry et al. (1996) examined

$\alpha_{ext,part}$ as a function of formation mechanisms for sulfate. If sulfate was formed by gas phase

reactions, lower humidity conditions led to smaller particles sizes; whereas when sulfate was

formed in aqueous processes, the higher relative humidity conditions led to larger particle sizes.

A simple example illustrating some of these concepts is shown in Figure 6 (Malm and

Kreidenweis, 1997). The insensitivity of the total computed scattering to the mixing assumption

is presented in Figure 6a. Two aerosol species with the same total volume, size distribution, and

index of refraction, but with densities differing by a factor of 2, are externally mixed. They have

mass scattering efficiencies of 3 m^2 g^{-1} and 6 m^2 g^{-1}, respectively. The externally mixed aerosol

contains 10 µg m^{-3} of species 1 and 5 µg m^{-3} of species 2, with each species contributing 30

Mm^{-1} to the total aerosol scattering of 60 Mm^{-1}.

Figure 6. (a) Diagram contrasting mass scattering efficiencies for internally versus externally mixed particles. (b) Partial scattering efficiencies for internally and externally mixed particles.

		Figure 6A		Figure 6B	
		species 1	species 2	species 1	species 2
mass	external case	10 µg/m^3	5 µg/m^3	10 µg/m^3	species 2 removed
aerosol type					
species density		2 g/cm^3	1 g/cm^3	2 g/cm^3	
specific mass scattering efficiency		3 m^2/g	6 m^2/g	3 m^2/g	
particle scattering		30 Mm^{-1}	30 Mm^{-1}	30 Mm^{-1}	
total scattering		60 Mm^{-1}		30 Mm^{-1}	
mass	internal case	15 µg/m^3		10 µg/m^3	
aerosol type					
species density		1.5 g/cm^3		2 g/cm^3	
specific mass scattering efficiency		4 m^2/g		2 m^2/g	
total scattering		60 Mm^{-1}		20 Mm^{-1}	

If species 1 and species 2 are now assumed to be internally mixed (see lower part of

Figure 6a), the specific mass scattering efficiency for the mixed particle is now required for

calculation of the total aerosol scattering. The specific mass scattering efficiency can be

computed as the mass-weighted average of the efficiencies of the individual species (4 m^2 g^{-1}),

assuming several conditions are met. The optical properties of the mixture must be similar to

those for the individual species (which must also be similar; this condition is met, for example,

by a mixture of ammonium sulfate and organics, with real refractive indices of 1.53 and 1.5, respectively). Volume conservation must be invoked, and the size distribution of the internal mixture must be similar to the size distributions of the external mixtures. By applying the specific mass scattering efficiency, a total aerosol b_{sp} for the sample is again computed as 60 Mm^{-1} (see Figure 6a).

However, the apportionment of scattering to species 1 and 2 is different under these two models. Using the externally mixed model, species 1 and 2 each contribute 50% of the total scattering. In the internally mixed case, species 1 contributes 66% of the scattering budget (since it makes up 66% of the total mass), while species 2 contributes 33%. This discrepancy arises because when the species are internally mixed, the same scattering efficiency is assigned to both species, although independently they have different efficiencies. *This discrepancy can only be resolved if the specific mass scattering efficiency of the mixed aerosol is prorated to its chemical constituents, based on their relative densities. The apportionment of scattering to specific species is therefore independent of whether an externally or internally mixed model is assumed.*

This simple example demonstrates that the contribution of each species to total extinction is sensitive to the assumed microscopic structure of the aerosol. White (1986) refers to this as the apportionment problem, distinct from the problem of computing total extinction from estimates of size-dependent chemical composition that we just demonstrated to be similar for the two cases in Figure 6a. For the externally mixed case, the total extinction for the mixture is calculated by computing the contribution of each species separately, and the species contribution to the total is well defined if we know the size distribution of each species. For the internally mixed case, it may be misleading to assign a percentage of the total extinction to each species on a mass-weighted basis, as demonstrated in Figure 6a.

The previous discussion concerns itself with apportioning extinction to a species as it resides in the ambient atmosphere. From a regulatory standpoint, the change in total scattering as a function of the removal of a species may be of interest. Total scattering can be computed for the mixture, and for the case when one species has been removed from the mixture; the difference between these values provides the contribution of the species to total scattering. As an example, we compute the partial scattering efficiency for species 2 under the assumptions of externally mixed particles. The partial scattering efficiency is obtained by computing the total aerosol scattering assuming only species 1 is present (30 Mm^{-1}, see Figure 6b). Subtracting this value from the total scattering obtained for the mixture (60 Mm^{-1}, see Figure 6a), we deduce that species 2 contributed 30 Mm^{-1} (half) to the mixed aerosol scattering. The derived partial scattering efficiency of 6 m^2 g^{-1} for species 2 [$\Delta b_{sp}/\Delta mass = (60-30$ $Mm^{-1})/(5$ μg $m^{-3})$] is the same as its mass scattering efficiency from Figure 6a.

Investigating the same scenario but for the internally mixed case (see the lower part Figure 6b), we assume that the removal of one species from the internal mixture would conserve particle number concentrations but reduce particle size. This size reduction alters the specific scattering efficiency of the mixture, which is now assumed to be 2 m^2 g^{-1}. The total aerosol scattering is thus 20 Mm^{-1}, which leads to the conclusion that the partial scattering efficiency of species 2 is 8 m^2 g^{-1} [$\Delta b_{sp}/\Delta mass = (60-20$ $Mm^{-1})/(5$ μg $m^{-3})$]. White (1986) presents a thorough discussion of the definitions of specific extinction and mass extinction efficiency and of the consequences of various assumptions of aerosol microstructure upon the apportionment of extinction to its chemical components.

Issues also arise when apportioning scattering to species that have different hygroscopic properties. Consider an external mixture of hygroscopic and nonhygroscopic aerosols species

with similar masses. The mass scattering efficiencies of the dry nonhygroscopic and hygroscopic species are each 3 m^2 g^{-1}, while that of the wet hygroscopic species is, because of associated water, 8 m^2 g^{-1}. When internally mixed, the wet specific mass scattering efficiency will be 3–8 m^2 g^{-1}, depending on the hygroscopic properties of the mixed aerosol. Several authors discuss aerosol growth characteristics as a function of RH and have successfully predicted the scattering characteristics of the mixed particles (Anderson et al., 1994; Sloane, 1983, 1986; Malm and Pitchford, 1997; Malm et al., 2000, 2003, 2005b). However, the apportionment of scattering to a particular species is still problematic. Typically, one growth curve is developed for the mixed species, and scattering due to water is apportioned proportionally among all aerosol components, even though only one of the species may be hygroscopic. An example would be a mixture of ammonium sulfate and a weakly hygroscopic organic species.

5.2.   *Methods for Deriving Mass Scattering Efficiencies*

The methods typically used to estimate mass scattering efficiencies depend on the type of measurements and data available. In this section we will discuss the most common methods used. We use the term "mass scattering efficiency" to refer to estimates that correspond to a single aerosol component such as dry ammonium sulfate, and although one could argue that species such as POM and soil correspond to a combination of chemical components, we will use this term to correspond to those efficiencies also. We use the term "specific mass scattering efficiency" to refer to aerosols composed of more than one species, for example, a "fine mode specific mass scattering efficiency". We will also use this term to refer to aerosols that include water mass. For example, if an efficiency for an inorganic salt particle with associated water mass is reported, we refer to it as a "specific mass scattering efficiency".

The simplest method for computing efficiencies is with measured mass concentrations from filter samples and measured light scattering coefficients from nephelometry. For an aerosol

population, a specific mass scattering efficiency α_{sp_spec} can be defined as the ratio of a light scattering coefficient corresponding to the mass concentration (M) of that population.

$$\alpha_{sp\_spec} = \frac{b_{sp}}{M} \tag{15}$$

The average specific mass scattering efficiency can be estimated by dividing the average scattering coefficient by the average mass concentration for a given set of measurements, or a linear regression can be performed on the data and the slope of the linear fit can be interpreted as the specific mass scattering efficiency. Specific mass scattering efficiencies derived in this manner represent an average aerosol that could be changing due to variations in relative humidity, size distribution, and composition during the sampling period. Mass concentrations used in this method could be either gravimetric mass or the sum of chemically analyzed masses, or be computed from integrated volume distributions using an assumed density.

A number of investigators have taken advantage of the form of equation 13 ($b_{ext} = \Sigma \alpha_{Mj} M_j$) to construct a multi-linear regression (MLR) model with b_{ext} as the independent variable, and the measured aerosol mass concentrations for each species j (M_j) as the dependent variables. The regression coefficients are then interpreted as mass extinction (or scattering or absorption) efficiencies. The assumptions required in this formulation are that all the components contributing to extinction are included, equation 13 is a reasonable approximation to the relationship between extinction and the various aerosol species, the number of samples is large enough to give stable results, and the concentrations of the species are uncorrelated.

However, as stated by White (1991), "Model simulations show the procedure to yield usefully accurate results under favorable conditions. An important liability is that the availability of standard software makes it easy to perform regression under unfavorable conditions." Regression-derived efficiencies are vulnerable to a variety of systematic and random errors. At

the most basic level, there is the issue that meteorologically driven fluctuations of the existing aerosol concentrations may cause aerosol mass concentrations of different species to be collinear. The high degree of collinearity commonly found among aerosol species can make regression results very sensitive to the choice of species to be included in the analysis. A more practical difficulty is that regression results can be biased by random uncertainties in the measurements. Standard regression models tend to overpredict the coefficients of species that have lower uncertainties (e.g., sulfates) and underpredict the coefficients of species with larger measurement uncertainties (e.g., organics), similar to the discussion in section 3.1.

The theoretical approach described at the beginning of this section (see equations 7–10) is often used to compute mass scattering efficiencies from mass (or number) distributions of aerosol species from impactor measurements or mobility or optical measurements. However, this method requires assumptions of the measured species chemical form and mixing properties of the aerosols, as well as their optical properties. Estimates from this method often assume an externally mixed aerosol, but if the size distribution measurement is obtained by mobility or optical measurements (number size distribution), an internally mixed aerosol is assumed, but perhaps for separate size modes. This method has been shown to accurately reconstruct light scattering. For example, measurements of size distributions have been incorporated with estimates of aerosol optical properties to reconstruct measured scattering (and estimate specific mass scattering efficiencies) on fine time scales (Hand et al., 2002; Malm et al., 2005a; McMeeking et al., 2005). These estimates have the added advantage of allowing for the investigation of the functional dependence of efficiencies on particle size, composition, and humidity. The theoretical method provides the most accurate estimate of efficiencies out of those discussed in this section. A disadvantage to this method is that size distribution measurements

are more analytically intensive and not often available for routine monitoring, so computing mass scattering efficiencies by this method is not routinely possible.

Estimating mass scattering efficiencies as the change in b_{ext} resulting from the removal (or addition) of a single species is different from assigning a fraction of measured extinction to a chemical species or a mixture of species. The change in extinction resulting from a change in aerosol species concentration was described previously (equation 14). As species are added or removed from an aerosol, the efficiency is dependent on change in composition as well as on change in aerosol size. Computing partial mass scattering efficiencies in this context requires a model to account for the effects of removal of mass on light scattering coefficients, such as the ELSIE (Elastic Light Scattering Interactive Efficiencies) model (Sloane, 1983; Sloane et al., 1991; Lowenthal et al., 1995; Omar et al., 1999). Among the assumptions in the ELSIE model are those associated with removing aerosol mass. Mass can be removed or added by assuming that the particle size changes but not the particle number, or that the particle number changes but not the particle size (Lowenthal et al., 1995). Unless the option is chosen to keep the size constant, the efficiencies derived from this method cannot be compared to efficiencies from other methods. Also, assumptions must be made regarding how to treat water mass associated with a removed species. Although this technique is useful in a regulatory context, in practice it is not possible to measure the change in light scattering due to a change in mass concentration, so more empirical approaches were adopted to estimate mass scattering efficiencies.

5.3. *Survey of Mass Scattering Efficiencies*

A review of ground-based measured mass scattering efficiencies from peer-reviewed literature since 1990 includes values derived from the four different methods described above (theoretical, measurement, multi-linear regression, and partial scattering approach) and are summarized by several tables (Tables 2–5 in Appendix 2). The tables can be understood in the

following way: the mass scattering efficiencies are listed by species (e.g., sulfate, POM) or as specific mass scattering efficiencies for mixtures of aerosols by size mode (i.e., fine, coarse, or total). The tables also list the study location, study name, aerosol characteristics (e.g., smoke) if noted, and the study time period. Each method table has a corresponding notes table that provides details of the measurements, size ranges, the relative humidity of the measurements, assumptions, and the wavelength at which the measurements were made if it was other than 550 nm; these can found in Appendix 2. Occasionally this information may also be found in a footnote in the mass scattering efficiency method table for quick reference. Citations are numbered consecutively in alphabetical order (a full citation list can also be found in Appendix 2). The "note" column in the table refers to the citation number as well as the entry in the notes table. When appropriate, we compute the average (and one standard deviation) for values in the cited literature and note it in the footnotes. Except for averages, values are listed as found in the literature, and furthermore, sulfate mass scattering efficiencies have been normalized to dry ammonium sulfate when possible. This normalization is performed because sulfate efficiencies are reported under a variety of conditions. For example, they may be reported in terms such as sulfate ion, ammonium sulfate mass, or ammoniated sulfate mass (depending on the acidity), and they may be reported for a range of relative humidity values corresponding to associated water mass. Sulfate mass scattering efficiencies reported for RH > 45% were converted to dry ammonium sulfate mass scattering efficiencies based on reported ammonium to sulfate molar ratios and f(RH) curves corresponding to ammonium sulfate. For all the entries, the original sulfate mass scattering efficiencies are reported, along with corrected dry ammonium sulfate mass scattering efficiencies in italicized font (if already reported in the cited manuscript), or noted with a (†) symbol if we performed the correction to a dry ammonium sulfate basis.

Occasionally there was not enough information available to do this correction. Other corrections in the table include normalizing the POM efficiencies to a multiplier of 1.8. Most of the estimates were reported corresponding to POM computed with multipliers of 1.2, 1.4, 1.6, or 2.1 (see notes table for each method). We normalized the efficiencies to $R_{oc} = 1.8$ so that estimates derived in the next section can be directly compared. Both efficiencies are listed in the tables but the normalized values are italicized.

We begin our review with the theoretical method efficiencies so that later discussions of efficiencies derived by more simple methods can be understood in the context of theoretical predictions. Theoretical mass scattering efficiencies are reported in Table 2. These efficiencies are the most representative estimates because the effects of particle size and composition can be included in the calculation for a single time period, and as previously mentioned, derived efficiencies accurately reconstruct scattering over very fine time resolutions. The theoretical method relies on computed scattering that is dependent on Mie theory and corresponding assumptions of spherical particles and optical properties.

5.3.1. Theoretical Method

The average fine mode dry ammonium sulfate mass scattering efficiency from the theoretical method is 2.5 ± 1.1 m^2 g^{-1} (see Table 6). Most of the values reported correspond to the fine mode, although coarse and total sulfate are reported and noted in Table 2 (see Appendix 2). The highest value in this table (6.0 m^2 g^{-1}) was reported for China by Li et al. (2000) and we have corrected it from ammonium bisulfate to ammonium sulfate but performed no humidity correction. It is unclear at what relative humidity this value is reported, although Li et al. (2000) state that particle growth based on Tang (1997) has been assumed. Having some water mass associated with this estimate would be consistent with its higher value compared to the other estimates. For example, wet specific mass scattering efficiencies reported for Hopi Point AZ,

Meadview AZ, Shenandoah National Park, and Great Smoky Mountains National Park correspond to different RH values (see notes table) and demonstrate the large effect water mass has on efficiencies, especially at Shenandoah where the ambient humidity is high in summer. Removing the highest value (6.0 m^2 g^{-1}, reported by Li et al., 2000) from the calculated average results in a mean dry ammonium sulfate mass scattering efficiency of 2.2 ± 0.6 m^2 g^{-1}. The lowest value in the table (1.12 m^2 g^{-1}) was observed in the Southern Ocean region south of Australia during the ACE-1 (Southern Hemisphere Aerosol Characterization Experiment) study (Quinn et al., 1998), corresponding to a small average surface mean diameter of 0.20 ± 0.04 µm. It is interesting that given the global distribution in the measurements, a fairly low variability in dry ammonium sulfate efficiencies is observed, perhaps a reflection of the robustness of this method for computing efficiencies, especially when the optical and hygroscopic properties are well understood.

The average POM mass scattering efficiency without corrections for R_{oc} differences was 5.9 ± 1.0 m^2 g^{-1} and was most likely affected by the assumptions in computing POM from measured organic carbon and the range of types of organics measured. To correct for the different multipliers used to compute POM, we normalized these values to an R_{oc} of 1.8, and the resulting normalized average POM mass scattering efficiency was 5.5 ± 1.6 m^2 g^{-1} (see Table 6). The normalization did not significantly change most of the estimates (see italicized values in the table) because most of the studies use R_{oc} values ranging from 1.4 to 2.1. This normalization did change the estimate by Li et al. (2000) in China because no R_{oc} was reported in that study, so we assumed they used a value of 1. Most of the authors in these studies applied R_{oc} values consistent with Turpin and Lim's (2001) suggested values that vary according to aerosol type. For example, during the Aerosols99 study, Quinn et al. (2001) reported values for locations ranging from the

Atlantic Ocean off the coast of Virginia to Cape Town, South Africa, with aerosol origins ranging from remote marine to African dust and biomass burning. They applied a POM multiplier of 1.6 for North American air masses (more urban aerosols) and 2.1 for all other air masses. With the exception of Li et al. (2001), these studies did not assume organics were hygroscopic; however, the RH corresponding to the value by Li et al. (2001) is unspecified.

Average fine, coarse, and total (fine + coarse) dust mass scattering efficiencies were 3.4 ± 0.5, 0.7 ± 0.2, and 1.2 ± 0.3 m^2 g^{-1}, respectively. It is probable that fine dust corresponds to the tail of the coarse mode dust distribution; however, the higher fine mode efficiencies are a result of these sizes interacting more efficiently with light, compared to the coarse mode. Mid-range values corresponding to the total aerosol mode reflect the integration over all sizes. The variability for each of these estimates is fairly low, considering differences in dust composition and size distributions, the study locations, and dust origins, which include Asia, the Indian Ocean, and off the coast of North Africa (Chiapello et al., 1999; Li et al., 2000; Quinn et al., 2001, 2002b, 2004).

The average fine and coarse mode specific mass scattering efficiencies were 4.3 ± 0.7 m^2 g^{-1} and 1.6 ± 1.0 m^2 g^{-1}, respectively. The fine mode values could include ammoniated salts, carbonaceous aerosols, and mineral aerosols. These efficiencies were reported for a range of humidities, and no corrections to a dry aerosol were performed because of the lack of information on the fine mode composition. The cut-off diameter for these modes may also vary from study to study, ranging from 1 to 2.5 μm. Given these differences, there is still a fairly narrow range of values reported for fine mode specific efficiencies. A much larger variation in the coarse mode efficiencies was observed. The composition, size distribution, and optical properties of the coarse mode may vary considerably given the studies reported here. For

example, the lowest value of 0.6 m^2 g^{-1} at Big Bend National Park (Hand, 2001) reflects the fact that soil dominated the coarse composition (~ 40% on average). In contrast, the values derived from the many cruise-based measurements (Quinn et al., 2001, 2002b, 2004) may be influenced by sea salt or other species.

Average fine, coarse, and total sea salt specific mass scattering efficiencies were 5.3 ± 0.8, 1.2 ± 0.3, and 2.3 ± 0.9 m^2 g^{-1}, respectively. Sea salt specific mass scattering efficiencies are not corrected for relative humidity and include the effects of aerosol water mass. Similar to what was observed with dust mass scattering efficiencies, the fine mode sea salt specific mass scattering efficiencies are larger than the coarse mode, with the total aerosol (fine + coarse) in the middle of the range.

5.3.2.   Measurement Method

Estimates of mass scattering efficiencies for the measurement method are reported in Table 3 (see Appendix 2 and Table 6). Most of these values correspond to specific mass scattering efficiencies for the fine or coarse mode because the measurements were performed for fine (or coarse) mass and measured light scattering. These values are not averaged together because the relative humidity at which the measurements are made, the types of mass data (gravimetric or sum of chemically analyzed), and the composition and size ranges corresponding to each mode vary; therefore normalizing these data to a common RH or composition is not possible. Some studies have several values reported (such as in the Maldives during the INDOEX study) because they are reported for ranges of light scattering coefficients and for different measurement methods (land- and cruise-based) by different investigators and averaging them together would be inappropriate. Even with these differences, some spatial patterns are noticeable. The highest fine mode specific mass scattering efficiencies (> 5 m^2 g^{-1}) are reported in urban locations such as Mexico City, Mexico (Chow et al., 2002), Fort Meade MD (Chen et

al., 2003), and the New England–mid-Atlantic region (Poirot and Husar, 2004). These values could be high due to relative humidity effects (especially in the eastern United States), or due to the aerosol composition. For example, the efficiency of 6 m^2 g^{-1} reported by Poirot and Husar (2004) corresponds to smoke aerosol that may have higher efficiencies (Malm et al., 2005a; McMeeking et al., 2005). With the exception of sites in Phoenix AZ and sites near Denver CO, the urban (e.g., Beijing, China, Atlanta GA, Dallas TX) fine mode specific mass scattering efficiencies are greater than 3 m^2 g^{-1}. Most of the rural sites in the southwestern United States correspond to lower specific efficiencies (less than ~ 2.5 m^2 g^{-1}) in Meadview AZ, Mount Zirkel in Colorado, and Spirit Mountain NV, which are close to the theoretical mass scattering efficiencies computed for dry ammonium sulfate. The exceptions to these low values are those reported for the northwestern United States (Mount Rainier WA and North Cascades WA) and in Bondville IL with efficiencies greater than 4 m^2 g^{-1}. Higher specific mass scattering efficiencies (usually greater than 3 m^2 g^{-1}) were observed during the INDOEX experiment in the Maldives. Specific mass scattering efficiencies for this study are ordered as a function of light scattering coefficients and no significant difference was observed for low scattering (b_{sp} < 25 Mm^{-1}) compared to high scattering periods (b_{sp} > 55 Mm^{-1}), in contrast to the relationship Lowenthal and Kumar (2004) observed for data from the IMPROVE network. The specific efficiencies reported for the Maldives are for an RH of 33%, so the effects of aerosol water mass are probably not significant for these data. Specific efficiencies corresponding to the total aerosol mode were reported for Yulin, China (Alfaro et al., 2003), during the ACE-Asia study. Values were higher during polluted periods compared to periods dominated by dust aerosols, probably because of the change in aerosol size distributions.

5.3.3. MLR Method

Estimates of mass scattering efficiencies obtained using the MLR method are summarized in Table 4 (see Appendix 2). These values are subject to variability based on how the regressions were performed (with or without intercepts, or accounting for measurement uncertainties) and the types of data used. Average fine mode specific mass scattering efficiencies were 3.1 ± 1.5 m^2 g^{-1}, which were somewhat lower than the average estimate derived from the theoretical method, although with much larger variability. The highest values (> 5 m^2 g^{-1}) were reported in Israel, and the lowest values ($2-3$ m^2 g^{-1}) were reported in the southwestern United States (Nevada, Arizona, and Colorado), which is similar to the spatial distribution seen with the results from the measurement method. Average coarse mode specific mass scattering efficiencies are 0.7 ± 0.6 m^2 g^{-1}, ranging from values greater than 1 m^2 g^{-1} in Nevada and Arizona to values less than 0.5 m^2 g^{-1} in Colorado, Arizona, and Israel. The variability of coarse mode composition and size distributions could result in large variability in derived efficiencies.

The average fine mode dry ammonium sulfate mass scattering efficiency was 4 ± 3 m^2 g^{-1}, higher than theoretically predicted for fine mode dry ammonium sulfate and with a large variability due to outliers. Removing the outliers (i.e., 10.9 and 8 ± 3 m^2 g^{-1}) results in an average dry ammonium sulfate efficiency of 3.2 ± 1.2 m^2 g^{-1}, much closer to what has been theoretically derived. It is possible that these high values are due to water associated with the nephelometer data, or due to uncertainties in the nephelometer data. Many of the sulfate mass scattering efficiencies reported in the MLR table were corrected to a dry ammonium sulfate basis, which could also contribute to uncertainties in these values. Variations in relative humidity or aerosol acidity could result in uncertainties in the corrections as these were applied in an average sense. The lowest value reported in the table (0.83 m^2 g^{-1}) corresponds to the total ($D_p <$ 10 μm) size distribution, demonstrating the effects of averaging over larger particles (higher

mass) that have less efficient light scattering properties. Also, it is probable that the chemical form of sulfate in the coarse mode was different from ammonium sulfate.

The unnormalized average value of POM mass scattering efficiency was 3 ± 4 m^2 g^{-1}, with the large variability reflecting the range in values reported. The average POM mass scattering efficiency normalized to an R_{oc} of 1.8 is 2 ± 3 m^2 g^{-1}. Outliers in these values are reported for Uniontown PA (12 ± 8 m^2 g^{-1}, Lowenthal et al., 1995), and removing that outlier from the normalized efficiencies results in an average value of 1.6 ± 0.6 m^2 g^{-1}, which is considerably lower than the average value of 5.5 ± 1.6 m^2 g^{-1} derived with the theoretical method. If we remove the cases that were computed assuming organics are somewhat soluble during higher RH periods, the average value is 2.3 ± 1.0 m^2 g^{-1}. Besides the outlier, the highest value reported is for Bondville IL (4.11 m^2 g^{-1}) (Koloutsou-Vakakis et al., 2001) and has not been normalized because it corresponds to a carbonaceous aerosol that includes both organic and light-absorbing carbon. The low values of POM mass scattering efficiency derived by this method provide a good example of how uncertainties associated with organics may result in an underprediction of derived mass scattering efficiencies.

The average ammonium nitrate mass scattering efficiency was 4 ± 2 m^2 g^{-1}. The highest values are reported for Meadview AZ and Mount Zirkel CO. However, no spatial dependence is seen, as the lowest values reported are also in the southwestern United States (Grand Canyon AZ, Canyonlands UT, and Phoenix AZ). The average fine, coarse, and total dust mass scattering efficiencies are 3 ± 2, 0.40 ± 0.08, and 0.7 ± 0.2 m^2 g^{-1}, respectively. Fine mode dust mass scattering efficiencies are quite similar to those derived using the theoretical method (3.4 ± 0.5 m^2 g^{-1}); however, coarse mode and total dust efficiencies are somewhat lower for the MLR

method. Given the range of assumptions and different measurements that are incorporated into these estimates, the convergence of fine dust efficiencies towards 3 $m^2 g^{-1}$ is notable.

The average sea salt specific mass scattering efficiencies for the fine, coarse, and total modes are 4.0 ± 1.6, 1.6 ± 1.2, and 2.2 (one number reported) $m^2 g^{-1}$, respectively. These values are also quite similar to those reported in the theoretical table. Sea salt is hygroscopic; therefore any water associated with measured scattering could be attributed to sea salt in the regression.

5.3.4.   Partial Scattering Method

Values of mass scattering efficiency derived from the partial scattering approach are reported in Table 5 (see Appendix 2). Most of these studies employed the ELSIE model, as described previously. Species included in the model are sulfate, POM, nitrate, dust, elemental carbon, and fine mode aerosols. The two entries listed in the table per site for the first eight entries correspond to model results using two scenarios: (1) assuming a homogeneous composition with constant particle size, and (2) a core/shell scenario with constant particle number. All estimates reported in the table using the constant size assumption are in bold font. It is not appropriate to average efficiencies computed with both scenarios because the second scenario corresponds to changing size distributions that would also change the efficiency. The entries listed for Hopi Point toward the end of the table all correspond to estimates made at different relative humidities.

The average dry ammonium sulfate partial scattering efficiency for the first scenario (including those we corrected) in Table 5 is 2.7 ± 0.4 $m^2 g^{-1}$, similar to the results from the theoretical method, as would be expected because the theoretical basis is the same. Most of the studies included in this table occurred in the western or southwestern United States with the exception of the rural sites of Bondville IL and Uniontown PA. The sites in the Southwest are mostly rural with the exception of Phoenix AZ. No strong spatial variation is noticeable. Values

derived in Meadview AZ are somewhat higher than those derived in Hopi Point. Both locations are near the Grand Canyon, with Hopi Point on the southern rim of the canyon and Meadview on the western edge of the canyon. Observations from Meadview have been used to characterize subregional aerosol and visibility in the Southwest (Measurement of Haze and Visual Effects, MOHAVE, study) (Turpin et al., 1997; Lowenthal et al., 2000). It is possible that the aerosols measured in Meadview were influenced by long-range transport and therefore probably aged, resulting in somewhat higher efficiencies. The average normalized POM mass scattering efficiency is 3.0 ± 1.4 m^2 g^{-1}. High values were measured in Uniontown PA, Denver CO, and the Grand Canyon (Hopi Point), a mix of rural and urban locations. The ELSIE model treats POM mass as partly soluble (values for these studies range from 25 to 60% solubility, and that fraction is as soluble as ammonium sulfate), so a direct comparison of POM partial scattering efficiency from this method to the other methods is not appropriate. The average ammonium nitrate partial scattering efficiency is 3.8 ± 1.5 m^2 g^{-1}, with an outlier value in Denver CO. The average fine dust mass scattering efficiency is 2.8 ± 1.0 m^2 g^{-1}. Especially high dust efficiencies were reported for Uniontown PA.

5.3.5.   Apportionment Method

As part of the 1991 National Acid Precipitation Assessment Program (NAPAP) Report 24 on visibility, mass scattering efficiencies were computed from light scattering coefficients and mass data based on several studies around the United States. Scattering was apportioned to major species such as ammonium sulfate and organics (White, 1991). The intention of the apportionment scheme was to provide the range of efficiencies based on extreme assumptions. Low estimates of sulfate mass scattering efficiencies were derived assuming that sulfates, nitrates, and POM scatter twice as efficiently as the remaining aerosol. The high estimates for sulfates were derived assuming that sulfates alone scatter twice as efficiently as all other fine

aerosols. Low estimates of POM mass scattering efficiency were derived assuming that POM and nonsulfate species scatter half as efficiently as sulfates. High POM mass scattering efficiencies were derived assuming that POM is three times as efficient, and sulfate is twice as efficient, as the remaining aerosol in the fine mode. The range of these values is reported in Table 6, along with a summary of efficiencies for all the methods. Values for POM mass scattering efficiencies are normalized to an R_{oc} multiplier of 1.8. The values reported in Table 6 for the apportionment method are from studies that occurred around urban and rural U.S. locations. The average specific mass scattering efficiency for the fine mode was 2.6 ± 0.8 m^2 g^{-1}, with higher values in the rural and urban eastern United States (4.5 ± 0.8 and 3.5 ± 0.4 m^2 g^{-1}, respectively). The lowest values were computed for the rural and urban western United States, especially San Jose CA (1.83 m^2 g^{-1}). The apportionment method fine mode specific mass scattering efficiency was the lowest of all the methods; however, it was closest to the MLR method. Although these values are reported as dry, it is possible that the RH environment where the measurements were made has an effect on the values derived, perhaps through associated water on the filter or aerosol processing effects.

Table 6. Summary of mass scattering efficiencies reported in Tables 2 through 5 (Appendix 2). The "Apportionment" column refers to results from White (1991). The "IMPROVE" column lists values used in the current IMPROVE formulation. Entries correspond to the fine mode unless otherwise stated in the row header. Sulfate efficiencies correspond to dry ammonium sulfate, and POM efficiencies have been normalized to an R_{oc} value of 1.8.

Summary of Mass Scattering Efficiencies from All Methods[*]					
Species/ Mode	Theoretical $(m^2 \, g^{-1})$	MLR $(m^2 \, g^{-1})$	Partial $(m^2 \, g^{-1})$	Apportionment[**] $(m^2 \, g^{-1})$	IMPROVE
Fine	4.3 ± 0.7 (26)	3.1 ± 1.5 (17)		2.6 ± 0.8 (30)	
Coarse	1.6 ± 1.0 (21)	0.7 ± 0.6 (13)			0.6
Total	2.2 ± 1.0 (9)				
Sulfate	2.5 ± 1.1 (16)	3.2 ± 1.2 (24)	2.7 ± 0.4 (6)	3.0 ± 0.9 – 3.9 ± 0.9 (30)	3.0
Nitrate		4 ± 2 (16)	3.8 ± 1.5 (6)		3.0
POM	5.5 ± 1.6 (20)	2.3 ± 1.0 (23)	3.0 ± 1.4 (6)	1.5 ± 0.3 – 3.2 ± 0.9 (30)	4.0
Fine Dust	3.4 ± 0.5 (19)	3 ± 2 (19)	2.8 ± 1.0 (4)		
Coarse Dust	0.7 ± 0.2 (21)	0.40 ± 0.08 (2)			1.0
Total Dust	1.2 ± 0.3 (9)	0.7 ±0.2 (3)			
Fine Sea Salt	5.3 ± 0.8 (22)	4.0 ± 1.6 (3)			
Coarse Sea Salt	1.2 ± 0.3 (20)	1.6 ± 1.2 (3)			
Total Sea Salt	2.3 ± 0.9 (9)	2.2 ± 0 (1)			

[*] Number of observations in parentheses
[**] Apportionment values from Table H-1 in Appendix H in White (1991) and references therein.

Dry ammonium sulfate mass scattering efficiencies derived from the apportionment method ranged from 3.0 ± 0.9 to 3.9 ± 0.9 m² g⁻¹ for the low and high apportionment strategies, respectively. These estimates are similar to the values derived from the other methods but are still larger than what is derived from the theoretical method. The POM mass scattering efficiencies are lower than other estimates reported in Table 6, although the MLR method estimates fall within the range of low and high values from the apportionment schemes. It is interesting that derived sulfate mass scattering efficiencies are fairly insensitive to the low and high apportionment scheme, while the POM efficiencies are approximately double, based on the

apportionment scheme, probably due to uncertainties associated with organic carbon measurements. The spatial variability in both sulfate and POM mass scattering efficiencies are similar to the fine mode specific efficiency. The highest values are derived in the eastern United States (both rural and urban) and the lowest values in the urban West.

5.3.6.   Mass Absorption Efficiencies

Reported estimates of mass scattering and absorption efficiencies of LAC, as well as for other species, are reported in Table 7 (see Appendix 2). Efficiencies listed in this table have been derived using all the methods described above, which is noted in the first column of the table. Typically, mass absorption efficiencies are computed by the measurement method, by dividing a light absorption coefficient measured by transmittance (measured with an aethalometer or particle soot absorption photometer) by the mass of LAC from thermal analyses. Light absorption coefficients measured with a photoacoustic technique also are used to derive mass absorption efficiencies (e.g., Arnott et al., 2003). The theoretical method can be used if the size distribution of LAC is measured, or by applying a complex refractive index to number or volume size distributions in the Mie calculation. In Table 7 the values reported for a wavelength other than 550 nm have been corrected to 550 nm assuming a λ^{-1} relationship (Bohren and Huffman, 1983). It is well known that large uncertainties surround the values of mass absorption efficiencies by LAC, as is evidenced by the range of values reported in the table. Much of the uncertainty stems from the fact that estimates of LAC mass concentrations are method-dependent (as described in section 2.3), as are light absorption efficiencies, on the wavelength at which the measurements are performed, due to the spectral dependence of light absorption. Uncertainties also arise due to the wide range in optical properties (i.e., complex refractive index) of LAC applied in theoretical methods.

Reconstructed extinction equations typically treat LAC as externally mixed (see equations 4 and 5), as well as assume that it is the only component of the aerosol that is absorbing solar radiation in the visible wavelengths. This formulation is based on the assumption that LAC refers only to "soot" particles; however, there is substantial evidence that some of the carbonaceous aerosol, especially biomass smoke, being characterized as LAC by thermal methods is not soot and in fact is probably refractory organic carbon. Others have reported that light-absorbing carbon and a significant fraction of organic carbon from biomass smoke have similar volatility and combustion temperatures, causing the split between LAC and OC to be poorly defined (and method-dependent) and leading to an overestimation of LAC and an underestimation of OC for biomass smoke (e.g., Novakov and Corrigan, 1995; Gelencsér et al., 2000; Mayol-Bracero et al., 2002; Formenti et al., 2003; Guyon et al., 2003). A previous study by Malm et al. (1994a) in the northwestern United States showed that light absorption coefficients (as measured independently) correlated well with higher temperature fractions of OC as well as LAC. Analyses of single particle data from Yosemite National Park (Hand et al., 2005) showed that both the measured LAC and OC from TOR analysis corresponded to a type of nongraphitic refractory carbonaceous particle called tar balls, which are efficient at both scattering and absorbing light. Caution should be taken in always interpreting data from TOR analyses only as externally mixed OC and LAC particles, because TOR analyses are based on the refractory properties of carbon particles and not necessarily on their light-absorbing characteristics.

Theoretical calculations performed by Fuller et al. (1999) suggest a reasonable LAC mass absorption efficiency of 6.5 m^2 g^{-1}; however, the average value of the empirical values listed in Table 7 is 13 ± 6 m^2 g^{-1}. The IMPROVE equation applies a value of 10 m^2 g^{-1}. The scattering due

to LAC is not considered in the IMPROVE equation. Estimates reported in Table 7 suggest an average fine mode LAC mass scattering efficiency of 3.6 ± 1.3 m^2 g^{-1}. Clearly, more work is needed to understand the absorption characteristics of carbonaceous aerosols.

The summary of the survey results for all methods, including values currently used in the IMPROVE formulation, is reported in Table 6. The results suggest that POM mass scattering efficiencies are higher than what is applied in the IMPROVE reconstruction equation, even though the current IMPROVE formulation assumes an R_{oc} multiplier of 1.4. However, in general, the IMPROVE efficiencies fall within the range of the variability seen in the survey results. Fine soil in the IMPROVE formulation is assumed to correspond to the tail of the coarse dust size distribution; therefore the mass scattering efficiency associated with dust in a reconstructed PM$_{2.5}$ b_{ext} calculation corresponds to a coarse dust mass scattering efficiency. If the fine dust concentration actually corresponds to a size distribution that peaks in the fine mode, the corresponding mass scattering efficiency would actually be quite higher (~ 3 m^2 g^{-1}). Size distribution measurements at IMPROVE sites suggest this is not typically the case (e.g., Hand et al., 2002; Lee et al., 2004a, 2004b).

Lowenthal and Kumar (2004) suggest that the mass scattering efficiencies applied in the IMPROVE formulation should be reevaluated based on a comparison of measured and reconstructed scattering that implies that scattering is overestimated 66% of the time on average at 20 IMPROVE sites. Dry ammonium sulfate mass scattering efficiencies from the survey are somewhat lower and ammonium nitrate efficiencies are somewhat higher than the IMPROVE values, but the IMPROVE mass scattering efficiencies fall within the variability seen in the survey results. Coarse mass (CM) efficiency is assumed to be 0.6 m^2 g^{-1}, and the absorption efficiency for light-absorbing carbon (LAC) is 10 m^2 g^{-1}, both falling within the range of

variability reported in the survey. In general the values of dry mass scattering efficiency applied in the IMPROVE equation are reasonable, given the range of ground-based values reported in the literature since 1990.

5.4.   Estimates of Dry Mass Scattering Efficiencies from IMPROVE Data

The form of the IMPROVE equation for reconstructing particle extinction is

$$b_{ext} = (3.0)f(RH)\{[(NH_4)_2SO_4] + [NH_4NO_3]\} + (4.0)[POM] + 1.0[Soil] + (0.6)[CM] + (10.0)[LAC] \qquad (16)$$

where b_{ext} is the extinction coefficient (Mm^{-1}) and enclosed in the brackets is the aerosol species mass concentration ($\mu g\ m^{-3}$). The parenthetically enclosed numerals in front of POM, soil, and coarse mass (CM) are the optimal dry mass scattering efficiencies as reviewed by White (1990) and Malm et al. (1994b). A nominal mass scattering efficiency value of 3.0 $m^2\ g^{-1}$ is applied for dry ammonium sulfate and dry ammonium nitrate. The ratio of wet and dry scattering as a function of RH is the relative humidity scattering enhancement factor f(RH).

In the IMPROVE monitoring program, nephelometers collocated with particle mass samplers have been operated at 22 sites, in some cases for more than 10 years. Therefore the validity of the assumptions associated with equation 16 can be explored and possibly refined by comparing measured and reconstructed scattering. Four methods will be used as part of this strategy to estimate mass scattering efficiencies. We describe each method below, followed by a comparison of results from each method for one site (Acadia National Park) and later for all sites. In addition to the uncertainties described in previous sections, the results from these methods are subject to uncertainties in the b_{sp} values measured by Optec NGN nephelometers at a wavelength of 550 nm.

Method 1 uses a simple linear regression technique that assumes the relationship between scattering and species mass concentrations can be represented by equation 17. POM is assumed to be 1.8·OC, sea salt is estimated as 1.6·Cl⁻, and soil and CM are grouped together.

$b_{sp} = a_o + a_1 f(RH)[(NH_4)_2SO_4] + a_2 f(RH)[NH_4NO_3] + a_3[POM] + a_4[soil + CM] + a_5[sea\ salt]$ (17)

The regression coefficients are interpreted as the mass scattering efficiencies and the f(RH) curves are those associated with ammonium sulfate assuming a mass mean diameter of $D_g = 0.4$ µm and geometric standard deviation of 2, and an ammonium sulfate D/D_o curve estimated using the AIM "no solids" model (assumes equilibrium below the crystallization point). The f(RH) was calculated on one-hour intervals and averaged to 24 hours to be commensurate with the one-day sampling duration of the aerosol samples.

Method 2 assumes an aerosol model of a fine mode internal mixture of inorganic ammonium salts (sulfate and nitrate) and POM that is externally mixed from soil, coarse mass, and sea salt. The measured fine mode mixture scattering (b_{mix}) is approximated by

$b_{mix} = b_{open} - b_{CM} - b_{soil} - b_{SS}$ (18)

where b_{open} is measured with the PM_{10} open air nephelometer, and b_{CM}, b_{soil}, and b_{SS} (scattering due to sea salt) are estimated using coarse mass, fine soil, and sea salt mass (1.6·Cl$^-$), respectively. Sea salt scattering is estimated by multiplying the sea salt mass by a mass scattering efficiency of 1.37 m^2 g^{-1} and the f(RH) value defined above. If the assumptions are met that allow scattering associated with an internal and external mixture to be approximately equal, then

$\alpha_{mix} M_{mix} = [(NH_4)_2SO_4 + NH_4NO_3]\alpha_{inorg} + 1.27[POM]\alpha_{inorg}$ (19)

where the specific mass scattering efficiency α_{mix} of the mixed aerosol mass ($M_{mix} = (NH_4)_2SO_4 + NH_4NO_3 + POM$) is prorated to its chemical constituents based on their relative densities (1.27 = 1.78/1.4). The specific mass scattering efficiency of ammonium sulfate and ammonium nitrate is α_{inorg}, and α_{POM} corresponds to the mass scattering efficiency of POM. Implicit assumptions in equation 19 are that the refractive indices of all the species are similar, the mixing ratios of the

species are independent of the size distribution of the mixed aerosols, and the organic density is known. Therefore the estimated scattering of the mixture (b_{mix_est}) is written as

$$b_{mix\_est} = (3.0)f(RH)[(NH_4)_2SO_4 + NH_4NO_3] + 3.81 \, [POM] \qquad (20)$$

where 3 m^2 g^{-1} is the nominal mass scattering efficiency assigned to ammonium sulfate and ammonium nitrate, and 3.81 m^2 g^{-1} is the density-weighted mass scattering efficiency of POM (3.81 = 1.27·3). A regression is performed for b_{mix} and b_{mix_est} with a regression coefficient of a_1. The inorganic and organic specific efficiencies can therefore be written as $\alpha_{inorg} = a_1 \cdot 3.0$ and $\alpha_{org} = a_1 \cdot 3.81$, respectively.

Both methods 1 and 2 assume that the discrepancy between measured and estimated scattering can be accounted for by a single multiplicative constant, either for each species or for the mixed aerosol. These approaches do not account for the possibility that mass scattering efficiencies vary as a function of mass concentration (due to its functional dependence on particle size, as described in the section 5.1). Therefore method 3 is used to investigate how mass scattering efficiencies may vary with mass concentrations. A scattering correction factor (SCF) is defined as the ratio of measured scattering of the mixture (b_{mix}) from equation 18 to the estimated scattering for the mixture (b_{mix_est}).

$$SCF = \frac{b_{mix}}{b_{mix\_est}} = \frac{b_{open} - b_{CM} - b_{soil} - b_{SS}}{3.0 f(RH)[(NH_4)_2 SO_4 + NH_4 NO_3] + 3.81[POM]} \qquad (21)$$

The SCF should equal 1 for all mass values if the assumptions used in computing b_{mix} and b_{mix_est} are appropriate and if there is no functional dependence between mass scattering efficiency and M_{mix}. The functional relationship of SCF with the mixture mass (M_{mix}) was explored using equation 22

$$SCF = a_o + a_1[M_{mix}] \qquad (22)$$

where a_o and a_1 are the regression coefficients determined using a Theil regression analysis, and *SCF* is the scattering correction factor computed from equation 21. In this case, a linear relationship is hypothesized; however, any functional relationship could be assumed. A new estimate of b'_{mix} can be calculated using

$$b'_{mix\_est} = SCF'[3f(RH)[(NH_4)_2SO_4 + NH_4NO_3] + 3.81[POM]] \tag{23}$$

where *SCF'* is the estimated scaling factor derived from equation 22. New inorganic and organic specific mass scattering efficiencies are then calculated as $\alpha'_{inorg} = 3.0 \cdot SCF'$ and $\alpha'_{org} = 3.81 \cdot SCF'$.

Methods 1–3 rely on statistical regressions between measured scattering coefficients and observed aerosol mass concentrations. For most sites, the mass scattering efficiencies increase as ambient aerosol mass concentrations increase, presumably because of heterogeneous aerosol processes that are related to the aging of the aerosol. The increase in mass scattering efficiency is primarily due to the aerosol size distribution growing into a size range that is more efficient at scattering light as mass concentrations increase. Method 4 takes into account changes in mass scattering efficiency as a function of mass due to shifts in particle size through a simple physical model of a linear combination of bimodal fine mode aerosol mass size distributions. One distribution is associated with the small size mode, lower mass concentrations, and lower mass scattering efficiencies, while the second size distribution corresponds to a larger size mode often observed under higher mass concentrations and higher mass scattering efficiencies. As was discussed in section 3.7, bimodal size distributions in the fine mode reflect different atmospheric processes. However, these processes include not only changes in particle size, but also changes in composition as the particles age and undergo processing. The implications for the omission of

compositional changes in method 4 will be discussed later for results corresponding to the Phoenix site.

The review of aerosol size distribution data reported in the peer-reviewed literature in section 3.7 indicates that low aerosol mass concentrations are typically associated with mass size distributions with mass mean diameters (D_g) around 0.2 μm and with larger geometric standard deviations (σ_g), while higher mass loadings correspond to size distributions with D_g near 0.5 μm and smaller values of σ_g. Therefore the two mass size distributions were assumed to be lognormals with a D_g of 0.2 μm and σ_g of 2.2, and D_g of 0.5 μm and σ_g of 1.2 for the small and large size modes, respectively. These size distributions were applied for all fine mode species (e.g., Hering et al., 1997) and used to compute dry mass scattering efficiencies. Humidification factors were computed for each size distribution and species also. The ambient scattering coefficient for a linear combination of the bimodal size distribution is computed using

$$b_{sp,j} = \alpha_s M_j f_s(RH)\frac{(M_l - M_j)}{(M_l - M_s)} + \alpha_l M_j f_l(RH)\frac{(M_j - M_l)}{(M_l - M_s)} \tag{24}$$

where α_s, α_l, M_s, M_l, f_s(RH), and f_l(RH) are the dry mass scattering efficiencies, mass concentrations, and humidification factors associated with the small and large mass size distributions, respectively. The species mass concentration is given by M_j. The mass scattering efficiencies associated with the small and large mass size distributions for each species are presented in Table 8. Unless otherwise stated, $M_s = 0.0$ μg m^{-3} and $M_l = 20.0$ μg m^{-3} for all species; when the species mass concentrations exceeded 20 μg m^{-3}, the dry mass scattering efficiency was set equal to the large values shown in Table 8.

Table 8. Values used for the dry mass scattering efficiencies for the large and small mass size distributions for each species.

$(m^2 \ g^{-1})$	Ammonium Sulfate	Ammonium Nitrate	POM
α_s (small)	2.2	2.4	2.8
α_l (large)	4.8	5.1	6.1

To demonstrate the differences in these four methods and their effects on reconstructed scattering, data from Acadia National Park (ACAD) will be presented for each method. Reconstructed total scattering (b_{sp_tot}) was computed using

$$b_{sp\_tot} = (3.0)f(RH)[(NH_4)_2SO_4 + NH_4NO_3] + 3.81[POM] + (1.0)[Soil] + (0.3)[CM] + (1.0)[Sea\ salt] \qquad (25)$$

We applied ammonium sulfate and ammonium nitrate mass scattering efficiencies of 3.0 $m^2 \ g^{-1}$, a POM mass scattering efficiency of 3.81 $m^2 \ g^{-1}$ (assuming a POM multiplier of 1.8), and a CM specific efficiency of 0.3 $m^2 \ g^{-1}$ to account for coarse particle truncation issues in the nephelometer. A statistical summary of the mass concentrations, RH, average number of hours in each 24-hour period of useable nephelometer data, average $f(RH)$ using ambient RH and RH inside the nephelometer chamber, and new and presently used $f(RH)$ curves for ACAD are provided in Table 9. A summary of measured and reconstructed total ambient scattering, absorption, and contributions to scattering from each species is found in Table 10. Also listed in Table 10 is estimated scattering due to absorbed water on the ammoniated salts. Reconstructed total ambient scattering associated with dry mass is overestimated by about 15% on average, and scattering due to absorbed water is about half of the scattering due to inorganic mass, emphasizing the importance of selecting an appropriate $f(RH)$ curve (see Appendix 3 for similar tables for all sites). The final row of Table 10 shows the bias in the calculation of reconstructed b_{sp}.

Table 9. A statistical summary of mass concentrations (µg m^{-3}) at Acadia National Park. CM and FM refer to gravimetric coarse mass and fine (PM$_{2.5}$) mass, respectively. AS and AN refer to ammonium sulfate and ammonium nitrate, respectively. POM is particulate organic matter using an R_{oc} factor of 1.8. Mass units are (µg m^{-3}). RH refers to ambient relative humidity. The number of nephelelometer data points in a 24-hr average is given by $N(b_{sp})$. The values of the revised f(RH) curves for the ambient RH (f(RH)$_{amb,new}$) and the nephelometer chamber RH (f(RH)$_{chamb,new}$) are also listed. Similar values are reported for the current f(RH) curves (f(RH)$_{amb,old}$ and f(RH)$_{chamb,old}$).

Variable	Mean	Std Dev	Minimum	Maximum	Valid
CM (µg m^{-3})	3.77	3.89	-0.45	76.19	1093
FM (µg m^{-3})	6.15	5.18	0.46	45.58	1120
AS (µg m^{-3})	2.96	3.12	0.18	28.37	1138
AN (µg m^{-3})	0.36	0.39	0.01	3.30	1125
POM (µg m^{-3})	1.87	1.72	0.05	28.43	1132
LAC (µg m^{-3})	0.24	0.18	-0.01	1.33	1132
Soil (µg m^{-3})	0.24	0.27	0.00	4.34	1139
Sea Salt (µg m^{-3})	0.08	0.37	0.00	5.44	1158
RH (%)	68.70	12.31	30.41	89.78	1052
b_{sp} (Mm^{-1})	21.79	25.46	1.96	240.92	406
$N(b_{sp})$	16.29	8.21	1.00	24.00	1158
f(RH)$_{chamb,new}$	2.28	0.51	1.33	4.26	1038
f(RH)$_{chamb,old}$	2.08	0.54	1.01	3.65	1038
f(RH)$_{chamb,small}$	2.29	0.56	1.07	4.35	1038
f(RH)$_{chamb,large}$	1.94	0.38	1.06	3.22	1038
f(RH)$_{chamb,NaCl}$	2.89	0.69	1.00	4.78	1038

Table 10. A summary of b_{sp} (Mm^{-1}) for Acadia National Park. Values correspond to measured total ambient scattering (b_{sp}), reconstructed total ambient scattering (b_{sp_recon}), measured scattering associated with inorganics and organics (b_{mix}), estimated scattering associated with inorganics and organics (b_{mix_est}), scattering due to ammonium sulfate ($b_{sp}(AS)$), ammonium nitrate ($b_{sp}(AN)$), particulate organic material ($b_{sp}(POM)$), soil and coarse mass ($b_{sp}(soil+CM)$), sea salt ($b_{sp}(SS)$), and water ($b_{sp}(H_2O)$). Light absorption (b_{ap}) was computed assuming a mass absorption efficiency of 10 m^2 g^{-1}. New f(RH) curves were used to estimate wet scattering. POM was computed assuming an R_{oc} factor of 1.8 and mass scattering efficiency of 3.8 m^2 g^{-1}.

Variable	Mean	Std Dev	Minimum	Maximum	Valid
b_{sp}	22.22	26.06	2.38	240.92	377
b_{sp_recon}	25.16	23.99	3.78	219.35	377
b_{mix}	20.69	25.75	0.82	240.16	377
b_{mix_est}	23.64	23.56	3.34	218.59	377
$b_{sp}(AS)$	14.14	18.25	1.28	184.85	377
$b_{sp}(AN)$	2.45	3.15	0.18	27.76	377
$b_{sp}(POM)$	7.05	5.94	0.83	67.24	377
$b_{sp}(Soil)$	0.28	0.22	0.01	2.27	377
$b_{sp}(CM)$	2.24	3.00	-0.21	45.71	377
$b_{sp}(SS)$	0.13	0.80	0.00	12.27	377
$b_{sp}(soil+CM)$	2.52	3.06	-0.07	46.20	377
b_{ap}	2.44	1.79	0.42	13.25	377
$b_{sp}(H_2O)$	8.48	11.26	0.75	112.63	377
$\dfrac{(b_{mix} - b_{mix\_est})}{b_{mix}}$	-0.14				

The fractional contribution of each species to total scattering using equation 25 is presented in Table 11. The results from method 1 are reported in Table 12. A comparison of measured total ambient scattering and reconstructed total scattering using equation 25 and method 1 is shown in Figure 7 (similar tables corresponding to method 1 for all sites can be found in Appendix 3 and figures can be found in Appendix 4). Notice that reconstructed scattering from equation 25 is underestimated for low values of b_{sp} and overestimated at high values of b_{sp}, suggesting that mass scattering efficiencies vary with mass concentration. Reconstructed b_{sp} derived from method 1 removes the biases observed at low and high b_{sp}, but at the expense of having what appears to be unrealistic mass scattering efficiencies. The soil + CM specific scattering efficiency is negative, which is unphysical, and the sea salt efficiency is 1.23 m^2 g^{-1} (see Table 12), similar to values reported by Quinn et al. (2001, 2002b, 2004) for higher RH values. The average ammonium sulfate and POM mass scattering efficiencies of 3.29 m^2 g^{-1}

and 3.43 m^2 g^{-1}, respectively, are physically reasonable. However, sulfate mass scattering

efficiencies may be overestimated and POM mass scattering efficiencies may be underestimated

due to the relative uncertainties in each of those measurements.

Table 11. Fractional contribution to total ambient scattering at Acadia National Park using equation 25. AS corresponds to ammonium sulfate and AN corresponds to ammonium nitrate. Particulate organic matter (POM) fraction was computed assuming an R_{oc} factor of 1.8. The coarse mode fraction is given by CM.

Species	Fraction of b_{sp}
AS	0.64
AN	0.11
POM	0.32
Soil	0.01
CM	0.10
Sea salt	0.01

Table 12. The results from method 1 for Acadia National Park (see equation 17). The regression coefficients (a_i) are listed, along with the standard error. Derived mass scattering efficiencies are also listed for ammonium sulfate (AS), ammonium nitrate (AN), particulate organic matter (POM = 1.8·OC), coarse mass combined with soil (soil+CM). and sea salt. The number of valid cases was 267 and there were 370 missing data points. The r^2 coefficient was 0.95.

Acadia National Park			
Variable	Coefficient (a_i)	Standard Error	Derived Mass Scattering Efficiency (m^2 g^{-1})
AS	1.10	0.03	3.29
AN	0.62	0.13	1.87
POM	0.90	0.07	3.43
Soil+CM	-0.23	0.13	-0.14
Sea salt	1.23	0.50	1.68

Figure 7. Method 1 measured total ambient scattering and reconstructed total scattering using equation 25 for Acadia National Park.

ACAD
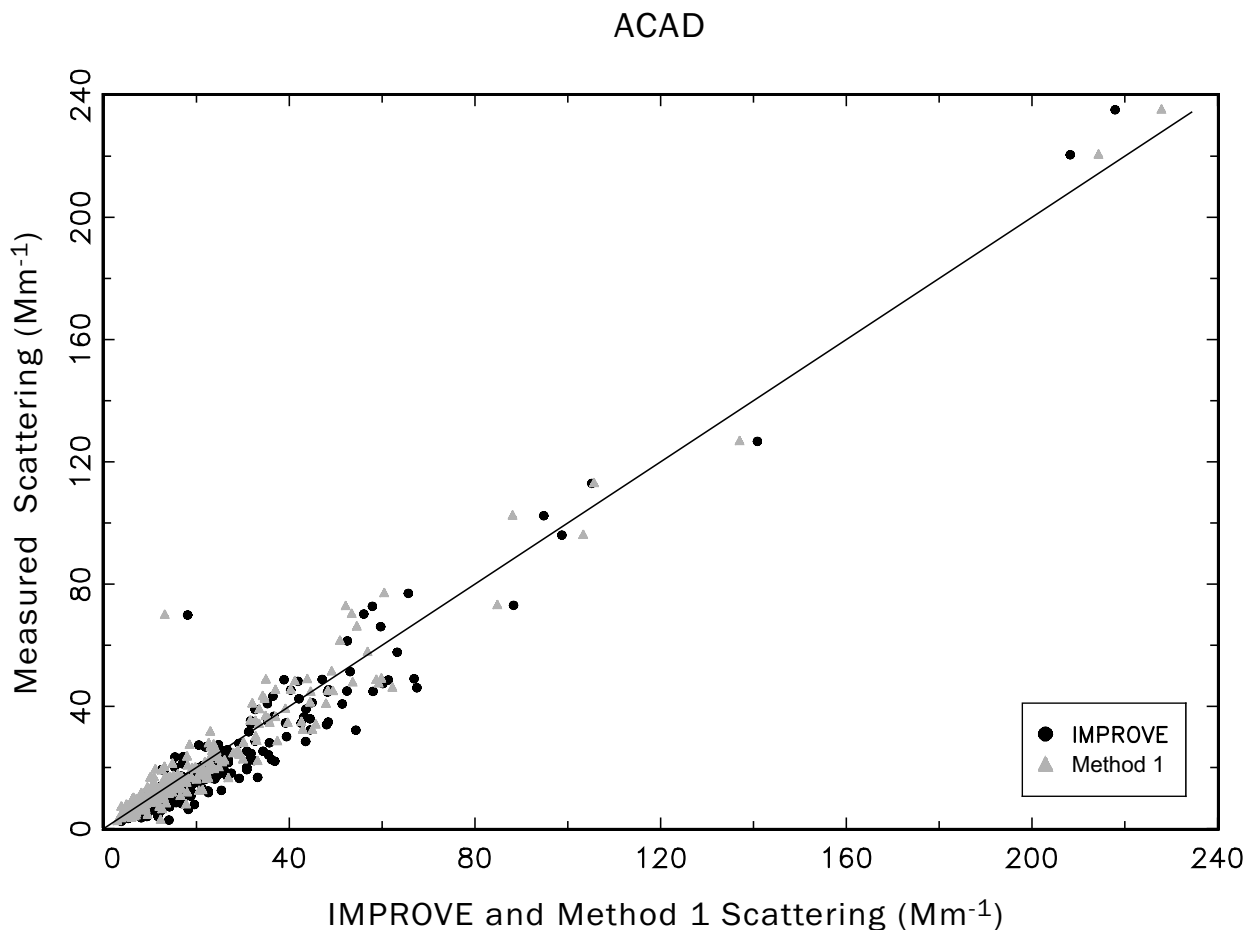
Estimates of specific scattering efficiencies for ammoniated salts (sulfates and nitrates) and POM mass scattering efficiency derived from method 2 are reported in the last two rows of Table 13. The derived sulfate and nitrate specific efficiency was 2.88 m^2 g^{-1} and the POM mass scattering efficiency was 3.65 m^2 g^{-1}. Comparisons of measured mixed b_{mix} to reconstructed mixed $b_{mix,est}$ using method 2 and equation 20 are shown in Figure 8 (similar tables corresponding to all sites for method 2 are found in Appendix 3 and figures are found in Appendix 4). The single multiplication factor derived from the regression between b_{mix} and b_{mix_est} that was used to correct the inorganic and organic mass scattering efficiencies does not

remove the biases observed at low and high scattering values. It only serves to make the average

method 2 reconstructed scattering equal that which is measured.

Figure 8. Method 2 reconstructed mixed scattering ($b_{mix,est}$, Mm^{-1}) compared to measured mixed scattering (b_{mix}, Mm^{-1}) using equation 20 (fine mode contributions) for Acadia National Park.
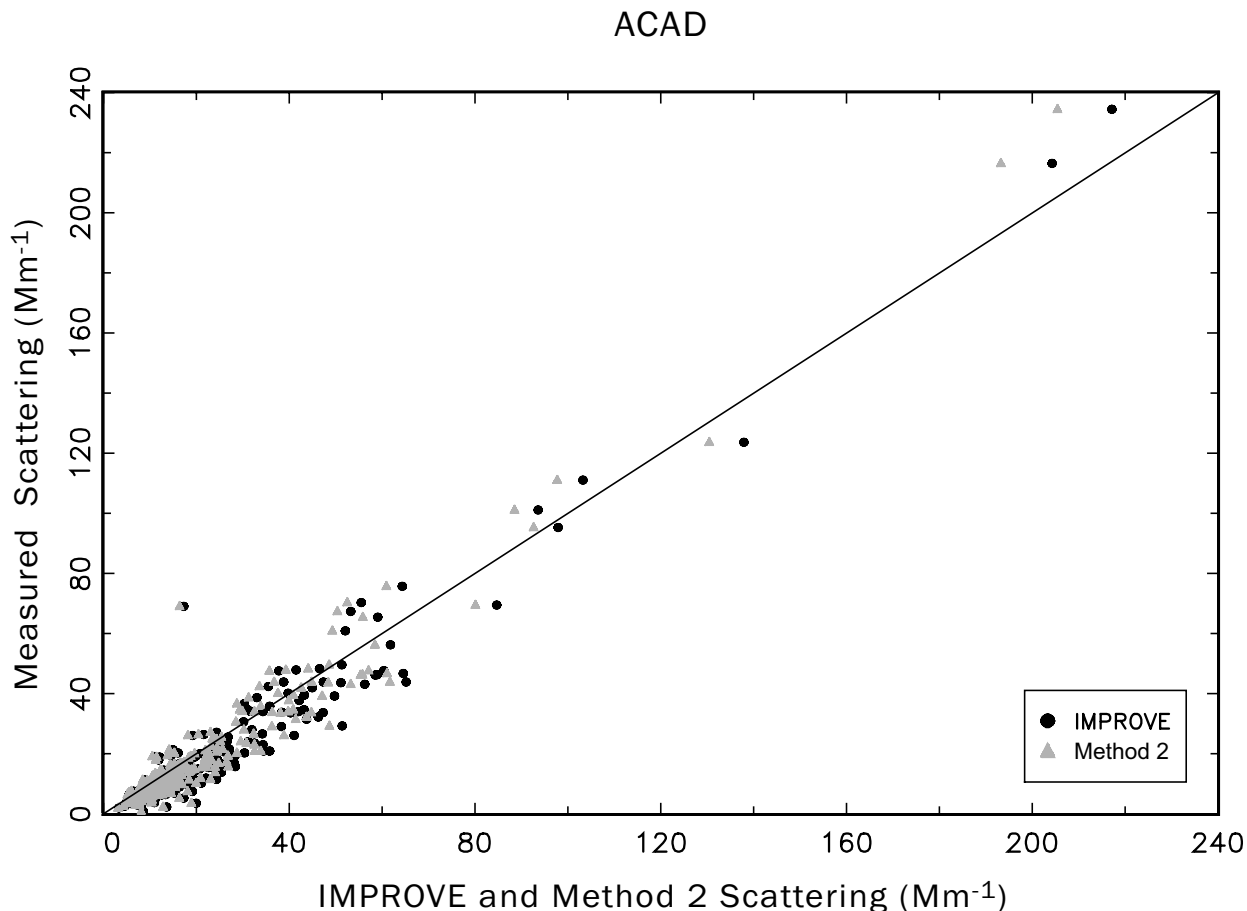
Table 13. Results for method 2 for estimating specific mass scattering efficiencies for inorganics (α_{inorg}) and organics (α_{org}) for Acadia National Park. See text for full description.

Results for Method 2 Regression (Acadia National Park)	
$a1$ coefficient	0.96
Standard error in $a1$	0.01
α_{inorg} (m^2 g^{-1})	2.88
α_{org} (m^2 g^{-1})	3.65

Statistical summaries of method 3 for Acadia National Park are reported in Tables 14–16.

The intercept and slope from the Thiel regression of *SCF* versus mass (M_{mix}) are presented in

Table 14. A slope of 0 corresponds to a constant mass scattering efficiency over the entire mass range, while the intercept is proportional to the over- or underestimation of the assumed mass scattering efficiencies for sulfates and POM (3 and 3.81 m^2 g^{-1}, respectively). An intercept of 1 and slope of 0 would imply that the assumed values provided good agreement between measured and reconstructed mixed (inorganic and POM) scattering. The comparison of fine mode inorganic and organic mass concentrations and *SCF* is shown in Figure 9 (similar tables for all sites corresponding to method 3 can be found in Appendix 3 and similar figures can be found in Appendix 4). The Thiel regression line is also shown, demonstrating a fairly flat slope as reported in Table 14. Mass scattering efficiencies for ammoniated salts and POM that are associated with the 15% upper and lower mass concentrations are reported in Table 15. Finally, the comparison of reconstructed and estimated mixed scattering using efficiencies derived from method 3 is shown in Figure 10. The summary of derived efficiencies from method 3 and the *SCF* factor are reported in Table 16. Accounting for the dependence of mass scattering efficiency on mass with method 3 removes these biases observed at low and high scattering by increasing the value of the efficiencies for low mass concentrations, and decreasing efficiencies that correspond to high mass concentrations (see Figure 10). As shown in Table 16, the average inorganic specific mass scattering efficiency using method 3 at Acadia National Park is 2.51 m^2 g^{-1} (ranging from 2.36 to 3.45 m^2 g^{-1}). The mean POM mass scattering efficiency was 3.18 m^2 g^{-1} (ranging from 3.00 to 4.39 m^2 g^{-1}).

Table 14. Results of the method 3 Thiel regression of *SCF* versus mass (M_{mix} = *inorganics* + *organics*) for Acadia National Park.

Method 3 Thiel Regression results (Acadia National Park)	
Intercept	0.78
Slope	0.011
Significance	0.04

Figure 9. The comparison of fine mode mixed inorganic and organic mass concentrations (M_{mix}, µg m^{-3}) and the *SCF* for Acadia National Park. The Thiel regression line is shown.
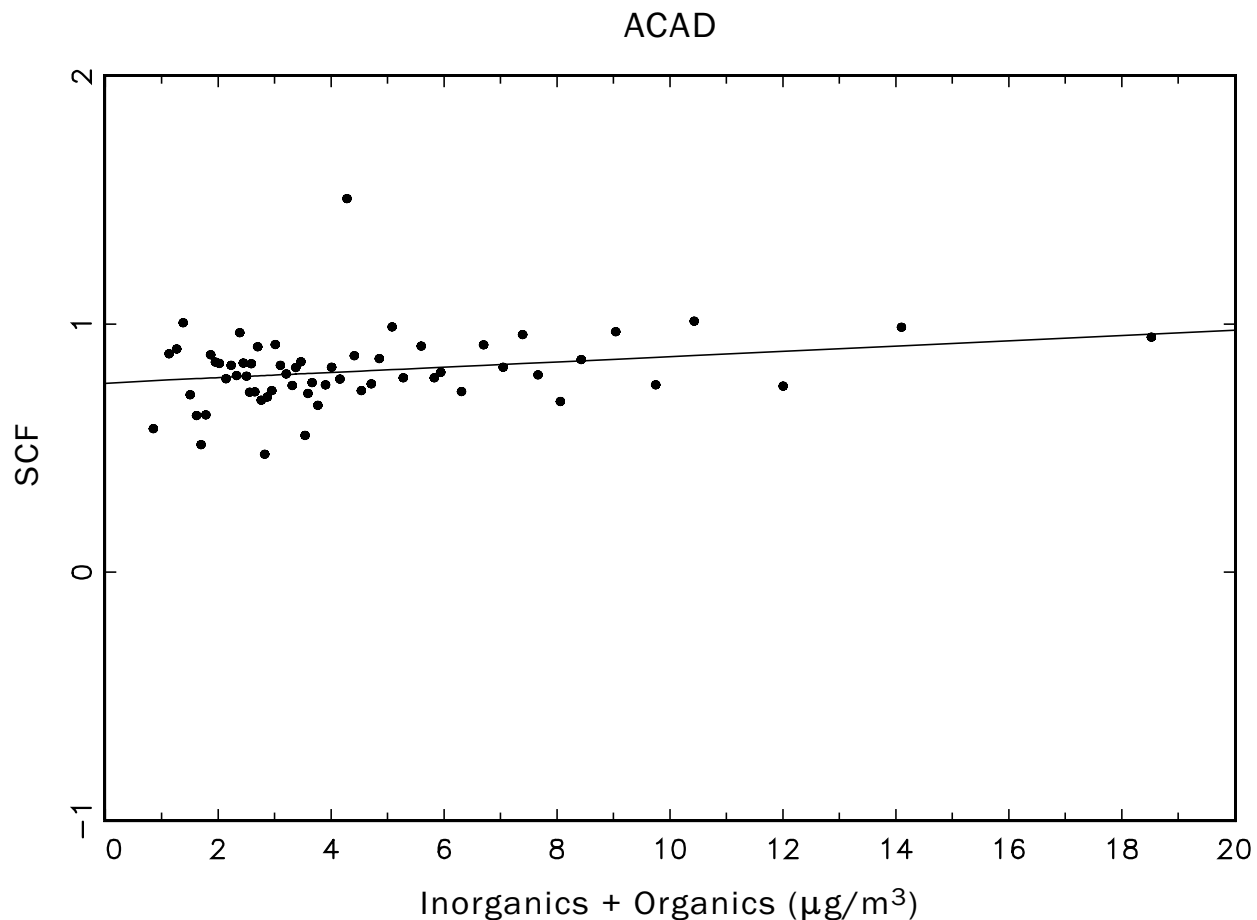
ACAD

Table 15. Method 3 estimates of the overall mean and upper and lower specific scattering efficiencies associated with the 15% upper and lower mass concentrations of mixed inorganic and organic mass for Acadia National Park.

Acadia National Park			
Specific Scattering Efficiency (m^2 g^{-1})	Lower	Mean	Upper
Inorganics (α_{inorg})	2.39	2.51	2.77
Organics (α_{org})	3.04	3.18	3.51

Figure 10. Comparisons of method 3 reconstructed mixed scattering ($b_{mix,est}$, Mm^{-1}) to measured mixed scattering (b_{mix}, Mm^{-1}) for Acadia National Park.
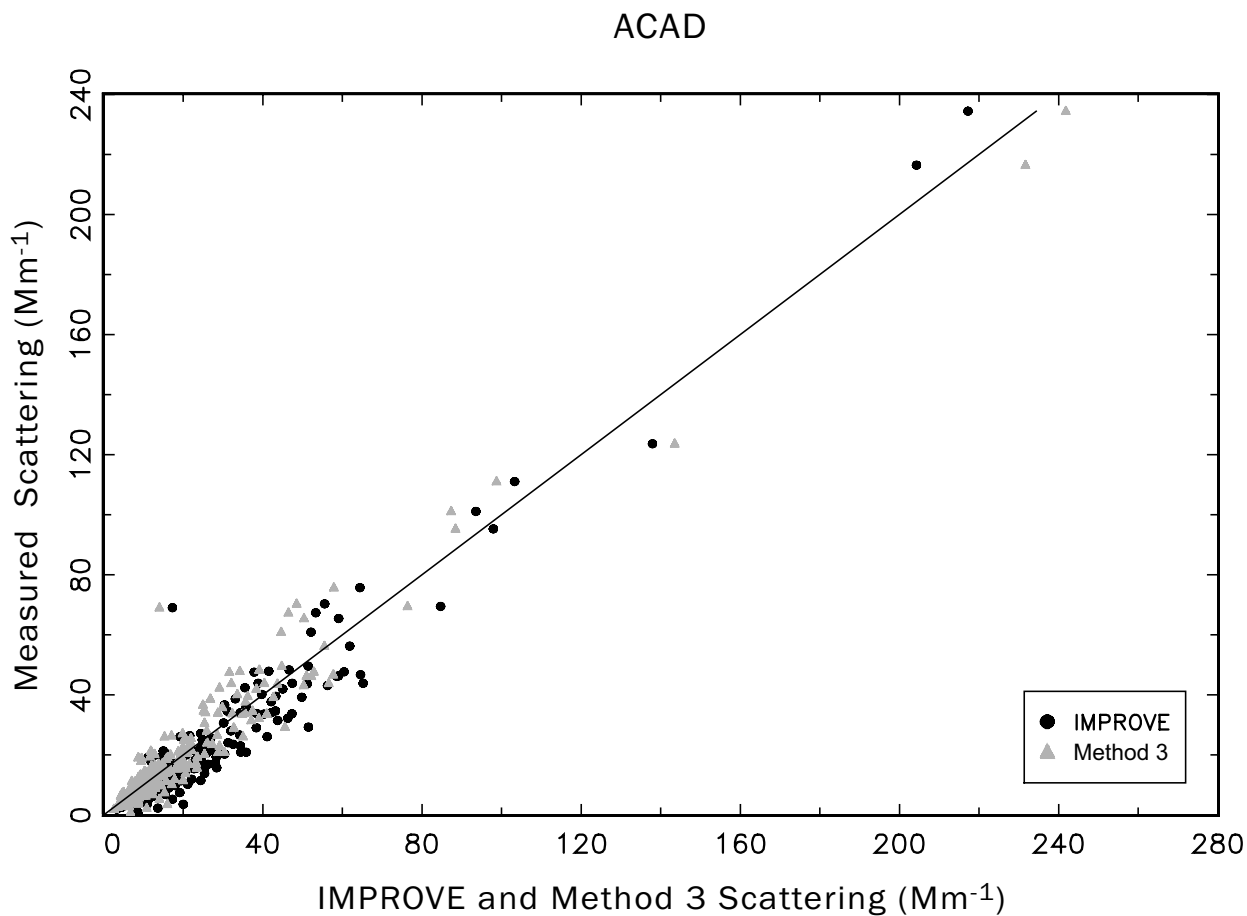
ACAD

Table 16. Summary of the method 3 *SCF* and specific mass scattering efficiencies for inorganics (α_{inorg}) and organics (α_{org}) for Acadia National Park.

Acadia National Park					
Variable	**Mean**	**Std Dev**	**Minimum**	**Maximum**	**Valid data**
SCF	0.84	0.28	0.09	3.06	377
α_{inorg} $(m^2\,g^{-1})$	2.51	0.14	2.36	3.45	1119
α_{org} $(m^2\,g^{-1})$	3.18	0.18	3.00	4.39	1119

From the discussion of these methods for data from Acadia National Park, it is clear that incorporating the dependence of mass scattering efficiencies on mass concentrations removed the biases observed between measured and reconstructed extinction, and improved the comparison of reconstructed and measured scattering. For most sites, a linear relationship between mass and

91

SCF appears to be a reasonable assumption, except at Great Smoky National Park (GRSM) where there seems to be a distinct nonlinearity. At GRSM the *SCF* is about 0.5 at lower mass concentrations ($< 5.0 \ \mu g \ m^{-3}$) and rapidly approaches one for higher mass concentrations.

The mass scattering efficiencies computed with method 4, based on a physical model, are quite similar to those derived using method 3, a statistical fitting approach. The method 3 specific mass scattering efficiencies associated with low mass concentrations are 2.39 $m^2 \ g^{-1}$and 3.04 $m^2 \ g^{-1}$ for inorganics and organics, respectively. Mass scattering efficiencies derived using method 4 are 2.28, 2.21, and 2.89 $m^2 \ g^{-1}$ for low concentrations of ammonium sulfate, ammonium nitrate, and POM, respectively (see Table 17). The difference between the two methods is on the order of 5%. The differences in sulfate mass scattering efficiencies corresponding to high mass concentrations between method 3 and method 4 were larger, with a difference of 10%. POM mass scattering efficiencies for high mass concentrations POM were very similar for both methods. A comparison of measured b_{sp} and reconstructed b_{sp} using method 4 is shown in Figure 11. The good agreement between the two estimates is demonstrated through an OLS regression forced through a zero intercept with a slope of 1.01 ± 0.013 and an $R^2 = 0.91$.

Table 17. Method 4 estimates of the mean, and the upper and lower mass scattering efficiencies ($m^2 \ g^{-1}$) associated with the 15% upper and lower mass concentrations for Acadia National Park.

Acadia National Park			
Mass Scattering Efficiency ($m^2 \ g^{-1}$)	Lower	Mean	Upper
Ammonium Sulfate	2.28	2.58	3.29
Ammonium Nitrate	2.21	2.25	2.34
POM	2.89	3.10	3.56

Figure 11. Method 4 estimates of reconstructed scattering compared to measured scattering (b_{sp}, *Mm^{-1}*) for Acadia National Park.

ACAD
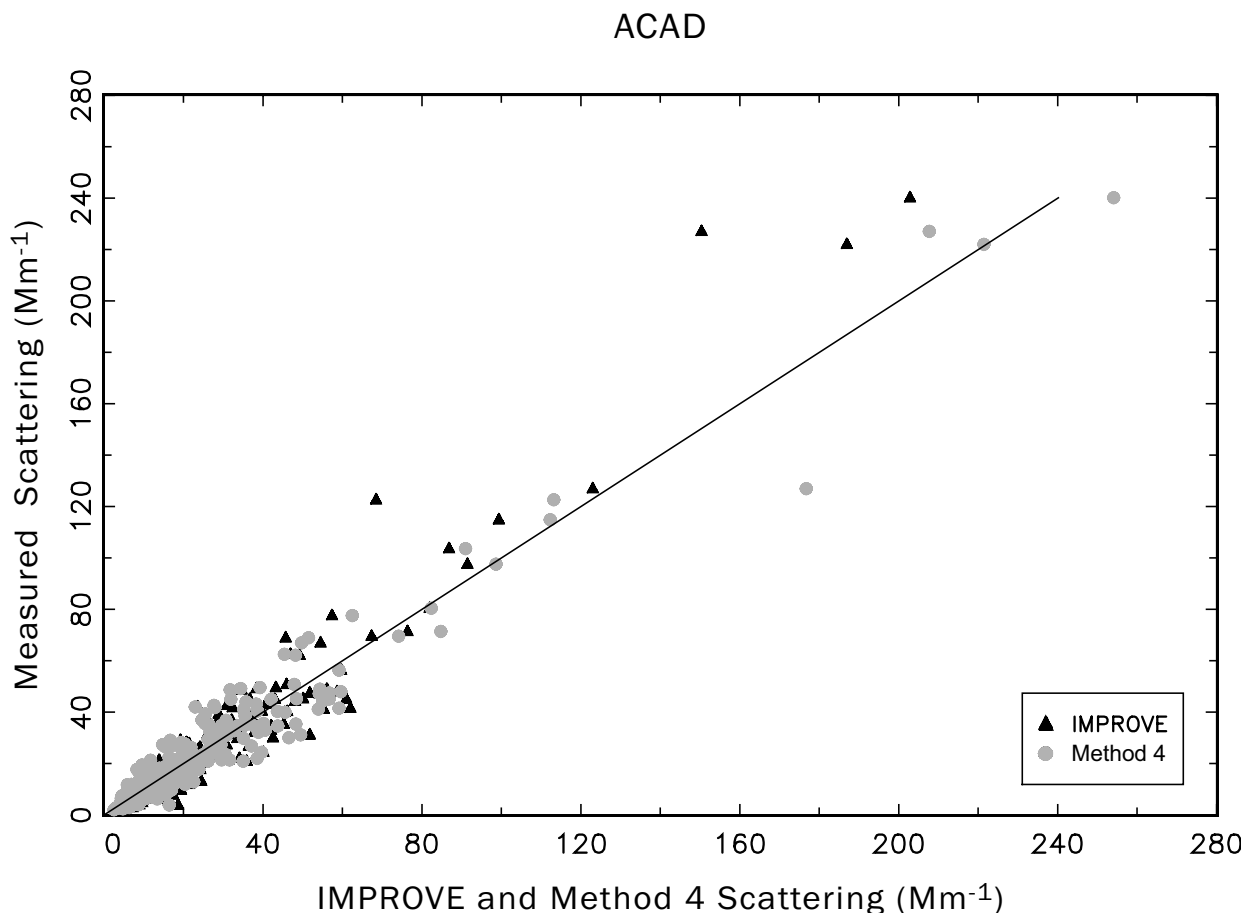
We now summarize and discuss these methods for all of the sites where the analyses were performed. The mass scattering efficiencies derived from method 1 are summarized in Table 18, along with the standard error associated with each estimate. For ammonium sulfate the regression coefficients are all statistically significant at 5%, except for Snoqualamie WA (SNPA), which is near the Cascade mountain range in the northwestern United States. The values are summarized for all sites in Figure 12, where the size of the circle corresponds to the magnitude of the mass scattering efficiency. The site in the Columbia River Gorge WA (CORI) is influenced by air masses from Portland, is in a high RH environment, and has a dry ammonium sulfate mass scattering efficiency that is greater than 3.0 m^2 g^{-1}. However, typically

the highest ammonium sulfate mass scattering efficiencies are found in the eastern United States, as well as Big Bend National Park TX (BIBE) where they are typically greater than 3.0 m^2 g^{-1}. In the southwestern United States, the values are near 2.0 m^2 g^{-1} with the site in Sycamore Canyon AZ (SYCA) having the lowest value at 1.40 m^2 g^{-1}. The average dry ammonium sulfate mass scattering efficiency for the sites that are statistically significant at 5% is 2.65 m^2 g^{-1}. This value is similar to the average values reported in the literature review of the theoretical method.

Table 18. Summary of mass scattering efficiencies (m^2 g^{-1}) and standard errors for all sites using method 1. Mass scattering efficiencies are listed for ammonium sulfate (AS), ammonium nitrate (AN), particulate organic matter (POM = 1.8·OC), soil and coarse mass (soil + CM), and sea salt.

Site	AS	AS Std Err	AN	AN Std Err	POM	POM Std Err	CM + Soil	CM+Soil Std Err	Sea Salt	Sea Salt Std Err
ACAD	3.29	0.08	1.87	0.40	3.43	0.28	-0.14	0.08	1.68	0.68
BIBE	3.20	0.08	1.38	0.76	3.58	0.21	0.29	0.02	56.03	58.17
BOWA	3.01	0.47	6.14	0.36	3.45	1.37	-0.56	0.33	2.26	5.98
CORI	3.59	0.24	5.15	0.20	2.54	0.22	0.06	0.05	0.84	0.55
DOSO	3.47	0.27	3.90	1.38	4.51	1.06	-1.19	0.44	0.00	0.00
GICL	1.66	0.15	2.38	1.18	5.73	0.08	0.11	0.04	1.55	24.88
HANC	2.44	0.21	6.68	0.73	3.81	0.20	0.20	0.04	0.00	83.57
GRSM	3.64	0.08	4.58	0.69	3.04	0.37	-0.85	0.19	0.00	532.74
IKBA	1.76	0.26	2.13	0.54	3.22	0.27	0.55	0.02	0.00	16.76
JARB	1.48	0.51	3.34	0.39	5.11	0.24	0.25	0.05	21.75	15.26
LOPE	2.77	0.28	4.77	0.13	3.30	0.23	0.13	0.06	4.48	37.51
MACA	3.36	0.15	4.52	0.23	2.66	0.52	-0.19	0.26	0.00	601.18
MORA	3.23	0.53	4.99	2.90	3.97	0.43	-0.36	0.27	3.45	5.56
OKEF	4.12	0.30	0.77	2.36	3.50	0.84	-0.17	0.29	0.00	0.00
PHOE	1.85	0.18	2.68	0.15	2.56	0.09	0.31	0.02	1.01	3.02
SENY	2.35	0.17	4.23	0.19	4.41	0.56	0.06	0.39	161.48	254.89
SHEN	3.44	0.10	2.64	0.35	2.33	0.51	-0.59	0.25	0.00	4895.51
SNPA	0.40	0.79	7.23	1.06	4.51	0.48	0.24	0.17	0.00	386.12
SYCA	1.40	0.30	5.06	0.85	4.56	0.16	0.24	0.02	-0.94	12.05
THIS	1.44	0.48	2.86	1.05	5.41	0.25	-0.02	0.10	0.59	7.74
UPBU	3.62	0.09	4.86	0.34	1.44	0.43	0.27	0.10	0.00	537.76
VIIS	3.15	0.29	9.47	1.51	-3.46	0.85	0.88	0.05	2.06	0.21
Avg	2.65		3.91		3.67		-0.06		12.10	

Figure 12. Map of the mean ammonium sulfate mass scattering efficiencies (m^2 g^{-1}) for the United States derived using method 1. The size of the circle reflects the magnitude of the efficiency, which is printed next to the circle.

Method 1 Sulfate Mass Scattering Efficiency
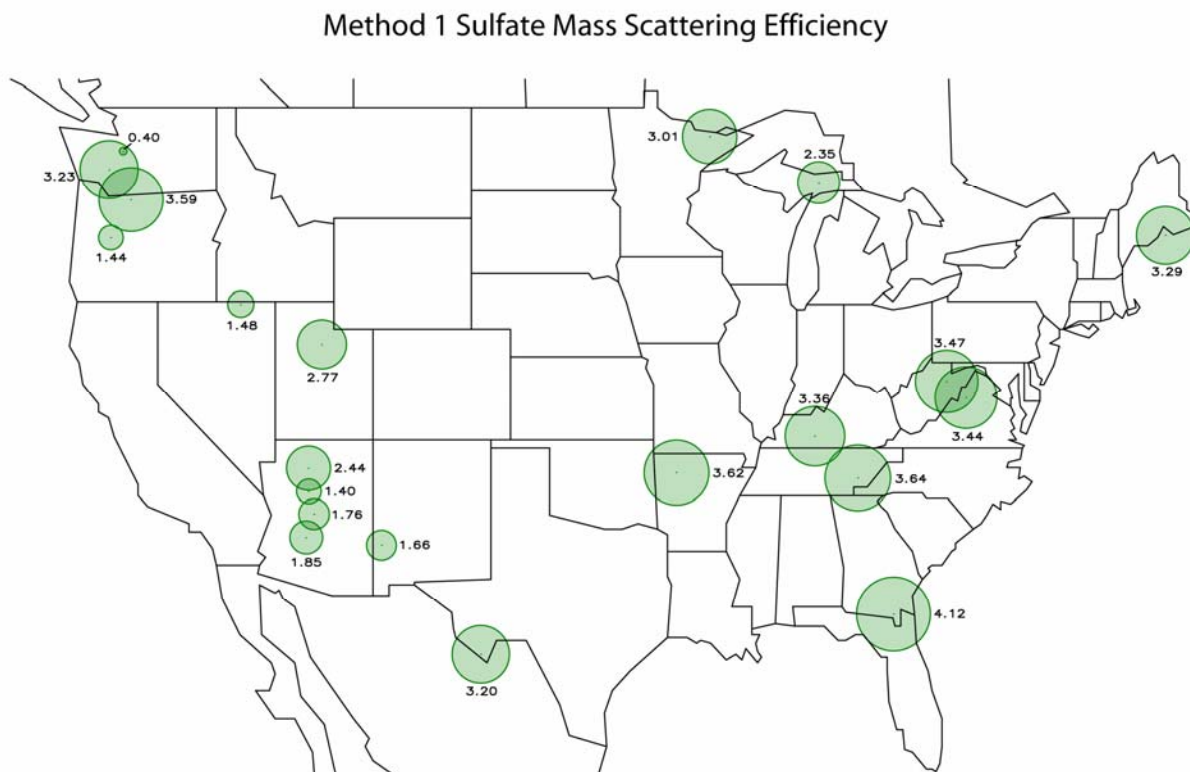
The derived mass scattering efficiencies for POM are statistically significant at 5% at all sites except at Dolly Sods WV (DOSO). The values are summarized in Figure 13. A negative value was derived at the Virgin Islands (VIIS) (not shown), which is unphysical. In the East, as with sulfates, the implied mass scattering efficiencies are near 3.0 m^2 g^{-1} or greater. In the West, the coefficients are higher and variable but all within ranges that would be considered physically reasonable. Those sites typically influenced by wild fires tend to have higher POM mass scattering efficiencies, consistent with recent analyses by Malm et al. (2005a) and Poirot and Husar (2004). The average POM mass scattering efficiency for statistically significant sites is 3.67 m^2 g^{-1} and is within range of the values reported in Table 6, although closest to the MLR

average value. The ratio of ammonium sulfate to POM mass scattering efficiencies on average is

1.38, which is similar to the ratio of POM to ammonium sulfate density of 1.21.

Figure 13. Map of the mean POM mass scattering efficiencies (m^2 g^{-1}) for the United States derived using method 1. The size of the circle reflects the magnitude of the efficiency, which is printed next to the circle.
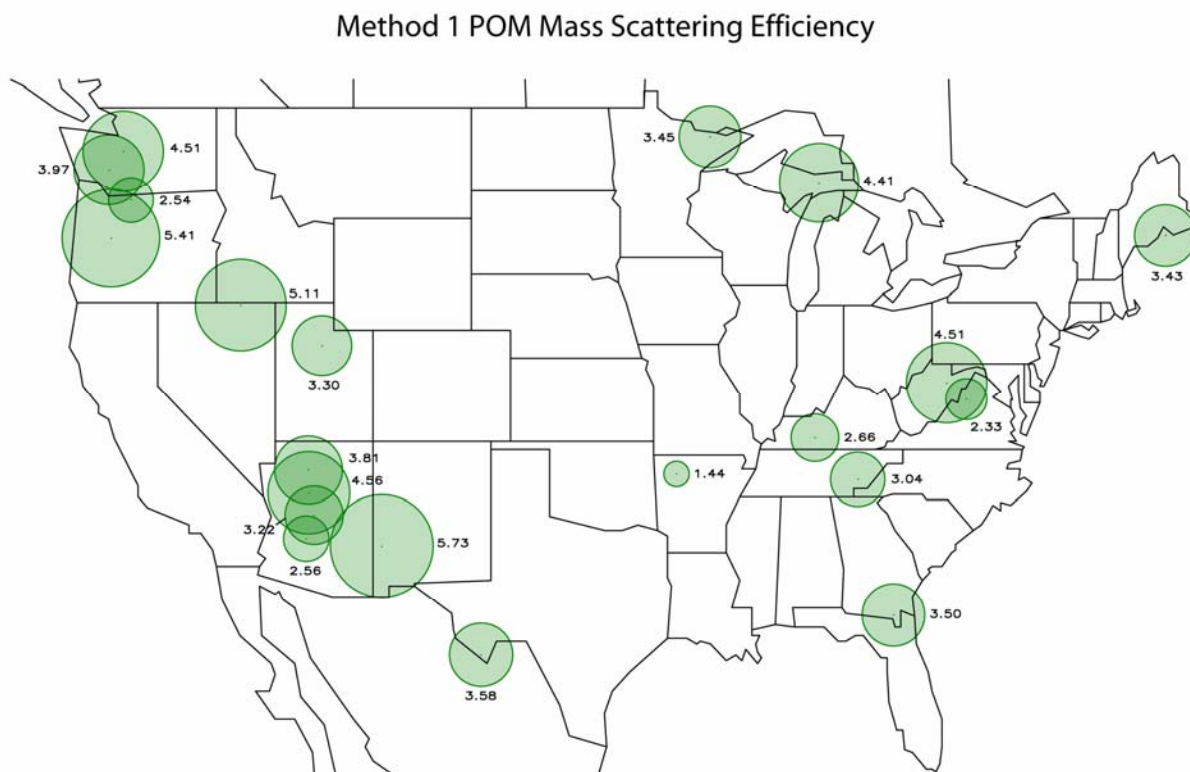
Many of the ammonium nitrate mass scattering efficiencies are higher than could be

reasonably expected, possibly because fine nitrate may be a surrogate for coarse particle nitrate

(see section 3.2). Coarse mass specific mass scattering efficiencies that are statistically

significant vary from a low of 0.06 m^2 g^{-1} at CORI and Seney MI (SENY) to a high of 0.88 m^2 g^{-1} at VIIS. Sea salt specific mass scattering efficiencies are only statistically significant at two

locations, ACAD and VIIS.

The specific mass scattering efficiencies for ammoniated salts (sulfate and nitrate) and

POM mass scattering efficiencies derived from method 2 are summarized for all of the sites in

Table 19. The values of α_{inorg} range from 2.02 to 5.41 m^2 g^{-1}, with an average of 2.87 m^2 g^{-1}. A

summary of the values is shown in Figure 14. The high value is in the Virgin Islands (not shown) where there is known to be large contributions to aerosol mass from sea salt and dust, so the inorganic salts could be influenced by those contributions. The low value occurred at Phoenix AZ (PHOE). The low and high values of efficiencies for POM also occurred at PHOE and VIIS, with 2.56 and 6.87 m^2 g^{-1}, respectively. These estimates are summarized in Figure 15. Throughout most of the United States, POM mass scattering efficiencies vary between about 3.5 and 4.0 m^2 g^{-1}, with the Arizona sites having the lowest values (Figure 15). POM mass scattering efficiencies are higher than those for inorganics; however, there is less spatial variability in POM mass scattering efficiencies compared to method 1 because of the internal mixing assumptions inherent in method 2. Because only one multiplicative factor is used to scale both the inorganics and the organics, the bias between measured and reconstructed scattering for low and high mass concentrations remains.

Table 19. Summary of specific mass scattering efficiencies (m^2 g^{-1}) **for inorganics** (α_{inorg}) **and organics** (α_{org}) **for all sites using method 2.**

Site	α_{inorg} (m^2 g^{-1})	α_{org} (m^2 g^{-1})
ACAD	2.87	3.65
BIBE	2.91	3.69
BOWA	3.72	4.72
CORI	2.97	3.78
DOSO	3.06	3.88
GICL	3.35	4.25
HANC	2.81	3.57
GRSM	3.13	3.97
IKBA	2.58	3.27
JARB	3.13	3.97
LOPE	3.21	4.08
MACA	3.11	3.95
MORA	2.85	3.62
OKEF	3.29	4.17
PHOE	2.02	2.56
SENY	2.98	3.79
SHEN	2.82	3.58
SNPA	2.99	3.80
SYCA	2.44	3.10
THIS	3.07	3.90
UPBU	3.14	3.99
VIIS	5.41	6.87
Avg	2.87	3.65

Figure 14. Map of inorganic specific mass scattering efficiencies (α_{inorg}, m² g⁻¹) for the United States using method 2. The size of the circle reflects the magnitude of the efficiency, which is printed next to the circle.

Method 2 Inorganic Mass Scattering Efficiency
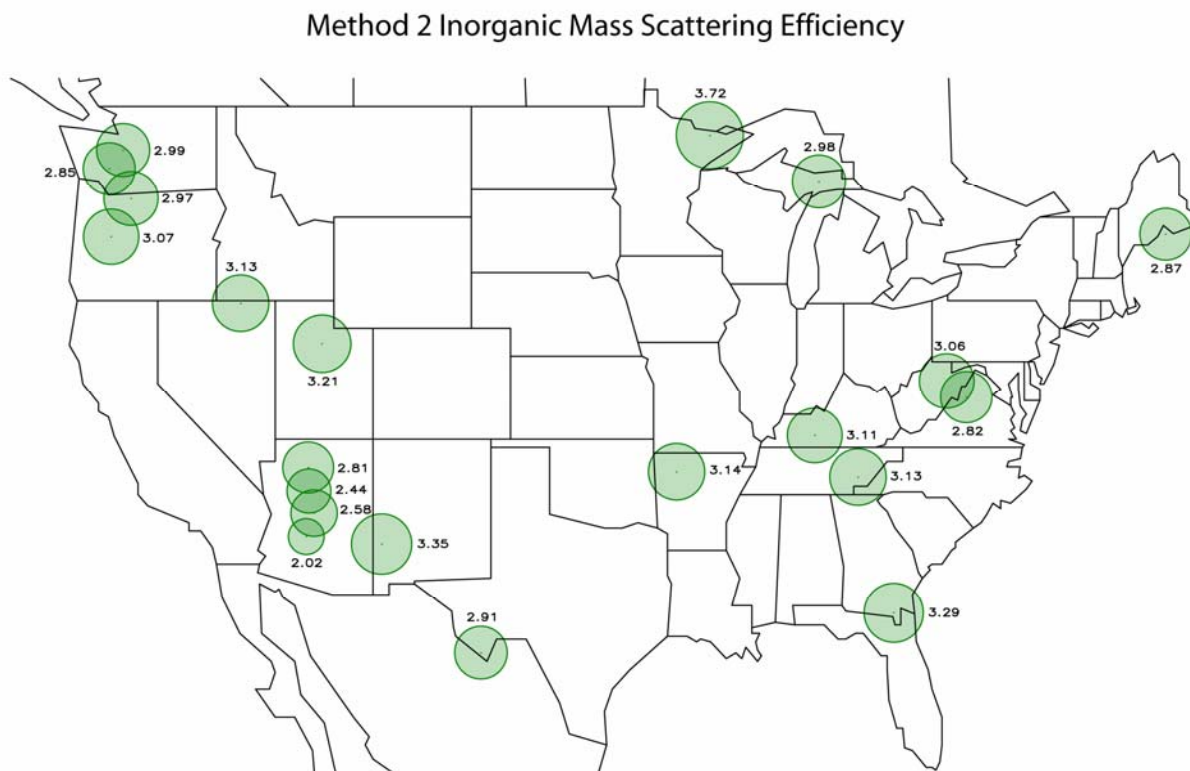
Figure 15. Map of organic (POM) mass scattering efficiencies (α_{org}, m^2 g^{-1}) for the United States using method 2. The size of the circle reflects the magnitude of the efficiency, which is printed next to the circle.

Method 2 POM Mass Scattering Efficiency
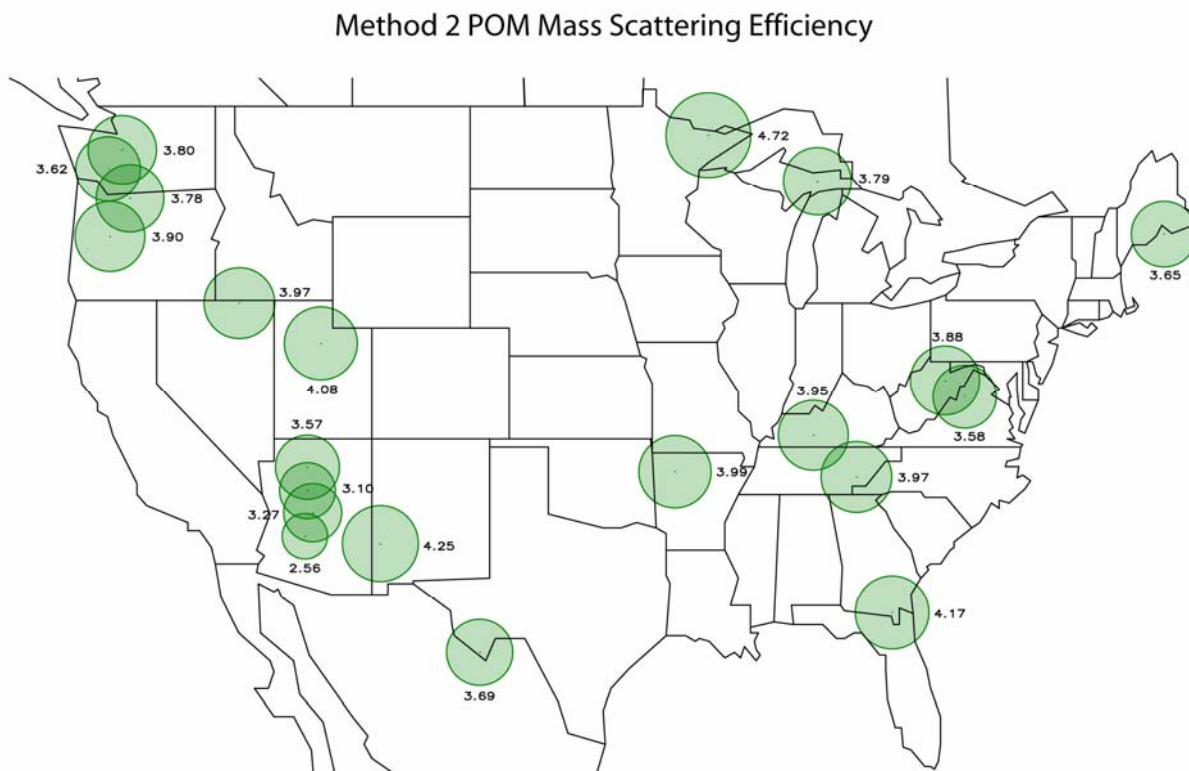
The results from method 3 using the Thiel regression of *SCF* and *M$_{mix}$* (intercept, slope, and t-values) from method 3 are listed in Table 20 for each site. As previously mentioned, a slope of 0 corresponds to a constant mass scattering efficiency over the entire mass range, while the intercept is proportional to the underestimation of the assumed mass scattering efficiencies for sulfates and POM (3 and 3.81 m^2 g^{-1}, respectively). An intercept of 1 and slope of 0 would imply that the assumed values provided good agreement between measured and reconstructed mixed (inorganic and POM) scattering. The average and one standard deviation intercept for all 22 sites is 0.76 ± 0.16, while the average slope is 0.02 ± 0.03.

Table 20. Summary of the results from method 3 using the Thiel regression of *SCF* and mass (M_{mix}) for each site. The fourth column corresponds to the percent change in specific mass scattering efficiency (either for inorganic or organics) from a doubling of the mixed inorganic and organic mass concentration (M_{mix}).

Site	Intercept	slope	t-value	% change
ACAD	0.78	0.01	0.04	2.62
BIBE	0.66	0.03	0.00	9.54
BOWA	1.01	0.00	0.96	-0.29
CORI	0.57	0.04	0.00	12.15
DOSO	0.78	0.01	0.10	2.75
GICL	0.65	0.05	0.00	13.73
HANC	0.95	-0.01	0.46	-2.52
GRSM	0.64	0.02	0.00	6.05
IKBA	0.47	0.10	0.00	28.96
JARB	0.92	0.01	0.72	3.00
LOPE	0.67	0.04	0.00	11.62
MACA	0.98	0.00	0.55	0.43
MORA	0.82	0.01	0.43	2.66
OKEF	0.65	0.04	0.00	10.55
PHOE	0.63	0.00	0.49	0.66
SENY	1.13	-0.01	0.16	-2.48
SHEN	0.72	0.01	0.00	3.94
SNPA	0.74	0.03	0.09	8.50
SYCA	0.72	0.01	0.37	2.54
THIS	0.69	0.05	0.02	12.05
UPBU	0.80	0.02	0.00	3.76
VIIS	2.52	-0.21	0.01	-20.22
Avg	0.76	0.02	0.21	6.20
Std Dev	0.16	0.03	0.29	7.21

The fourth column in Table 20 corresponds to the percent change in mass scattering efficiency (either for inorganic or organics) resulting from a doubling of the mixed inorganic and organic mass concentration (M_{mix}). The results in the final column are shown in graphical form in Figure 16. Notice that the percent change in mass scattering efficiency resulting from a doubling of mass concentration is lowest in the eastern United States, with only a few percent change along the Ohio River valley. Great Smoky Mountains National Park TN (GRSM) has a 6% change in mass scattering efficiency for a doubling of mass, while OKEF (Okefenokee GA) has an 11% change. Sites in the western United States exhibit the largest change in mass scattering efficiency as a function of mass. Sites in the Northwest and Great Basin region all have percent

changes between about 10 and 15%, while sites in Arizona vary from about a 1% change to as high as 29% at IKBA (Ikes Backbone AZ). The intercept data are shown in Figure 18. Sites along the Ohio River valley have intercepts between 0.9 and 1.0, implying 3.0 m^2 g^{-1} and 3.81 m^2 g^{-1} are reasonable choices for dry mass scattering efficiencies. In the western United States, the intercepts range between 0.5 and 0.7, with a low value of 0.47 at IKBA, implying a lower mass scattering efficiency would be more appropriate there. This result is consistent with what is observed at other sites in that region.

Figure 16. Map of percent change in specific mass scattering efficiency (for either α_{inorg} or α_{org}) due to a doubling of mixture mass (M_{mix}) using method 3. The size of the circle reflects the magnitude of the change, which is printed next to the circle.

Percent Change in Efficiency in Doubling of Mass
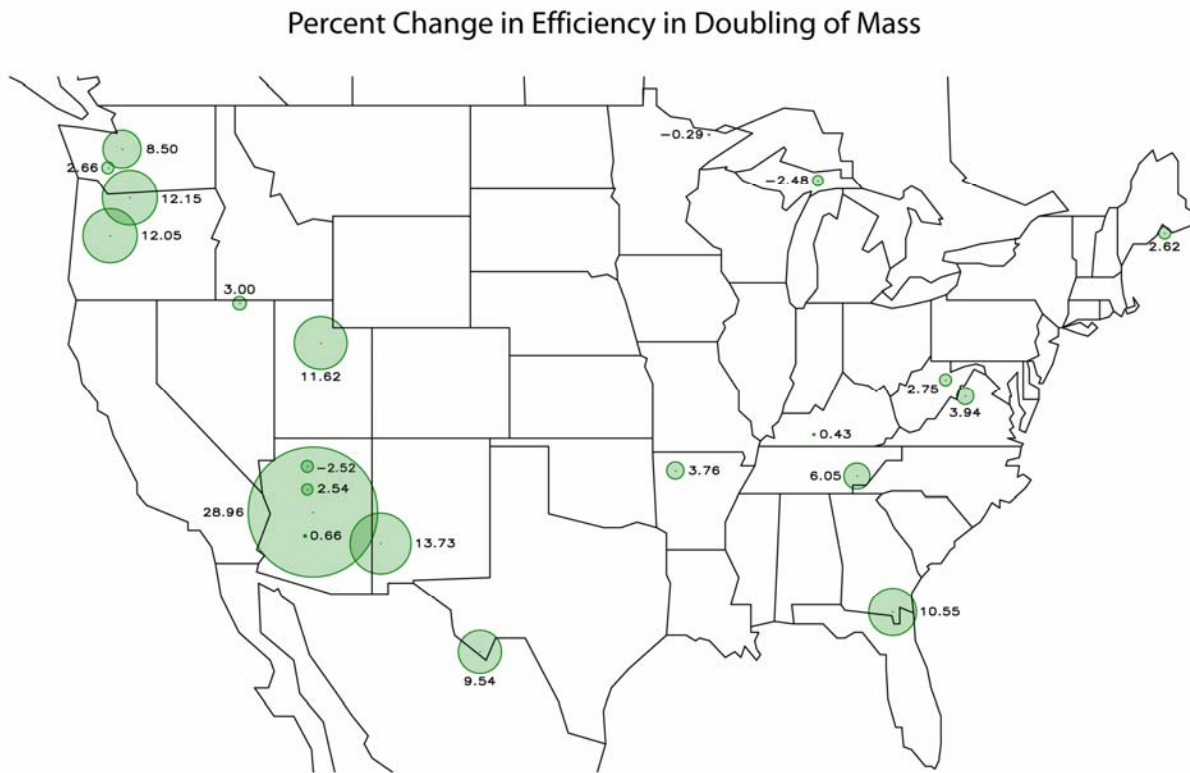
Figure 17. Map of the intercept from the Theil regression in method 3. The size of the circle reflects the magnitude of the intercept, which is printed next to the circle.

Method 3: Intercept
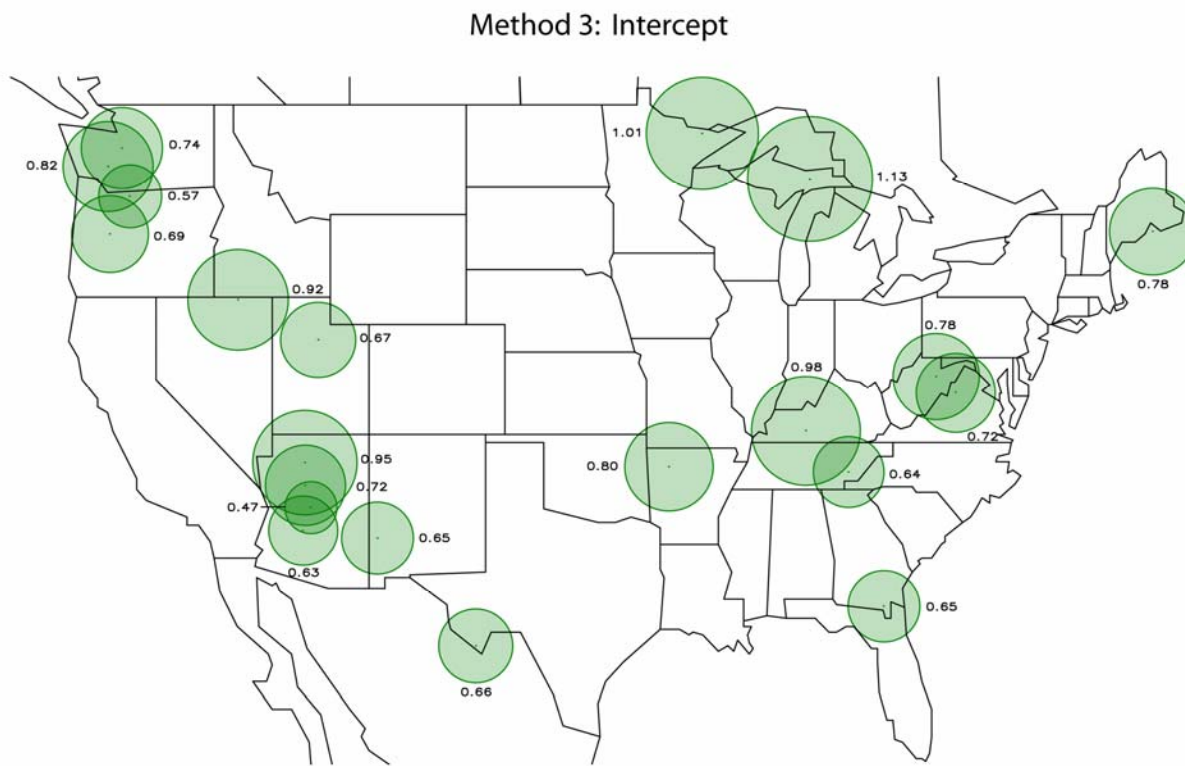
The mean, upper, and lower specific mass scattering efficiencies for the mixed ammonium salts and POM mass scattering efficiencies are reported in Table 21. The upper and lower mass scattering efficiencies are calculated by averaging the mass scattering efficiencies associated with the upper and lower 15% mixed mass concentrations (M_{mix}). The percent change between the upper and lower mass scattering efficiencies (either inorganics or organics) is reported in the last column. The highest average inorganic specific mass scattering efficiencies are found in the southeast United States, where they are near 3 m^2 g^{-1} or less (see Figure 18 for spatial distribution). The inorganic specific scattering efficiencies decrease towards the western United States. The lowest inorganic specific mass scattering efficiencies (near 2.0 m^2 g^{-1}) are found in Arizona. (IKBA, PHOE, and SYCA). The average inorganic specific mass scattering efficiency is 2.35 ± 0.34 m^2 g^{-1}.

Table 21. The mean, upper, and lower specific scattering efficiencies for inorganics (α_{inorg}) and organics (α_{org}) computed with method 3. The upper and lower estimates are calculated by averaging the specific scattering efficiencies associated with the upper and lower 15% mixed mass concentrations (M_{mix}). The percent change between the upper and lower mass scattering efficiencies (final column) corresponds to both (α_{inorg}) and (α_{org}).

Site	α_{inorg} (m² g⁻¹) Lower	α_{inorg} (m² g⁻¹) Mean	α_{inorg} (m² g⁻¹) Upper	α_{org} (m² g⁻¹) Lower	α_{org} (m² g⁻¹) Mean	α_{org} (m² g⁻¹) Upper	Percent Change α_{Inorg} & α_{Org}
ACAD	2.39	2.51	2.77	3.04	3.18	3.51	15.65
BIBE	2.13	2.48	3.06	2.71	3.15	3.89	43.47
BOWA	2.98	3.01	3.02	3.78	3.82	3.84	1.40
CORI	1.89	2.33	3.16	2.40	2.96	4.01	66.84
DOSO	2.46	2.71	3.17	3.12	3.44	4.02	29.02
GICL	2.10	2.51	3.60	2.67	3.19	4.57	71.51
HANC	2.68	2.77	2.83	3.40	3.52	3.59	5.75
GRSM	2.13	2.58	3.39	2.70	3.27	4.30	59.27
IKBA	1.75	2.25	2.90	2.23	2.85	3.68	65.39
JARB	2.78	2.84	2.97	3.53	3.61	3.77	6.75
LOPE	2.20	2.51	3.08	2.79	3.19	3.91	40.08
MACA	2.98	3.03	3.10	3.79	3.85	3.94	3.95
MORA	2.47	2.58	2.74	3.14	3.27	3.48	10.74
OKEF	2.41	3.00	3.92	3.06	3.81	4.97	62.53
PHOE	1.91	1.94	2.01	2.43	2.47	2.55	5.15
SENY	2.76	3.14	3.32	3.50	3.99	4.21	20.34
SHEN	2.27	2.55	3.04	2.88	3.23	3.86	33.94
SNPA	2.29	2.54	2.97	2.90	3.22	3.77	29.89
SYCA	2.20	2.25	2.36	2.79	2.86	2.99	7.33
THIS	2.11	2.44	3.11	2.68	3.10	3.95	47.15
UPBU	2.54	2.83	3.29	3.22	3.59	4.18	29.87
VIIS	4.90	6.22	6.97	6.22	7.90	8.86	42.34
Avg	2.35	2.61	3.04	2.99	3.31	4.08	31.24
Std Dev	0.34	0.30	0.40	0.44	0.38	0.50	23.70

Figure 18. Map of mean inorganic specific mass scattering efficiencies (α_{inorg}, m^2 g^{-1}) from method 3. The size of the circle reflects the magnitude of the efficiency, which is printed next to the circle.
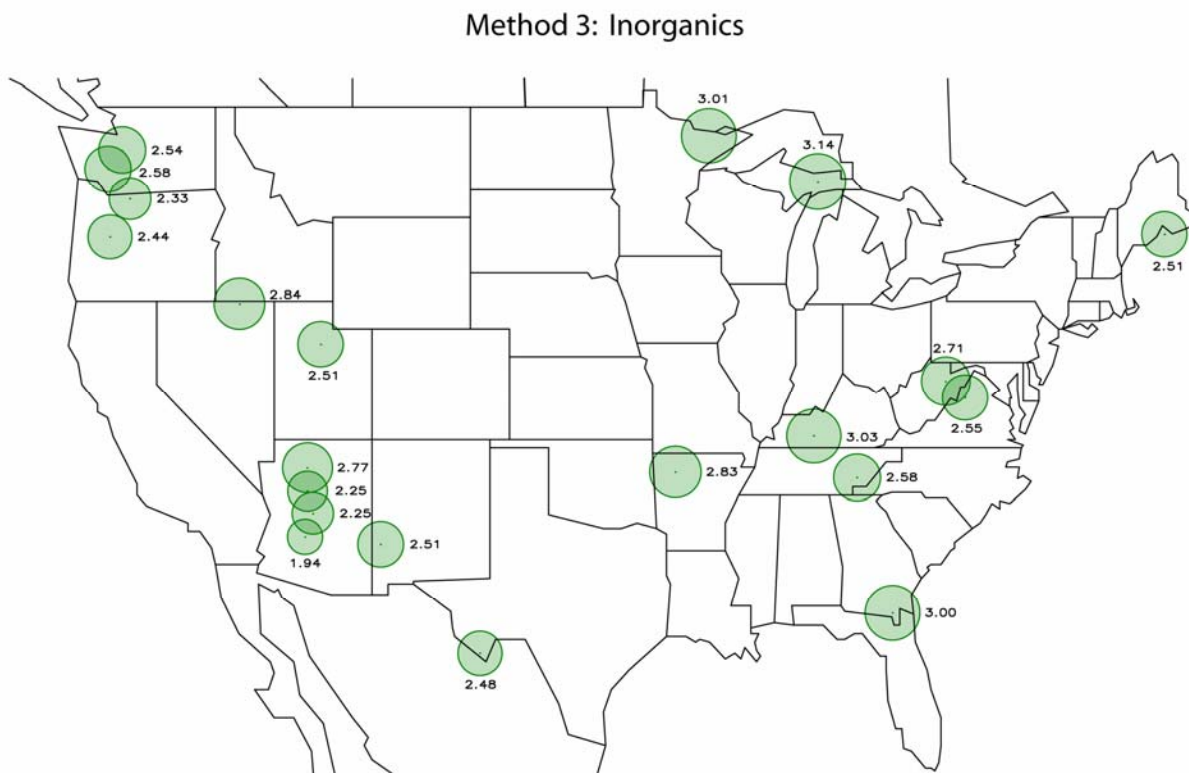
The spatial distribution of POM mass scattering efficiencies from method 3 is shown in Figure 19. Inorganic and organic aerosols were assumed to be internally mixed; therefore the POM scattering efficiencies are scaled to inorganic efficiencies by the ratio of their densities (1.31) and the spatial variability across the United States is the same for both. Notice, however, that in the central eastern United States the POM scattering efficiencies approach 4.0 m^2 g^{-1}, the value currently assumed in the Regional Haze Rule guidance. Also note that at GRSM there is less than a 6% change in mass scattering efficiency for a doubling of mass concentration, but that the actual variability in observed mass results in a 60% change in mass scattering efficiency between the upper and lower estimates when the functional dependence on mass is accounted for by this method. The average POM mass scattering efficiency is 3.31 ± 0.38 m^2 g^{-1}, similar to that derived for inorganics.

Figure 19. Map of organic mass scattering efficiencies (α_{org}, m^2 g^{-1}) from method 3. The size of the circle reflects the magnitude of the efficiency, which is printed next to the circle..

Method 3: POM
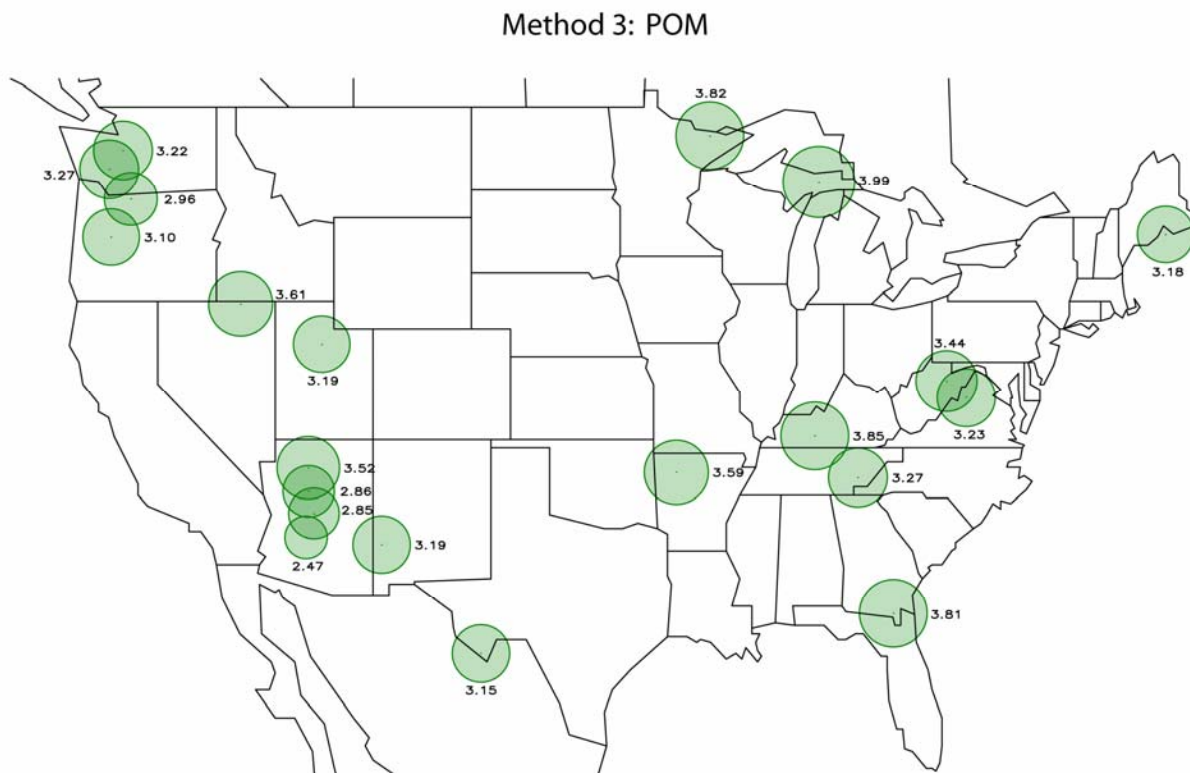
In the eastern United States the POM mass scattering efficiencies for method 3 are similar to method 1. However, method 3 results are quite different from method 1 in the western part of the country, where the efficiencies were near 2.0 m^2 g^{-1} or lower. One interesting feature showing up in both analyses is lower mass scattering efficiencies in Arizona compared to adjacent monitoring sites.

Table 22, like Table 20 for method 3, provides the mean, lower, and upper mass scattering efficiencies for each species as derived using method 4. The upper and lower estimates are computed by averaging the mass scattering efficiencies associated with the upper and lower 15% mass concentrations. Although results for VIIS are reported, calculations of the average and standard deviation in mass scattering efficiencies do not include data from VIIS. The results derived with method 4 are quite similar to those from method 3, with similar values of the

average mean, lower, and upper mass scattering efficiencies for all the sites. However, there is much greater variability in the results from method 3 compared to those from method 4. Method 3 also yields a significantly lower POM mass scattering efficiency for the urban area of Phoenix compared to method 4 (mean values of 2.47 versus 3.71 m^2 g^{-1}). In fact, method 4 yields the highest POM mass scattering efficiencies (3.71 m^2 g^{-1}) compared to other sites because it has some of the highest POM mass concentrations; however, results from method 3 indicate that PHOE has the lowest POM mass scattering efficiencies of all the sites. A possible reason for this discrepancy is the calculation of POM. An R_{oc} factor of 1.8 is used on all sites in methods 3 and 4; however, the MLR regression in section 3.1 suggests that Phoenix has a much lower average R_{oc} factor (1.3). If POM mass is overestimated in Phoenix due to a high R_{oc} factor, the efficiencies derived with method 4 will be more strongly affected that those derived using method 3 because of how masses are weighted in the respective algorithms. If we correct the method 4 Phoenix POM mass scattering efficiency for an R_{oc} factor of 1.3, the value decreases to 2.68 m^2 g^{-1} and we obtain a closer agreement with method 3 (2.47 m^2 g^{-1}). These differences in mass scattering efficiencies between method 3 and 4 generally occur for all monitoring sites in the Southwest, suggesting that the difference in composition of the two size modes, not just the change in size, is potentially important and is not included in the method 4 formulation. These differences are highlighted by comparing Figures 18 and 19 to Figures 20 and 21 where the mass scattering efficiencies for each monitoring site and species are shown. The effects of the different mass scattering efficiencies on estimated scattering will be investigated in section 7, where we present the biases between measured and estimated scattering for all the methods.

Table 22. The mean, upper, and lower specific scattering efficiencies (m^2 g^{-1}) for ammonium sulfate (AS), ammonium nitrate (AN), and particulate organic matter (POM) computed with method 4. The upper and lower estimates are calculated by averaging the mass scattering efficiencies associated with the upper and lower 15% mass concentrations. The percent changes between the upper and lower mass scattering efficiencies are shown in the final three columns.

m^2 g^{-1}	α_{AS}	α_{AS}	α_{AS}	α_{AN}	α_{AN}	α_{AN}	α_{POM}	α_{POM}	α_{POM}	AS	AN	POM
Site	lower	mean	upper	lower	mean	upper	lower	mean	upper	% diff	% diff	% diff
ACAD	2.28	2.58	3.29	2.21	2.25	2.34	2.89	3.10	3.56	43.95	6.03	23.48
BIBE	2.29	2.58	3.06	2.21	2.24	2.30	2.87	3.07	3.50	33.25	4.00	22.05
BOWA	2.26	2.44	2.79	2.20	2.27	2.56	2.86	3.09	3.60	23.49	15.99	25.68
CORI	2.25	2.39	2.62	2.22	2.33	2.72	2.92	3.27	3.95	16.64	22.87	35.49
DOSO	2.40	3.05	4.27	2.21	2.28	2.45	2.98	3.33	3.82	78.28	10.51	28.22
GICL	2.25	2.36	2.53	2.20	2.22	2.25	2.76	3.09	3.85	12.39	1.96	39.59
HANC	2.23	2.31	2.44	2.20	2.23	2.28	2.82	2.99	3.33	9.31	3.32	17.93
GRSM	2.40	3.05	4.22	2.21	2.26	2.41	2.97	3.39	4.02	75.47	8.68	35.29
IKBA	2.25	2.35	2.49	2.21	2.25	2.32	2.88	3.02	3.27	10.77	4.93	13.75
JARB	2.22	2.27	2.34	2.20	2.22	2.26	2.85	3.03	3.45	5.39	2.47	21.25
LOPE	2.25	2.34	2.48	2.22	2.30	2.61	2.89	3.11	3.49	10.08	17.82	20.74
MACA	2.48	3.11	4.20	2.23	2.34	2.65	3.03	3.41	4.02	69.20	19.01	32.90
MORA	2.22	2.35	2.61	2.20	2.23	2.28	2.86	3.20	3.81	17.57	3.33	33.02
OKEF	2.43	2.87	3.62	2.22	2.26	2.33	3.01	3.34	3.87	49.04	5.11	28.78
PHOE	2.29	2.42	2.60	2.24	2.37	2.83	3.14	3.71	4.98	13.24	26.64	58.21
SENY	2.28	2.54	3.24	2.21	2.32	2.76	2.85	3.14	3.69	42.31	25.05	29.25
SHEN	2.37	2.97	4.09	2.22	2.30	2.49	2.92	3.23	3.84	72.77	12.30	31.72
SNPA	2.23	2.35	2.56	2.21	2.25	2.34	2.84	3.10	3.62	15.08	5.85	27.20
SYCA	2.24	2.32	2.43	2.21	2.24	2.30	2.90	3.13	3.57	8.88	4.28	23.03
THIS	2.21	2.29	2.45	2.20	2.22	2.26	2.82	3.11	3.76	10.75	2.45	33.37
UPBU	2.34	2.81	3.67	2.22	2.34	2.66	2.97	3.33	3.93	57.30	19.97	32.19
VIIS	2.26	2.33	2.46	2.21	2.23	2.26	2.8	2.9	3.1	8.85	2.26	10.71
Avg	2.27	2.49	2.91	2.21	2.26	2.39	2.91	3.18	3.74	32.15	10.60	29.20
Std Dev	0.078	0.289	0.689	0.009	0.046	0.190	0.086	0.172	0.353	25.433	8.261	9.293

Figure 20. Map of the mean ammonium sulfate mass scattering efficiencies (α_{AS}, m^2 g^{-1}) from method 4. The size of the circle reflects the magnitude of the efficiency, which is printed near the circle.

Method 4 SO$_4$ Mean Efficiency
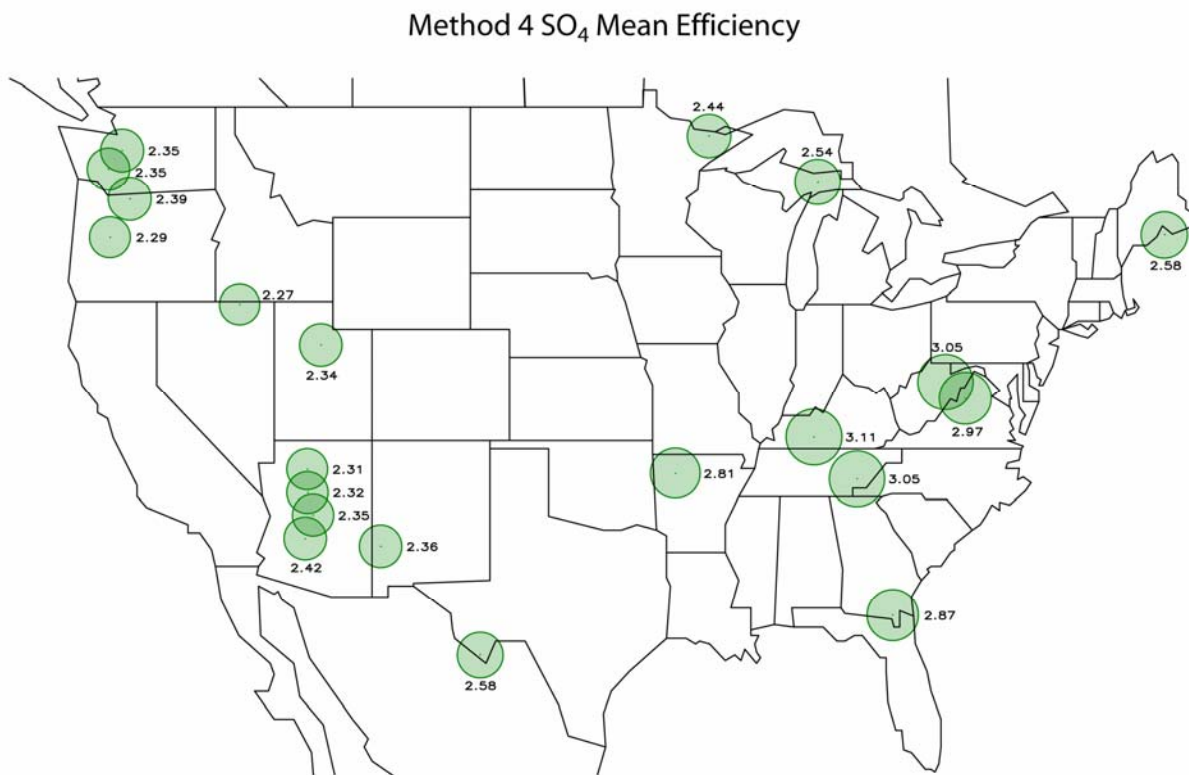
Figure 21. Map of mean POM mass scattering efficiencies (α_{POM}, m^2 g^{-1}) from method 4. The size of the circle reflects the magnitude of the efficiency, which is printed near the circle.

Method 4 POM Mean Efficiency
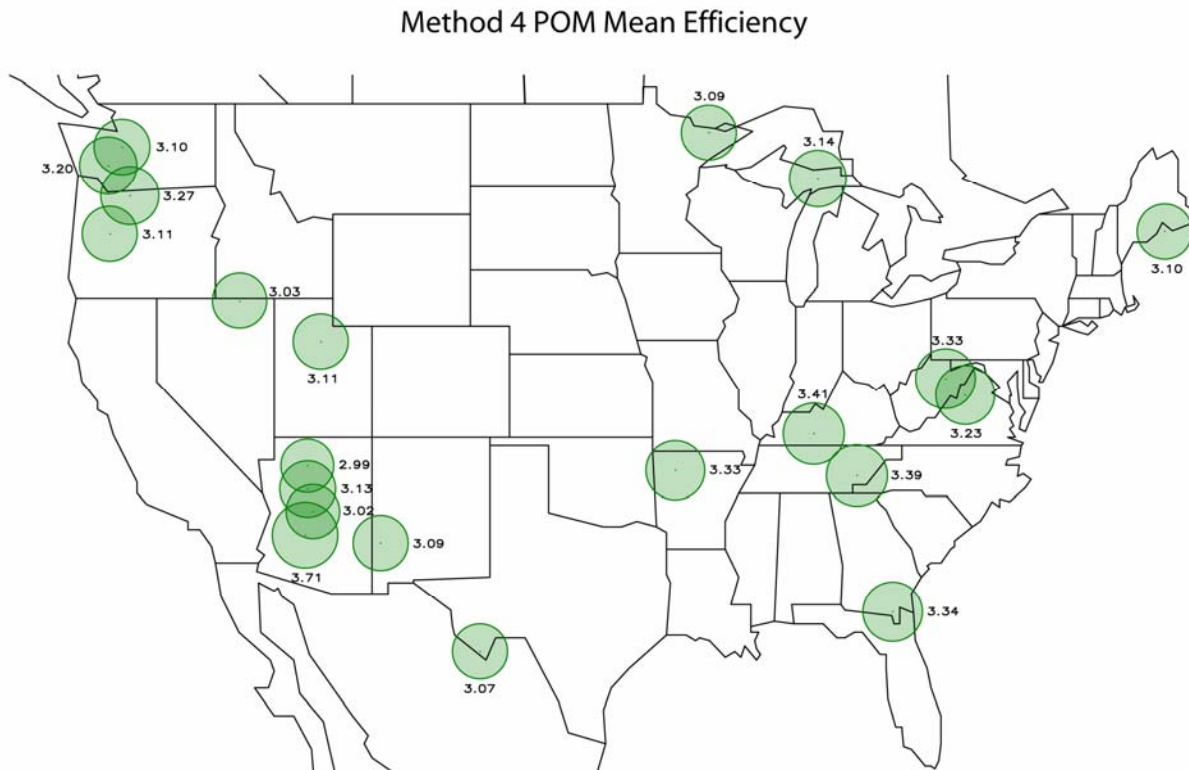
6.   Evaluation of the Combined Data Set

Section 5 focused on the various methods for estimating mass scattering efficiencies for each site individually. We now apply methods 3 and 4 to a combined data set from all the sites. Data from PHOE and VIIS were not included in this combined data set because the results from these sites were consistent outliers. When analyses are performed on a per-site basis, site specific coefficients are applied to data from each site; however, in this section we apply only one set of assumptions to the combined data set. We will refer to results from methods 3 and 4 as applied to the combined data set as "M3-C" and "M4-C", respectively. Method 3 yields an intercept and slope for the combined data set of 0.8 and 0.015, respectively, and can be compared to the values

derived for individual sites from Table 20. The average intercept and slope of all the individual

sites was 0.69 and 0.04, respectively.

Table 23 presents a statistical summary of aerosol mass concentrations for each species,

relative humidity, total aerosol scattering, and the average f(RH) estimates corresponding to the

ammonium sulfate small size mode, large size mode, current IMPROVE estimate, and sodium

chloride for the combined data from all the sites and time periods (except PHOE and VIIS).

Ammonium sulfate composes 43% of the fine mass while POM contributes 34%. Soil

contributes 10% of the fine mass, ammonium nitrate is 7%, and light-absorbing carbon is 4%.

Sea salt contributes less than 1%.

Table 23. A statistical summary of mass concentrations (μg m^{-3}) for the combined data set (all optical monitoring sites except Phoenix and the Virgin Islands). CM and FM refer to gravimetric coarse mass and fine (PM$_{2.5}$) mass, respectively. AS and AN refer to ammonium sulfate and ammonium nitrate, respectively. POM is particulate organic matter using an R_{oc} factor of 1.8. RH refers to ambient relative humidity. The number of nephelometer data points in a 24-hr average is given by $N(b_{sp})$. The values of the f(RH) corresponding to the nephelometer chamber for the ammonium sulfate small mode, large mode, current IMPROVE estimate, and NaCl curves are also listed. The contribution to fine mass is provided in parentheses.

Variable	Mean	Std Dev	Minimum	Maximum	Valid
CM (μg/m^3)	4.71	5.09	-17.74	116.56	13217
FM (μg/m^3)	7.15	6.35	-0.71	68.04	13630
AS (μg/m^3)	3.05 (43%)	3.90	0.00	46.69	13982
AN (μg/m^3)	0.51 (7%)	0.92	-0.06	16.92	13695
POM (μg/m^3)	2.45 (34%)	2.68	-0.19	104.41	13794
LAC (μg/m^3)	0.30 (4%)	0.30	-0.02	13.39	13768
Soil (μg/m^3)	0.68 (10%)	1.34	0.00	29.26	13881
Sea Salt (μg/m^3)	0.02 (<1%)	0.14	0.00	5.44	15051
RH (%)	61.48	18.02	5.85	90.00	13300
b_{sp} (Mm^{-1})	25.92	31.28	0.04	325.96	5899
$N(b_{sp})$	15.86	8.83	1.00	24.00	15051
f(RH)$_{c,small}$	2.09	0.59	1.04	4.35	12727
f(RH)$_{c,large}$	1.80	0.40	1.04	3.22	12727
f(RH)$_{c,IMPROVE}$	1.87	0.59	1.00	3.65	12727
f(RH)$_{c,NaCl}$	2.54	0.86	1.00	4.78	12727

Table 24. A summary of the low, mean, and high mass scattering efficiencies (m^2 g^{-1}) for the combined data set with method 4 (M4-C), two statistical corrections to method 4 results (M4-C1 and M4-C2, see text), and results from method 3 applied to the combined data (M3-C). Results correspond to ammonium sulfate (AS), ammonium nitrate (AN), and particulate organic material (POM).

α (m^2 g^{-1})	AS			AN			POM		
Case	low	mean	high	low	mean	high	low	mean	high
M4-C	2.23	2.52	3.28	2.21	2.25	2.41	2.87	3.18	3.80
M4-C1	2.19	2.47	3.22	4.12	4.21	4.49	2.59	2.87	3.43
M4-C2	2.28	2.57	3.36	2.26	2.31	2.46	2.94	3.25	3.89
M3-C	2.45	2.67	3.14	2.45	2.67	3.14	3.10	3.38	3.97

Using the combined data, we now investigate the performance of method 4 by evaluating different statistical regressions between the method 4 estimated and measured scattering. The results of the regressions are summarized in Table 24. The mean and lower and upper mass scattering efficiencies for the combined data set as derived by method 4 are referred to as "M4-C". The first statistical approach (M4-C1) corresponds to a regression of the scattering estimates from method 4 for each species against the measured scattering, b_{mix}, with adjustments to the method 4 dry mass scattering efficiencies by the regression coefficients corresponding to each species. The regression coefficients were near 1, indicating that method 4 results in average mass scattering efficiencies that are representative of the actual mass scattering efficiencies. The statistical approached referred to as "M4-C2" is similar to M4-C1 except the regression is between fine mode (summed inorganics and organics, b_{mix_est}) scattering from method 4 and measured b_{mix} (similar to method 2), resulting in a single regression coefficient instead of coefficients corresponding to each species. The regression coefficient is not statistically different from 1, implying again that dry mass scattering efficiencies derived with method 4 are representative of actual values. Finally, results from method 3 applied to the combined data (M3-C) are very similar to the results from method 4 (see last row in Table 24). The values in Table 24 should be contrasted to those used in the current IMPROVE equation for estimating

scattering. The current IMPROVE ammonium sulfate, ammonium nitrate, and POM mass scattering efficiencies are 3.0, 3.0, and 4.0 m^2 g^{-1}, respectively, roughly 20–25% higher than estimates obtained from method 4 (2.52, 2.25, and 3.18 m^2 g^{-1} for ammonium sulfate, ammonium nitrate, and POM, respectively).

A summary of measured and reconstructed total b_{sp} and accumulation mode b_{mix} using method 4 is presented in Table 25. Also presented are estimates of scattering associated with each species, fine particle absorption, and scattering due to water. There is only about a 3% difference on average between estimated and measured scattering for both fine and total scattering. Ammonium sulfate and POM contribute 41 and 27%, respectively, to total extinction, while CM contributes 12%. Nitrate and soil each contribute less than 10% of total scattering, and sea salt contributes less than 0.2 of one percent.

Table 25. A summary of b_{sp} (Mm^{-1}) for the combined data set (all monitoring sites except Phoenix and the Virgin Islands). Values correspond to measured total ambient scattering (b_{sp}), reconstructed total ambient scattering (b_{sp_recon}), measured scattering associated with fine mode inorganics and organics (b_{mix}), estimated scattering associated with inorganics and organics (b_{mix_est}), scattering due to ammonium sulfate (b_{sp}(AS)), ammonium nitrate (b_{sp}(AN)), particulate organic material (b_{sp}(POM)), sea salt (b_{sp}(SS)), and water (b_{sp}(H$_2$0)). Light absorption (b_{ap}) was computed assuming a mass absorption efficiency of 10 m^2 g^{-1}. New f(RH) curves were used to estimate wet scattering.

Variable (Mm^{-1})	Mean	Std Dev	Minimum	Maximum	Valid
b_{sp}	25.56	30.00	0.04	273.50	5090
b_{sp_recon}	24.80	27.83	0.27	301.00	5090
b_{mix}	22.74	29.92	-11.01	271.99	5090
b_{mix_est}	21.98	27.61	0.10	298.70	5090
b_{sp}(AS)	11.92	21.84	0.39	292.39	5090
b_{sp}(AN)	2.27	4.90	-0.19	74.16	5090
b_{sp}(POM)	7.79	9.01	-0.36	194.13	5090
b_{sp}(Soil)	1.02	1.66	0.01	29.26	5090
b_{sp}(CM)	3.52	3.68	-3.12	69.94	5090
b_{sp}(SS)	0.04	0.41	0.00	15.12	5090
b_{ap}	2.74	2.15	-0.11	30.25	5090
b_{sp}(H$_2$O)	6.31	11.55	0.06	158.15	5090

7. Biases between Reconstructed and Measured Scattering

In this section we present a brief summary of the skill with which each method reconstructs total scattering as measured by the Optec ambient open air nephelometer. We compute the average bias as $(b_{sp\_recon} - b_{sp\_meas})/b_{sp\_meas}$ for time periods with low (10–20%), median (45–55%), and high (80–90%) measured scattering values. The results for each of the five methods (current IMPROVE and methods 1–4) are presented in Tables 26–28 and Figures 22–26.

The poorest performance for all the methods corresponds to time periods with the 10–20% lowest measured scattering coefficients. The statistical models (methods 1–3) demonstrate the weakest performance, with average biases across all sites for method 1 and method 2 of 63 and 82%, respectively. Methods 3 and 4 perform the best, with average biases of 46 and 44%, respectively. The biases for all the methods tend to increase and decrease for each sites similarly (see Figure 22). The bias was near 150% at Ikes Backbone AZ (IKBA) and Jarbridge Wilderness NV (JARB) and near zero at Shenandoah National Park VA (SHEN), Three Sisters Wilderness OR (THIS), and Upper Buffalo Wilderness AR (UPBU). The biases corresponding to the eastern monitoring sites were the lowest, ranging from 25–30 % for methods 3 and 4.

The lowest average biases corresponding to time periods with the median (45–55%) measured scattering coefficients were 4.3 and 1.2%, corresponding to methods 3 and 4, respectively. The highest average biases for this case were 13 and 22%, corresponding to methods 1 and 2, respectively. Note that the bias at Phoenix is smallest (<10%) for the methods that were applied on a site-by-site basis (methods 1–3), compared to the highest bias (~ 30%) for method 4, which was applied similarly to the entire data set. Phoenix has relatively high concentrations of POM with quite low mass scattering efficiencies, as compared to more remote

nonurban locations; these unique conditions are accounted for in the site-by-site evaluations (methods 1–3), but not in the site-independent algorithm applied in method 4.

Methods 1 and 2 have the lowest biases (1–2%) corresponding to the highest (80–90%) scattering values; however, all models performed well under these conditions, with biases of less than 10%. Method 4 has an average bias across all sites of -9%. Methods 1–3 perform the best for the Phoenix site for the reasons discussed above.

Table 26. Average biases for time periods with low (10–20%) measured scattering values for methods 1–4 and the current IMPROVE equation.

Site	Method 1	Method 2	Method 3	Method 4	IMPROVE
ACAD	0.433	0.510	0.270	0.213	0.320
BIBE	0.779	0.866	0.402	0.518	0.577
BOWA	0.440	1.341	0.790	0.485	0.571
CORI	1.105	1.419	0.640	0.965	1.109
DOSO	0.637	0.732	0.485	0.308	0.265
GICL	0.875	1.450	0.478	0.676	0.858
HANC	0.556	0.568	0.515	0.188	0.359
GRSM	0.423	0.565	0.097	0.235	0.242
IKBA	1.455	1.421	0.819	1.199	1.383
JARB	1.358	1.800	1.328	1.066	1.277
LOPE	0.521	0.841	0.380	0.345	0.428
MACA	0.308	0.376	0.318	0.087	0.125
MORA	1.536	1.530	0.956	1.025	1.157
OKEF	0.563	0.754	0.374	0.288	0.336
PHOE	0.109	0.201	0.096	0.421	0.468
SENY	-0.027	0.031	0.140	-0.211	-0.093
SHEN	0.429	0.584	0.317	0.336	0.404
SNPA	0.405	0.554	0.243	0.225	0.336
SYCA	0.810	0.837	0.677	0.774	0.857
THIS	0.327	0.456	0.116	0.099	0.182
UPBU	0.210	0.398	0.130	0.050	0.099
Avg	0.631	0.821	0.456	0.442	0.536

Figure 22. The average biases for each site corresponding to time periods with low measured scattering values (10–20%) (see Table 26).
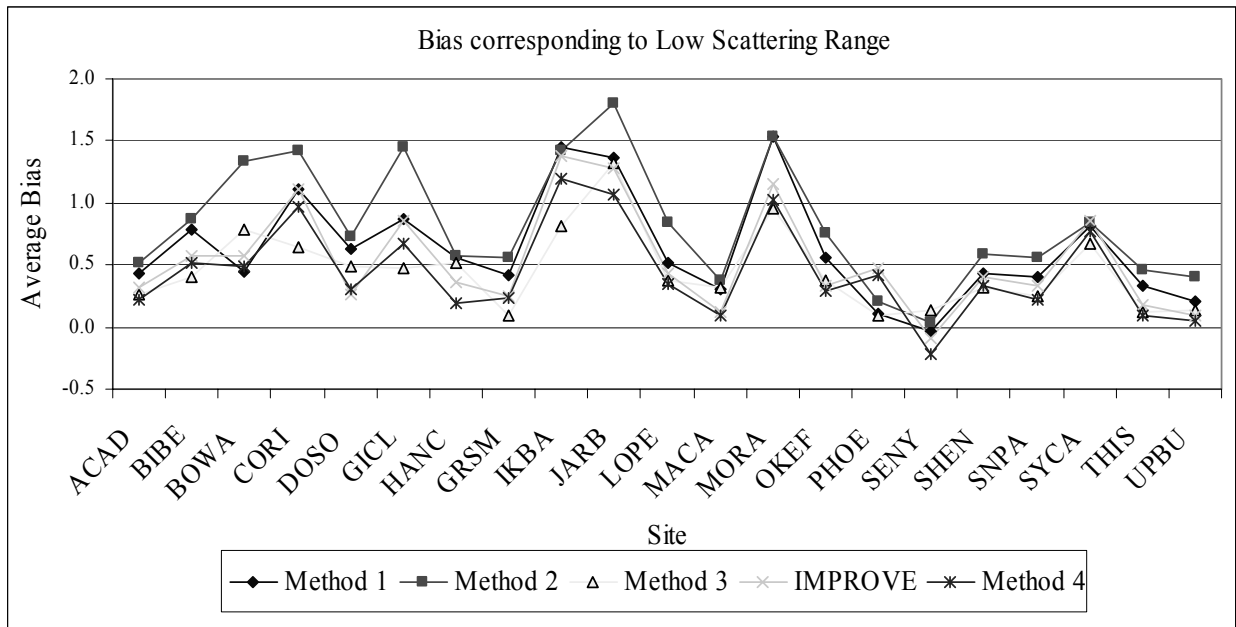
Table 27. Average biases for time periods with the median (45–55%) measured scattering values for methods 1–4 and the current IMPROVE equation.

Site	Method 1	Method 2	Method 3	Method 4	IMPROVE
ACAD	0.140	0.186	0.016	-0.028	0.054
BIBE	0.204	0.232	0.002	0.027	0.038
BOWA	-0.043	0.248	-0.041	-0.208	-0.117
CORI	0.250	0.432	0.052	0.201	0.246
DOSO	0.362	0.239	0.090	-0.023	-0.057
GICL	0.097	0.489	0.000	0.043	0.123
HANC	0.232	0.235	0.202	0.014	0.072
GRSM	0.190	0.258	0.010	0.077	0.045
IKBA	0.169	0.194	0.020	0.097	0.163
JARB	0.152	0.299	0.133	-0.011	0.049
LOPE	0.160	0.392	0.100	0.043	0.080
MACA	0.110	0.114	0.076	-0.062	-0.072
MORA	0.224	0.218	0.045	0.075	0.093
OKEF	0.097	0.170	0.027	-0.081	-0.069
PHOE	-0.020	0.062	-0.018	0.331	0.299
SENY	-0.118	-0.057	0.028	-0.256	-0.151
SHEN	0.085	0.184	0.037	0.054	0.073
SNPA	0.187	0.257	0.107	0.042	0.072
SYCA	-0.007	0.035	-0.050	0.003	0.055
THIS	0.042	0.157	-0.010	-0.087	-0.043
UPBU	0.134	0.231	0.069	-0.010	-0.014
Avg	0.126	0.218	0.043	0.012	0.045

116

Figure 23. The average biases for each site corresponding to time periods with median measured scattering values (45–55%) (see Table 27).

Table 28. Average biases for time periods with high (80–90%) measured scattering values for methods 1–4 and the current IMPROVE equation.

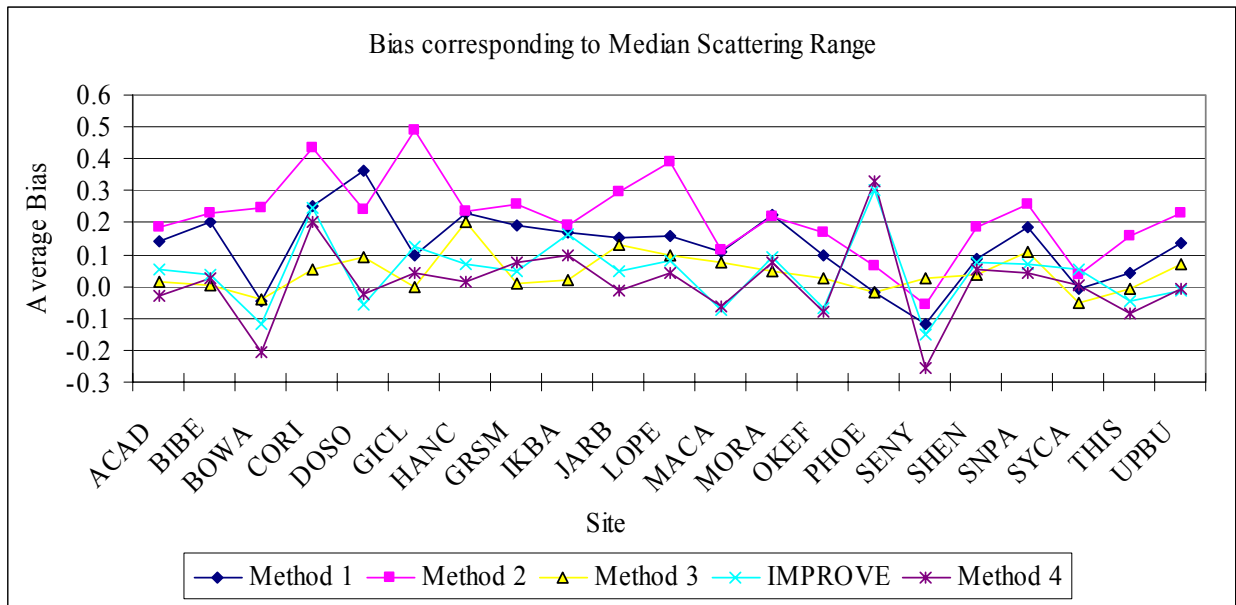| Site	Method 1	Method 2	Method 3	Method 4	IMPROVE
ACAD	0.093	0.119	0.020	-0.016	0.024
BIBE	-0.022	-0.020	-0.073	-0.121	-0.152
BOWA	-0.006	0.224	-0.027	-0.191	-0.115
CORI	-0.054	0.106	-0.057	-0.006	-0.031
DOSO	0.140	0.056	-0.011	-0.098	-0.139
GICL	0.049	0.182	-0.047	-0.117	-0.113
HANC	-0.152	-0.149	-0.166	-0.270	-0.254
GRSM	0.002	-0.008	-0.029	-0.016	-0.131
IKBA	-0.068	-0.071	-0.007	-0.110	-0.088
JARB	-0.144	-0.080	-0.147	-0.275	-0.250
LOPE	-0.042	0.025	-0.132	-0.208	-0.181
MACA	-0.016	-0.039	-0.063	-0.140	-0.169
MORA	-0.012	-0.020	-0.095	-0.093	-0.109
OKEF	-0.002	-0.004	0.015	-0.155	-0.194
PHOE	-0.057	-0.025	-0.067	0.456	0.193
SENY	0.005	-0.003	0.011	-0.154	-0.108
SHEN	-0.006	0.046	0.000	0.028	-0.021
SNPA	-0.010	-0.049	-0.096	-0.178	-0.183
SYCA	-0.068	-0.072	-0.128	-0.039	-0.056
THIS	0.009	0.045	0.061	-0.088	-0.152
UPBU	-0.053	-0.024	-0.069	-0.135	-0.161
Avg	**-0.020**	**0.011**	**-0.053**	**-0.092**	**-0.114**

Figure 24. The average biases for each site corresponding to time periods with high measured scattering values (80–90%) (see Table 28).
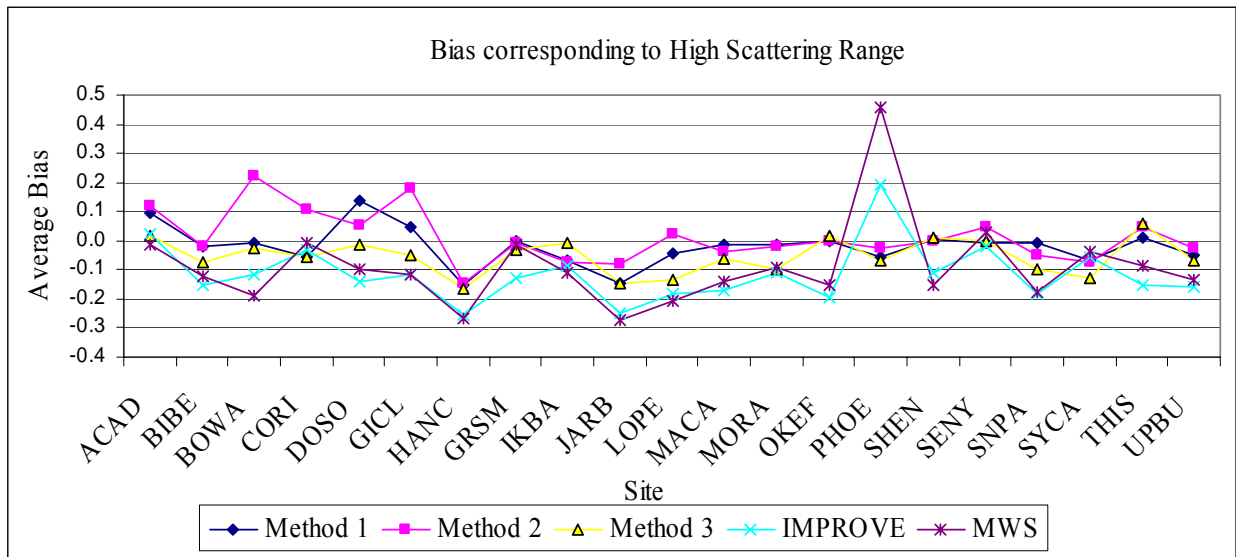
Figure 25. Average biases for the combined data set (all sites and time) for time periods with low (10–20%), median (45–55%), and high (80–90%) scattering ranges, as calculated using methods 3 and 4, and the current IMPROVE algorithm. Also shown is the average of the per-site biases from Tables 26–28. The *f*(RH) curves were calculated for continuous growth from 1 < RH < 90%.
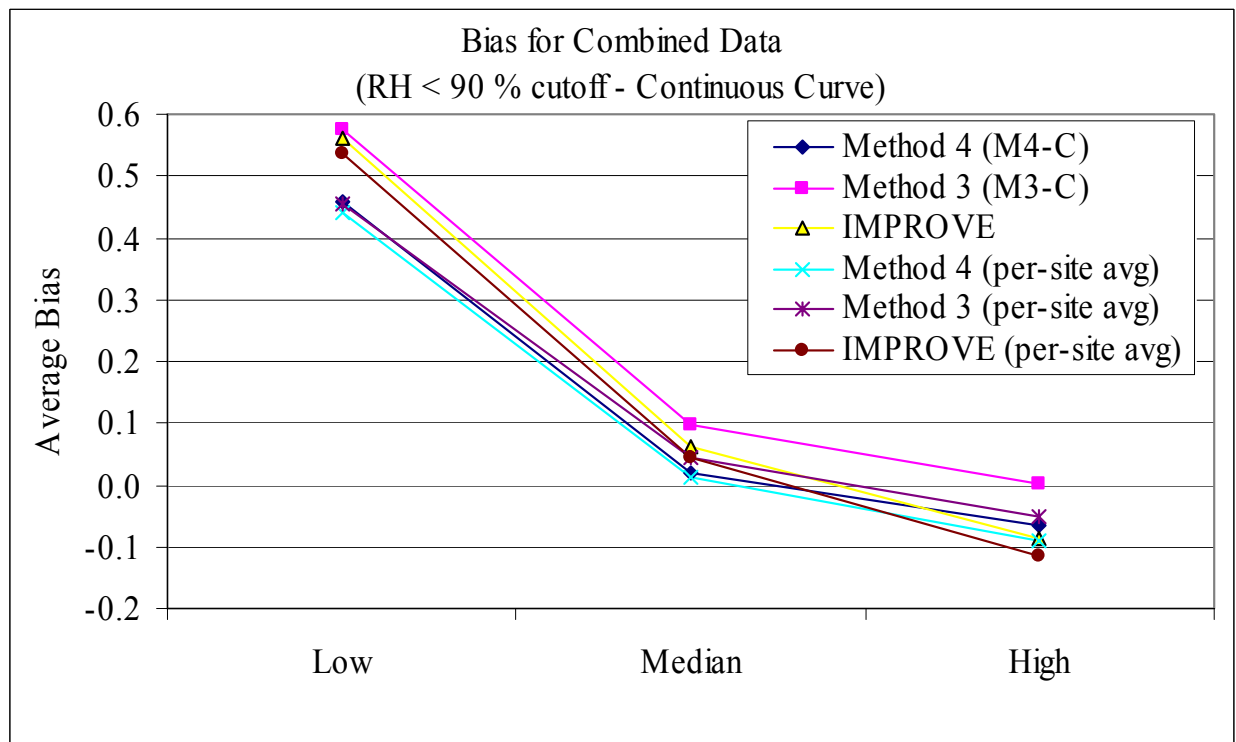
Figure 26. Average biases for the combined data set (all sites and time) for time periods with low (10–20%), median (45–55%), and high (80–90%) scattering ranges, as calculated using methods 3, 4, and the current IMPROVE algorithm. The *f*(RH) curves were calculated from 1 < RH < 95% assuming crystallization growth curves.
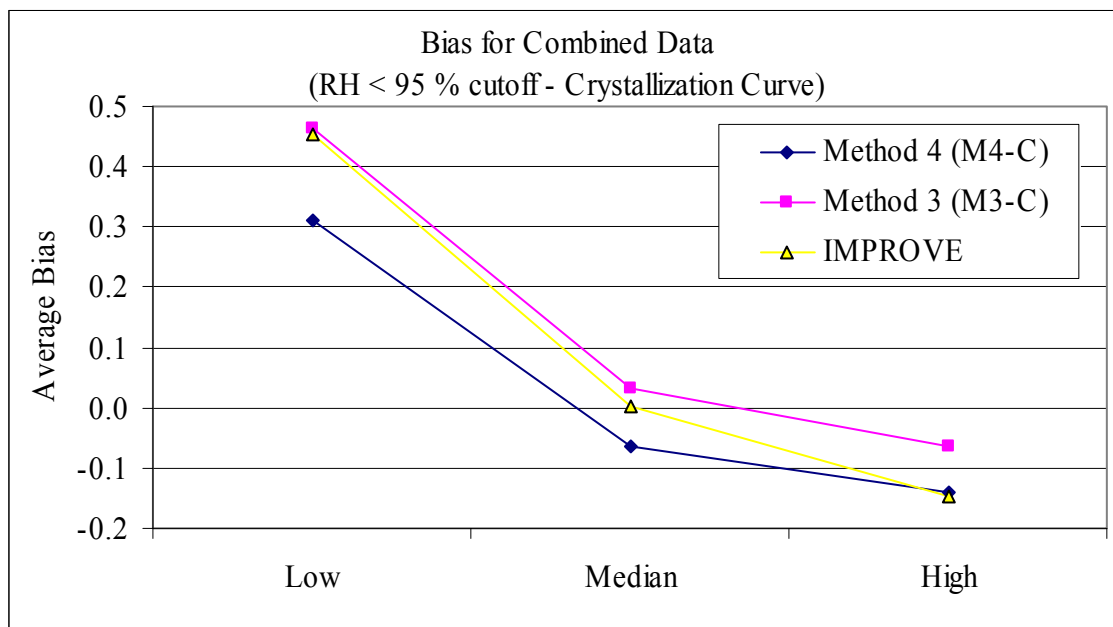
The biases were also computed for the combined data set of all sites and time periods. In this analysis the bias is calculated for each 24-hour sampling period and then averaged, thus biasing the results toward those monitoring sites that have been operating over longer periods of time. This approach should be contrasted against the bias computed as the grand average of all the site average biases, thus weighting each monitoring site or geographic location equally. Figures 25 and 26 show the average bias corresponding to time periods with low, median, and high scattering periods for method 4 (MC-4), method 3 (MC-3), and the current IMPROVE algorithm for the combined data set. Two *f*(RH) curves were used in these calculations. Because the Regional Haze Rule suggests using an RH cutoff of 95%, the bias calculations were computed using RH cutoff values of both 90 and 95%. Figure 25 presents the biases computed assuming a 90% RH cutoff and continuous (1 < RH < 90%) *f*(RH) curves for both the combined data set and the site-by-site average, while Figure 26 presents the same biases computed with a

95% RH cutoff and f(RH) curves corresponding to the crystallization branch for the combined data set only.

For the f(RH) curve corresponding to a 90% cutoff RH, the biases corresponding to the low scattering values are the largest for all the methods, ranging from 45 to almost 60%. The biases corresponding to the median scattering values range from 0–10%, and the biases corresponding to the highest scattering values are negative (-10–0%) (see Figure 25). The biases computed for an average of all the sites are lower than biases computed for the combined data set, by about 10% for the low scattering range, 5% at the median scattering range, and within a few percent at the high scattering range. The lower bias corresponding to the averaged per-site estimates is consistent with the earlier example of better performance at the Phoenix site when analyses are performed on a per-site basis. The biases computed from method 3 as applied to the combined data set (M3-C) were highest for the low and median scattering range, and the method 4 average of the per-site analyses had the lowest biases for the low and median scattering ranges. For the time periods with the highest scattering range, M3-C had the lowest bias, while the current IMPROVE formulation had the largest (most negative) bias. Overall, M4 for the per-site analyses had the lowest bias. Computing the biases with f(RH) curves corresponding to a higher RH cutoff (95%) resulted in lowering the biases for all the methods compared to an RH cutoff of 90%. This decrease in bias does not imply that the bias was necessarily improved, because a bias could decrease from -10 to -20%, reflecting a larger difference between measured and predicted scattering. The biases corresponding to the low scattering range dropped by about 10%, and the median and high bias dropped by about 6–8%. Method 4 (M4-C) results are biased negatively by about 14% for the high scattering values, negatively by 6% for the median values, and positively by 31% for low scattering values.

8. Summary of Suggested Refinements to the IMPROVE Equation

The current equation used to estimate extinction associated with measured aerosol species is

$$b_{ext} = \alpha_{AS}f(RH)_{AS}[AS] + \alpha_{AN}f(RH)_{AN}[AN] + \alpha_{POM}[POM] + \alpha_{soil}[Soil] + \alpha_{CM}[CM] + \alpha_{LAC}[LAC] \qquad (25)$$

where it is assumed that the dry mass scattering and absorption efficiencies α_{AS}, α_{AN}, α_{POM}, α_{soil}, α_{CM}, and α_{LAC} are 3.0, 3.0, 4.0, 1.0, 0.6, and 10.0 m^2 g^{-1}, respectively, and the f(RH) curve is calculated on an hourly basis and averaged to 24 hours to be commensurate with the 24-hour average aerosol mass measurements. The f(RH) curve is a "smoothed" ammonium sulfate curve that reflects continuous particle growth starting at 40% RH. The forms assumed for each of the aerosol species are ammonium sulfate and ammonium nitrate, 1.4·OC, soil, and gravimetric coarse mass (PM$_{10}$–PM$_{2.5}$).

Uncertainty in estimated extinction is dependent on not only the assumed forms of each of the aerosol species and their respective mass scattering efficiencies and growth factors, but also on measurement and analytic accuracy and precision. One uncertainty of special concern is the variation in flow rate associated with the IMPROVE monitoring system, because uncertainties in the flow rate affect the cutpoint of the inlet. The IMPROVE 2.5 μm inlet intersects the size range corresponding to the coarse mode; therefore any changes in the cutpoint of the inlet (due to variations in the flow rate) cause significant and varying amounts of coarse material to be characterized as fine mass. The fine mode mass scattering efficiency associated with the fine tail of the coarse mode can vary significantly. This issue is especially important for sites where soil mass contributes significantly to estimated extinction (e.g., most sites in the West during spring months) and for sites where coarse particle nitrate concentrations are high. Some of the issues associated with measurement uncertainty have been discussed, but this report

does not make any recommendations on changes in measurement methodology or analytic procedures.

Another significant uncertainty in reconstructed b_{ext} is the chemical form of each of the aerosol species. Again, this issue is discussed in some detail in this report, but because the ammonium ion is not measured, the current assumption of interpreting sulfate and nitrate in the fine mode as ammonium sulfate and ammonium nitrate is not changed. However, the multiplication factor (R_{oc} = 1.4) used to estimate particulate organic material from measured organic carbon mass in the current equation is undoubtedly low. Based on recent literature review and an analysis of IMPROVE data, we recommend a value of 1.8. We also recommend the inclusion of fine sea salt in the IMPROVE equation as 1.8·Cl per the above discussion. Recognizing that fine sea salt is probably the fine tail of coarse mode sea salt, a new f(RH) function and dry mass scattering efficiency for sea salt was developed. No new recommendation of fine mass absorption efficiency is made.

Because coarse mass is not speciated, we cannot recommend a change in coarse mass scattering efficiency. Coarse mass is not composed only of crustal material but also contains significant fractions of organic and inorganic species, some of which are hygroscopic and light absorbing and therefore have mass scattering efficiencies that differ significantly from the currently assumed value of 0.6 m^2 g^{-1}. Thus it should be recognized that coarse mass extinction is only a very rough estimate. Coarse mass concentrations are also only approximate because the $PM_{2.5}$ cutpoint intersects the size range that corresponds to the peak of the coarse mode mass size distribution, and flow rate variability can cause the cutpoint to vary substantially.

At most monitoring sites, dry mass scattering efficiencies increase with increasing mass concentration. This relationship was observed at most of the rural sites and at the one urban site

(Phoenix) in the optical monitoring network. The trend toward increasing mass scattering efficiency with mass concentrations was treated with two separate approaches. A variety of statistical regressions of mass concentration and scattering coefficients were applied (methods 1–3); however, results from statistical regressions are only as robust as the data themselves. Therefore the second approach (method 4) was based on a physical model of a bimodal fine mode size distribution. The small size mode corresponds to lower mass concentrations and particles that are less efficient at scattering light, while the large size mode is associated with higher mass concentrations and particles that are more efficient at scattering light. The mass scattering efficiencies were computed for a simple linear mixing of these size modes as a function of mass. This model was applied to those species typically found in the fine ($D_p < 2.5$ μm) mode, namely sulfates, nitrates, and POM.

The fine mode bimodal mass size distributions were assumed to be lognormal distributions with mass mean diameters (D_g) of 0.2 μm and 0.5 μm for the small and large size modes, respectively, and with geometric standard deviations (σ_g) of 2.2 and 1.2, respectively, consistent with what is reported in the literature. The ambient scattering coefficient for each species is calculated using the same size distribution parameters. An ammonium sulfate f(RH) curve is calculated for each size distribution and the ambient scattering for each species is calculated using

$$b_{sp,j} = \alpha_s M_j f_s(RH)\frac{(M_l - M_j)}{(M_l - M_s)} + \alpha_l M_j f_l(RH)\frac{(M_j - M_l)}{(M_l - M_s)} \tag{26}$$

where α_s, α_l, M_s, M_l, f_s(RH), and f_l(RH) are the dry mass scattering efficiencies, mass concentrations, and humidification factors associated with the small and large mode mass size distributions, respectively. The species mass concentration is given by M_j. The mass scattering efficiencies associated with the small and large mass size distributions for each species are

presented in Table 29. Unless otherwise stated, $M_s = 0.0$ µg m^{-3} and $M_l = 20.0$ µg m^{-3}; when the species mass concentrations exceeded 20 µg m^{-3}, the dry mass scattering efficiency was set equal to the large values shown in Table 29.

Table 29. Values used for the dry mass scattering efficiencies (m^2 g^{-1}) for the large and small mass size distributions for each species (ammonium sulfate, ammonium nitrate, and particulate organic material, POM).

m^2 g^{-1}	Ammonium sulfate	Ammonium nitrate	POM
α_s (small)	2.2	2.4	2.8
α_l (large)	4.8	5.1	6.1

The bias between modeled and measured scattering is similar for method 3 (statistical approach) and method 4 (physically based model) as applied to the combined data set; however method 4 has an advantage of being less dependent on the data set in its formulation.

A substantial number of measurements of D/D_o and f(RH) curves indicate that aerosol growth occurs at low RH values well below the crystallization points. New f(RH) curves are recommended that are based on an ammonium sulfate D/D_o "no solids" growth curve with a mass size distribution corresponding to those mass size distributions discussed above. The "no solids" curve extends the D/D_o curve to relative humidity values below the ammonium sulfate crystallization point. However, there is little difference in the bias between estimated and measured scattering for the case when f(RH) is assumed to be 1 below the crystallization point compared to when continuous growth between $1 < RH < 90\%$ is assumed. Currently, organic mass is not assumed to be hygroscopic and no change is recommended in this assumption, although there is some evidence that ambient organics may be very weakly hygroscopic at high RH values (RH > 85%).

The form of the extinction equation using method 4, and including site-specific Rayleigh scattering and absorption by gaseous NO$_2$, is

$$
\begin{aligned}
b_{ext} \approx\ & 2.2 \times f_S(RH) \times [Small\ (NH_4)_2\,SO_4] + 4.8 \times f_L(RH) \times [Large\ (NH_4)_2\,SO_4] \\
& + 2.4 \times f_S(RH) \times [Small\ NH_4NO_3] + 5.1 \times f_L(RH) \times [Large\ NH_4NO_3] \\
& + 2.8 \times [Small\ POM] + 6.1 \times [Large\ POM] \\
& + 10 \times [Elemental\ Carbon] \\
& + 1 \times [Fine\ Soil] \\
& + 1.4 \times f_{SS}(RH) \times [Sea\ Salt] \\
& + 0.6 \times [Coarse\ Mass] \\
& + Rayleigh\ Scattering\,(Site\ Specific) \\
& + EE_{NO2} \times [NO_2]
\end{aligned}
\tag{27}
$$

The apportionment of the total concentrations of ammonium sulfate ($(NH_4)_2SO_4$) into the concentrations of the small and large size fractions is accomplished using the following equations:

$$
[Large\ (NH_4)_2\,SO_4] = \frac{[Total\ (NH_4)_2\,SO_4]}{20} \times [Total\ (NH_4)_2\,SO_4]
\tag{28}
$$

$$
[Small\ (NH_4)_2\,SO_4] = [Total\ (NH_4)_2\,SO_4] - [Large\ (NH_4)_2\,SO_4]
\tag{29}
$$

Similar equations are used to apportion total ammonium nitrate (NH_4NO_3) and total particulate organic material (POM = 1.8·OC) concentrations into the small and large size fractions.

REFERENCES

Adam, M., M. Pahlow, V. A. Kovalev, J. M. Ondov, M. B. Parlange, and N. Nair, The Baltimore Supersite experiment during the Canadian forest fire smoke intrusion, *J. Geophys. Res., 109(D16),* doi:10.1029/2003JD004047, 2004.

Alfaro, S. C., L. Gomes, J. L. Rajot, S. Lafon, A. Gaudichet, B. Chatenet, M. Maille, G. Cautenet, F. Lasserre, H. Cachier, and X. Y. Zhang, Chemical and optical characterization of aerosols measured in spring 2002 at the ACE-Asia supersite, Zhenbeitai, China, *J. Geophys. Res., 108(D23),* 8641, doi:10.1029/2002JD003214, 2003.

Ames, R. B., J. L. Hand, S. M. Kreidenweis, D. E. Day, and W. C. Malm, Optical measurements of aerosol size distributions in Great Smoky Mountains National Park: dry aerosol characterization, *J. Air Waste Manage., 50*, 665-676, May 2000.

Anderson, T. L., R. J. Charlson, W. H. White, and P. H. McMurry, Comment on: Light scattering and cloud condensation nucleus activity of sulfate aerosol measured over the northeast Atlantic Ocean, *J. Geophys. Res., 99,* 25947-25949, 1994.

Andrews, E., and S. M. Larson, Effect of surfactant layers on the size changes of aerosol particles as a function of relative humidity, *Environ. Sci. Technol., 27,* 857-865, 1993.

Andrews, E., P. Saxena, S. Musarra, L. M. Hildemann, P. Koutrakis, P. H. McMurry, I. Olmez, and W. H. White, Concentration and composition of atmospheric aerosols from the 1995 SEAVS experiment and a review of the closure between chemical and gravimetric measurements, *J. Air Waste Manage., 50,* 648-664, May 2000.

Arnott, W. P., H. Moosmuller, P. J. Sheridan, J. A. Ogren, R. Raspet, W. V. Slaton, J. L. Hand, S. M. Kreidenweis, and J. L. Collett, Jr., Photoacoustic and filter-based ambient aerosol light absorption measurements: Instrument comparisons and the role of relative humidity, *J. Geophys. Res.*, *108(D1)*, 4034, doi:10.1029/2002JD002165, 2003.

Ashbaugh, L. L., and R. A. Eldred, Loss of particle nitrate from Teflon sampling filters: Effects on measured gravimetric mass in California and in the IMPROVE network, *J. Air Waste Manage., 54,* 93-104, January 2004.

Ashbaugh, L. L., C. E. McDade, W. H. White, P. Wakabayashi, J. L. Collett, Jr., and X.-Y. Yu, Efficiency of IMPROVE network denuders for removing nitric acid, Paper # 32, A&WMA Specialty conference: Regional and Global Perspectives on Haze: Causes, Consequences and Controversies, Asheville, NC, October 25-29, 2004.

Bohren, C. F., and D. R. Huffman, *Absorption and Scattering of Light by Small Particles*, Wiley Interscience, New York, 1983.

Brooks, S. D., P. J. DeMott, and S. M. Kreidenweis, Water uptake by particles containing humic materials and mixtures of humic materials with ammonium sulfate, *Atmos. Environ., 38,* 1859-1868, 2004.

Busch, B., C. Sprengard-Eichel, K. Kandler, and L. Schültz, Hygroscopic properties and water soluble fraction of atmospheric particles in the diameter rang efrom 50 nm to 3.8 μm during the Aerosol Characterization Experiment in Lindenberg 1998, *J. Aerosol Sci., 30(S1),* S513-S514, 1999.

Cabada, J. C., S. Rees, S. Takahama, A. Khlystov, S. Pandis, C. I. Davidson, and A. L. Robinson, Mass size distributions and size resolved chemical composition of fine particulate matter at the Pittsburgh supersite, *Atmos. Environ., 38,* 3127-3141, 2004.

Carrico, C. M., M. J. Rood, J. A. Ogren, C. Neusüß, A. Wiedensohler, and J. Heintzenberg, Aerosol optical properties at Sagres, Portugal, during ACE-2, *Tellus, 52B,* 694-715, 2000.

Carrico, C. M., M. H. Bergin, J. Xu, K. Baumann, and H. Maring, Urban aerosol radiative properties: Measurements during the 1999 Atlanta Supersite Experiment, *J. Geophys. Res., 108(D7)*, 8422, doi:10.1029/2001JD001222, 2003.

Carrico, C. M., S. M. Kreidenweis, W. C. Malm, D. E. Day, T. Lee, J. Carrillo, G. R. McMeeking, and J. L. Collett, Jr., Hygroscopic growth behavior of a carbon-dominated aerosol in Yosemite National Park, *Atmos. Environ., 39*, 1393-1404, 2005.

Chan, M.-N., and C. K. Chan, Hygroscopic properties of two model humic-like substances and their mixtures with inorganics of atmospheric importance, *Environ. Sci. Technol., 37,* 5109-5115, 2003.

Chen, L.-W. A., J. C. Chow, B. G. Doddridge, R. R. Dickerson, W. F. Ryan, and P. K. Mueller, Analysis of a summertime $PM_{2.5}$ and haze episode in the Mid-Atlantic region, *J. Air Waste Manage., 53*, 946-956, Aug 2003.

Chiapello, I., G. Bergametti, B. Chatenet, F. Dulac, I. Jankowiak, C. Liousse, and E. Santos Soares, Contribution of the different aerosol species to the aerosol mass load and optical depth over the northeastern tropical Atlantic, *J. Geophys. Res, 104(D4)*, 4025-4035, 1999.

Chow, J. C., J. G. Watson, L. C. Pritchett, W. R. Pierson, C. A. Frazier, and R. G. Purcell, The DRI thermal/optical reflectance carbon analysis system: Description, evaluation and applications in U.S. air quality studies, *Atmos. Env., 27A(8)*, 1185-1201, 1993.

Chow, J. C., J. G. Watson, D. H. Lowenthal, and L. W. Richards, Comparability between $PM_{2.5}$ and particle light scattering measurements, *Environ. Mon. Assess. 79,* 29-45, 2002.

Chu, S.-H., $PM_{2.5}$ episodes as observed in the speciation trends network, *Atmos. Environ., 38,* 5237-5246, 2004.

Clegg S.L., P. Brimblecombe, and A.S. Wexler, A thermodynamic model of the system H+-NH4+-SO42--NO3--H2O at tropospheric temperatures, *J. of Phys. Chem., 102A*, 2137-2154, 1998a.

Clegg S.L., P. Brimblecombe, and A.S. Wexler, A thermodynamic model of the system H+-NH4+-Na+-SO42—NO3—Cl—H2O at 298.15 K, *J. of Phys. Chem., 102A,* 2155-2171, 1998b.

Cocker, D. R., N. E. Whitlock, R. C. Flagan, and J. H. Seinfeld, Hygroscopic properties of Pasadena, California aerosol, *Aerosol Sci. Technol., 35,* 637-647, 2001.

Countess, R. J., G. T. Wolff, and S. H. Cadle, The Denver winter aerosol: A comprehensive chemical characterization, *J. Air Pollution Control Assoc., 30,* 1194-1200, 1980.

Day, D. E., W. C. Malm, and S. M. Kreidenweis, Seasonal variations in aerosol composition and acidity at Shenandoah and Great Smoky Mountains national parks, *J. Air Waste Manage., 47,* 411-418, March 1997.

Day, D. E., W. C. Malm, and S. M. Kreidenweis, Aerosol light scattering measurements as a function of relative humidity, *J. Air Waste Manage., 50,* 710-716, May 2000.

Day, D. E. and W. C. Malm, Aerosol light scattering measurements as a function of relative humidity: a comparison between measurements made at three different sites, *Atmos. Environ., 35,* 5169-5176, 2001.

Dick, W. D., P. Saxena, and P. H. McMurry, Estimation of water uptake by organic compounds in submicron aerosols measured during the Southeastern Aerosol and Visibility Study, *J. Geophys. Res., 105(D1),* 1471-1479, 2000.

Dixon, J. K, The absorption coefficient of nitrogen dioxide in the visible spectrum, *J. Chem. Phys., 8(2),* 157-160, 1940.

Eldering, A., J. A. Ogren, Z. Chowdhury, L. S. Hughes, and G. R. Cass, Aerosol optical properties during INDOEX based on measured aerosol particle size and composition, *J. Geophys. Res.,107(D22),* 8001, doi:10.1029/2001JD001572, 2002.

El-Zanan, H. S., D. H. Lowenthal, B. Zielinska, J. C. Chow, and N. Kumar, Determination of the organic aerosol mass to organic carbon ratio in IMPROVE samples, *Chemosphere, 60(4),* 485-496, July 2005.

Ferron, G. A., E. Karg, B. Busch, and J. Heyder, Hygroscopicity of ambient particles, *J. Aerosol Sci. 30(S1),* S19-S20, 1999

Formenti P., W. Elbert, W. Maenhaut, J. Haywood, S. Osborne, and M. O. Andreae, Inorganic and carbonaceous aerosols during the South African Regional Science Initiative (SAFARI 2000) experiment: Chemical characteristics, physical properties, and emission data for smoke from African biomass burning, *J. Geophys. Res., 108(D13),* 8488, doi:10.1029/2002JD002408, 2003.

Frank, N. H., Retained nitrate, hydrated sulfate and carbonaceous mass in Federal Reference Method PM2.5 for six eastern U.S. cities, *Submitted to J. Air Waste Manage.,* 2005.

Fridlind, A. M., and M. Z. Jacobson, Point and column aerosol radiative closure during ACE 1: Effects of article shape and size, *J. Geophys. Res., 108(D3),* 4094, doi:10.1029/2001JD001553, 2003.

Fuller, K. A., W. C. Malm, and S. M. Kreidenweis, Effects of mixing on extinction by carbonaceous particles, *J. Geophys. Res., 104,* 15941-15954, 1999.

Gao, S., M. Keywood, N. L. Ng, J. Surratt, V. Varutbangkul, R. Bahreini, R. C. Flagan, and J. H. Seinfeld, Low-molecular-weight and oligomeric components in secondary organic aerosol from the ozonolysis of cycloalkenes and α-pinene, *J. Phys. Chem. A., 108,* 10147-10164, 2004.

Gasparini, R., R. Li, and D. R. Collins, Integration of size distributions and size-resolved hygroscopicity measured during the Houston Supersite for compositional categorization of the aerosol, *Atmos. Environ., 38,* 3285-3303, 2004.

Gebhart, K. A., W. C. Malm, and D. E. Day, Examination of the effects of sulfate acidity and relative humidity on light scattering at Shenandoah National Park, *Atmos. Environ., 28(5),* 841-849, 1994.

Gelencsér, A., A. Hoffer, A. Molnár, Z. Krivácsy, Gy. Kiss, E. Mészáros, Thermal behaviour of carbonaceous aerosol from a continental background site, *Atmos. Env., 34,* 823-831, 2000.

Grosjean, D., and S. K. Friedlander, Gas-particle distribution factors for organics and other pollutants in the Los Angeles atmosphere, *J. Air Pollution Control Assoc., 25,* 1038-1044, 1975.

Guyon, P., B. Graham, G. C. Roberts, O. L. Mayol-Bracero, W. Maenhaut, P. Artaxo, and M. O. Andreae, In-canopy gradients, composition, sources, and optical properties of aerosol over the Amazon forest, *J. Geophys. Res., 108(D18)*, 4591, doi:10.1029/2003JD003465, 2003.

Gysel, M., E. Weingartner, S. Nyeki, D. Paulsen, U. Baltensperger, I. Galambos, and G. Kiss, Hygroscopic properties of water-soluble matter and humic-like organics in atmospheric fine aerosol, *Atmos. Chem. Phys., 4,* 35-50, 2004.

Hand, J. L., A new technique for obtaining aerosol size distributions with applications to estimates of aerosol properties, Ph.D. Dissertation, Colorado State University, 2001.

Hand, J. L., and S. M. Kreidenweis, A new method for retrieving particle refractive index and effective density from aerosol size distribution data, *Aerosol Sci. Technol., 36,* 1012-1026, 2002.

Hand, J. L., R. B. Ames, S. M. Kreidenweis, D. E. Day and W. C. Malm, Estimates of particle hygroscopicity during the Southeastern Aerosol and Visibility Study, *J. Air Waste Manage., 50,* 677-685, May 2000.

Hand, J. L., S. M. Kreidenweis, D. E. Sherman, J. L. Collett, Jr., S. V. Hering, D. E. Day, W. C. Malm, Aerosol size distributions and visibility estimates during the Big Bend Regional Aerosol Visibility and Observational Study (BRAVO), *Atmos. Environ., 36*, 5043-5055, 2002.

Hand, J. L., N. M. Mahowald, Y. Chen, R. L. Siefert, C. Luo, A. Subramaniam, and I. Fung, Estimates of atmospheric-processed soluble iron from observations and a global mineral aerosol model: Biogeochemical implications, *J. Geophys. Res., 109(D17205)*, doi:10.1029/2004JD004574, 2004.

Hand J.L., W. C. Malm, D. E. Day, T. Lee, C. Carrico, J. Carrillo, J. L. Collett, Jr., A. Laskin, C. Wang, J. P. Cowin, M. J. Iedema, Optical, physical and chemical properties of tar balls during the Yosemite Aerosol Characterization Study, *J. Geophys. Res., 110(D21),* doi:10.1029/2004JD005728, 2005.

Hansson, H.-C., M. J. Rood, S. Koloutsou-Vakakis, K. Hämeri, D. Orsini, and A. Wiedensholer, NaCl aerosol particle hygroscopicity dependence on mixing with organic compounds, *J. Atmos. Chem., 31,* 321-346, 1998.

Hasan, H. and T. G. Dzubay, Apportioning light extinction coefficients to chemical species in the atmospheric aerosol, *Atmos. Environ., 17,* 1573-1581, 1983.

Hegg, D. A., R. J. Ferek, and P. V. Hobbs, Aerosol size distributions in the cloudy atmospheric boundary layer of the North Atlantic Ocean, *J. Geophys. Res., 98(D5),* 8841-8846, 1993.

Hering, S., and G. Cass, The magnitude of bias in the measurement of $PM_{2.5}$ arising from volatilization of particulate nitrate from Teflon filters, *J. Air Waste Manage., 49,* 725-733, June 1999.

Hering, S. V. and S. K. Friedlander, Origins of aerosol sulfur size distributions in the Los Angeles Basin, *Atmos. Environ., 16(11),* 2647-2656, 1982.

Hering, S., A. Eldering, and J. H. Seinfeld, Bimodal character of accumulation mode aerosol mass distributions in southern California, *Atmos. Environ., 31(1),* 1-11, 1997.

Hodkinson, J. R., Calculations of color and visibility in urban atmospheres polluted by gaseous NO2, *Air Water Pollut., 10(2),* 137-144, 1966.

Hogrefe O., J. J. Schwab, F. Drewnick, G. G. Lala, S. Peters, K. J. Demerjian, K. Rhoads, H. D. Felton, O. V. Rattigan, L. Husain, and V. A. Dutkiewicz, Semicontinuous $PM_{2.5}$ sulfate and nitrate measurements at an urban and rural location in New York: PMTACS-NY summer 2001 and 2002 campaigns, *J. Air Waste Manage., 54,* 1040-1060, September 2004.

Huebert, B. J., and R. J. Charlson, Uncertainties in data on organic aerosols, *Tellus, 52B(5),* 1249-1255, 2000.

Im, J.-S., V. K. Saxena, and B. N. Wenny, An assessment of hygroscopic growth factors for aerosols in the surface boundary layer for computing direct radiative forcing, *J. Geophys. Res., 106(D17)*, 20213-20224, 2001

Jaffe, D., J. Snow, and O. Cooper, The April 2001 Asian dust events: Transport and substantial impact on surface particulate matter concentrations across the United States, *Eos, Transactions*, November 18, 2003.

Jaffe, D., S. Tamura, and J. Harris, Seasonal cycle and composition of background fine particles long the west coast of the U.S., *Atmos. Environ., 39,* 297-306, 2005.

Japar, S. M., A. C. Szkarlat, R. A. Gorse, Jr., E. K. Heyerdahl, R. L. Johnson, J. A. Rau, and J. J. Huntzicker, Comparison of solvent extraction and thermal optical carbon analysis methods: Application to diesel vehicle exhaust aerosol, *Environ. Sci. Techonol., 18,* 231-234, 1984.

John, W., S. M. Wall, J. L. Ondo, and W. Winklmayr, Modes in the size distributions of atmospheric inorganic aerosol, *Atmos. Environ., 24A(9)*, 2349-2359, 1990.

Kim, Y, P., J. H. Seinfeld, P. Saxena, Atmospheric gas-aerosol equilibrium 2. Analysis of common approximations and activity-coefficient calculation methods, *Aerosol Sci. Technol., 19(2),* 182-198, 1993.

Koloutsou-Vakakis, S., C. M. Carrico, P. Kus, M. J. Rood, Z. Li, R. Shrestha, J. A. Ogren, J. C. Chow, and J. G. Watson, Aerosol properties at a midlatitude Northern Hemisphere continental site, *J. Geophys. Res., 106(D3)*, 3019-3032, 2001.

Kreisberg, N. M., M. R. Stolzenburg, S. V. Hering, W. D. Dick, and P. H. McMurry, A new method for measuring the dependence of particle size distributions on relative humidity, with the application to the Southeastern Aerosol and Visibility Study, *J. Geophys. Res., 106(D14),* 14935-14949, 2001.

Lee, T., S. M. Kreidenweis, and J. L. Collett, Jr., Aerosol ion characteristics during the Big Bend Regional Aerosol and Visibility Observational Study, *J. Air Waste Manage., 54,* 585-592, May 2004a.

Lee, T., X-Y. Yu, B. Ayres, J. Carrillo, C. Carrico, P. Herckes, G. R. McMeeking, G. Engling, S. M. Kreidenweis, J. L. Collett, Jr., D. E. Day, and W. C. Malm, Characteristics of aerosol nitrate at several IMPROVE monitoring sites, Paper # 38, A&WMA Specialty conference: Regional and Global Perspectives on Haze: Causes, Consequences and Controversies, Asheville, NC, October 25-29, 2004b.

Lefer, B. L., and R. W. Talbot, Summertime measurements of aerosol nitrate and ammonium at a northeastern U.S. site, *J. Geophys. Res., 106(D17),* 20365-20378, 2001.

Li, S-M., J. Tang, H. Xue, and D. Toom-Sauntry, Size distribution and estimated optical properties of carbonate, water soluble organic carbon, and sulfate in aerosols at a remote high altitude site in western China, *Geophys. Res. Letts., 27(8),* 1107-1110, 2000.

Li, X., H. Maring, D. Savoie, K. Voss, and J. M. Prospero, Dominance of mineral dust in aerosol light-scattering in the North Atlantic trade winds, *Nature, 380,* 416-419, 1996.

Lightstone, J. M., T. B. Onasch, D. Imre, and S. Oatis, Deliquescence, efflorescence, and water activity in ammonium nitrate and mixed ammonium nitrate/succinic acid microparticles, *J. Phys. Chem. A., 104,* 9337-9346, 2000.

Liu L.-J. S., R. Burton, W. E. Wilson, and P. Koutrakis, Comparison of aerosol acidity in urban and semi-rural environments, *Atmos. Environ., 30(8),* 1237-1245, 1996.

Lowenthal, D. H., C. F. Rogers, P. Saxena, J. G. Watson, and J. C. Chow, Sensitivity of estimated light extinction coefficients to model assumptions and measurement errors, *Atmos. Environ., 29,* 751-766, 1995.

Lowenthal, D. H., J. G. Watson, P. Saxena, Contributions to light extinction during project MOHAVE, *Atmos. Environ., 34,* 2351-2359, 2000.

Lowenthal, D. H., and N. Kumar, $PM_{2.5}$ and light extinction reconstruction in IMPROVE, *J. Air Waste Manage., 53,* 1109-1120, September 2003.

Lowenthal, D. H., and N. Kumar, Variation of mass scattering efficiencies in IMPROVE, *J. Air Waste Manage., 54,* 926-934, August 2004.

Lowenthal, D. H., and N. Kumar, Light scattering from sea salt aerosols in IMPROVE, *Prepared for submission to J. Air Waste Manage.,* 2005.

Malm, W. C. and D. E. Day, Optical properties of aerosols at Grand Canyon National Park, *Atmos. Environ., 34,* 3373-3391, 2000.

Malm W.C. and D. E. Day, Estimates of aerosol species scattering characteristics as a function of relative humidity, *Atmos. Environ., 35,* 2845-2860, 2001.

Malm, W. C. and S. M. Kreidenweis, The effects of models of aerosol hygroscopicity on the apportionment of extinction, *Atmos. Environ., 31(13),* 1965-1976, 1997.

Malm W. C. and M. Pitchford, Comparison of calculated sulfate scattering efficiencies as estimated from size-resolved particle measurements at three national locations, *Atmos. Environ., 31(9),* 1315-1325, 1997

Malm, W. C., K. A. Gebhart, J. Molenar, T. Cahill, R. Eldred, and D. Huffman, Examining the relationship between atmospheric aerosols and light extinction at Mount Rainier and North Cascades National Parks, *Atmos. Environ., 28(2),* 347-360, 1994a.

Malm, W. C., J. F. Sisler, D. Huffman, R. A. Eldred, and T. A. Cahill, Spatial and seasonal trends in particle concentration and optical extinction in the United States, *J. Geophys. Res., 99(D1),* 1347-1370, 1994b.

Malm, W. C., D. E. Day, and S. M. Kreidenweis, Light scattering characteristics of aerosols as a function of relative humidity: Part 1: A comparison of measured scattering and aerosol concentrations using the theoretical models, *J. Air Waste Manage., 50,* 686-700, 2000

Malm W.C., D. E. Day, S. M. Kreidenweis, J. L. Collett, Jr., and T. Lee, Humidity dependent optical properties of fine particles during the Big Bend Regional Aerosol and Visibility Observational study (BRAVO), *J. Geophys. Res. 108(D9),* 4279, doi:10.1029/2002JD002998, 2003.

Malm W.C., D. E. Day, C. Carrico, S. M. Kreidenweis, J. L. Collett, Jr., G. McMeeking, T. Lee, and J. Carrillo, Inter-comparison and closure calculations using measurements of aerosol species and optical properties during the Yosemite Aerosol Characterization Study, *J. Geophys. Res., 110(D14),* Art. No. D14302, July 19, 2005a.

Malm, W. C., D. E. Day, S. M. Kreidenweis, J. L. Collett, Jr., C. Carrico, G. McMeeking, and T. Lee, Hygroscopic properties of an organic-laden aerosol*, Atmos. Environ., 39(27),* 4969-4982, September 2005b.

Martins, J. V., P. Artaxo, P. V. Hobbs, C. Liousse, H. Cachier, Y. J. Kaufman, and A. Plana-Fattori, Particle size distributions, elemental compositions, carbon measurements, and optical properties of smoke from biomass burning in the Pacific Northwest of the United States, in: *Global Biomass Burning and Global Change,* edited by Levine, J. S., pp. 716-732, MIT Press, Cambridge, 1996.

Mayol-Bracero, O. L., P. Guyon, B. Graham, G. Roberts, M. O. Andreae, S. Desesari, M. C. Facchini, S. Fuzzi, and P. Artaxo, Water-soluble organic compounds in biomass burning aerosols over Amazonia 2. Apportionment of the chemical composition and importance of the polyacidic fraction, *J. Geophys. Res., 107(D20),* 8091, doi:10.1029/2001JD000522, 2002.

McDade, C. E., R. A. Eldred, and L. L. Ashbaugh, Artifact corrections in IMPROVE, Paper # 15, A&WMA Specialty conference: Regional and Global Perspectives on Haze: Causes, Consequences and Controversies, Asheville, NC, October 25-29, 2004.

McMeeking G.R., S. M. Kreidenweis, C. Carrico, T. Lee, J. L. Collett, Jr., and W. C. Malm, Observations of smoke-influenced aerosol during the Yosemite Aerosol Characterization Study: Size distributions and chemical composition, *J. Geophys. Res., 110(D09),* doi:10.1029/2004JD005389, 2005.

McMurry, P. H., X. Zhang, and C.-T. Lee, Issues in aerosol measurements for optics assessment, *J. Geophys. Res., 101,* 19189-19197, 1996.

McMurry, P. H., X. Wang, K. Park, and K. Ehara, The relationship between mass and mobility for atmospheric particles: A new technique for measuring particle density, *Aerosol Sci. Technol., 36,* 227-238, 2002.

Meng Z., and J. H. Seinfeld, On the source of the submicrometer droplet mode of urban and regional aerosols, *Aerosol Sci. Technol., 20,* 253-265, 1994.

Mie, G., Beitraege zur optic trueber medien, speziell kolloidaler metalosungen, *Ann. Physik, 25,* 377-445, 1908.

Mikhilov, E., S. Vlasenko, R. Niesner, and U. Pöschl, Interaction of aerosol particles composed of protein and salts with water vapor: hygroscopic growth and microstructural rearrangement, *Atmos. Chem. Phys., 4,* 323-350, 2004.

Nenes A., S. N. Pandis, C. Pilinis, ISORROPIA: A new thermodynamic equilibrium model for multiphase multicomponent inorganic aerosols, *Aqua. Geochem., 4,* 123-152, 1998.

Neusüß, C., H. Wex, W. Birmili, A. Wiedensohler, C. Kozier, B. Busch, E. Brüggemann, T. Gnauk, M. Ebert, and D. S. Covert, Characterization and parameterization of atmospheric particle number-, mass-, and chemical-size distributions in central Europe during LACE 98 and MINT, *J. Geophys. Res., 107(D21),* 8127, doi:10.1029/2001JD000514, 2002.

Novakov, T., and C. E. Corrigan, Thermal characterization of biomass smoke particles, *Mikrochim. Acta., 119,* 157-166, 1995.

Omar, A. H., S. Biegalski, S. M. Larson, S. Landsberger, Particulate contributions to light extinction and local forcing at a rural Illinois site, *Atmos. Environ., 33,* 2637-2646, 1999.

Peng, C., M.-N. Chan, and C. K. Chan, The hygroscopic properties of dicarboxylic and multifunctional acids: Measurements and UNIFAC predictions, *Environ. Sci. Technol., 35,* 4495-4501, 2001.

Penner, J. E., R. J. Charlson, J. M. Hales, N. Laulainen, R. Leifer, T. Novakov, J. Ogren, L. F. Radke, S. E. Schwarz, and L. Travis, Quantifying and minimizing uncertainty of climate forcing by anthropogenic aerosols, *Bull. Am. Met. Soc., 75,* 375-400, 1993.

Perry, K. D., T. A. Cahill, R. A. Eldred, and D. D. Dutcher, Long-range transport of North African dust to the eastern United States, *J. Geophys. Res., 102(D10),* 11225-11238, 1997.

Pilinis, C., S. N. Pandis, and J. H. Seinfeld, Sensitivity of direct climate forcing by atmospheric aerosols to aerosol size and composition, *J. Geophys. Res.,100,* 18739-18754, 1995.

Poirot, R. L., and R. B.Husar, Chemical and physical characteristics of wood smoke in the northeastern U.S. during July 2002: Impacts from Quebec forest fires, Paper # 94, A&WMA Specialty conference: Regional and Global Perspectives on Haze: Causes, Consequences and Controversies, Asheville, NC, October 25-29, 2004.

Prenni, A. J., P. J. DeMott, and S. M. Kreidenweis, Water uptake of internally mixed particles containing ammonium sulfate and dicarboxylic acids, *Atmos. Environ., 37,* 4243-4251, 2003.

Quinn, P. K., D. J. Coffman, V. N. Kapustin, T. S. Bates, and D. S. Covert, Aerosol optical properties in the marine boundary layer during the First Aerosol Characterization Experiment (ACE 1) and the underlying chemical and physical aerosol properties, *J. Geophys. Res., 103(D13),* 16547-16563, 1998.

Quinn, P. K., D. J. Coffman, T. S. Bates, T. L. Miller, J. E. Johnson, K. Voss, E. J. Welton, and C. Neususs, Dominant aerosol chemical components and their contribution to extinction

during the Aerosols99 cruise across the Atlantic, *J. Geophys. Res., 106(D18),* 20783-20809, 2001.

Quinn, P.K., T. L. Miller, T. S. Bates, J. A. Ogren, E. Andrews, and G. E. Shaw, A 3-year record of simultaneously measured aerosol chemical and optical properties at Barrow, Alaska, *J. Geophys. Res., 107(D11),* 4130, 10:1029/2001JD001248, 2002a.

Quinn, P. K., D. J. Coffman, T. S. Bates, T. L. Miller, J. E. Johnson, E. J. Welton, C. Neususs, M. Miller, and P. J. Sheridan, Aerosol optical properties during INDOEX 1999: Means, variability, and controlling factors, *J. Geophys. Res., 107(D19),* 8020, doi:10.1029/2000JD000037, 2002b.

Quinn, P. K., D. J. Coffman, T. S. Bates, E. J. Welton, D. S. Covert, T. L. Miller, J. E. Johnson, S. Maria, L. Russell, R. Arimoto, C. M. Carrico, M. J. Rood, and J. Anderson, Aerosol optical properties measured on board the *Ronald H. Brown* during ACE-Asia as a function of aerosol chemical composition and source region, *J. Geophys. Res., 109(D19),* doi:10.1029/2003JD004010, 2004.

Radke, L., D. A. Hegg, J. H. Lyons, C. A. Brock, P. V. Hobbs, R. Weiss, R. Rassmussen, Airborne measurements on smokes from biomass burning, in *Aerosols and Climate*, edited by P. V. Hobbs and M. P. McCormick, pp. 411-422, Deepak Publishing, Hampton VA, 1988.

Radke, L. F., D. A. Hegg, P. V. Hobbs, J. D. Nance, J. H. Lyons, K. K. Laursen, R. E. Weiss, P. J. Riggan, and D. E. Ward, Particulate and trace emissions from large biomass fires in North America, in: *Global Biomass Burning: Atmospheric, Climatic and Biospheric Implications,* edited by J. S. Levine, pp. 209-224, MIT Press, Cambridge MA, 1991.

Reid, J. S., and P. V.Hobbs, Physical and optical properties of smoke from individual biomass fires in Brazil, *J. Geophys. Res., 103,* 32013-32031, 1998.

Reid, J. S., R. Koppmann, T. F. Eck, and D. P. Eleuterio, A review of biomass burning emissions, Part II: Intensive physical properties of biomass burning particles, *Atmos. Chem. Phys., 5,* 799-825, 2005.

Rees, S. L., A. L. Robinson, A. Khlystov, C. O. Stanier, and S. N. Pandis, Mass balance closure and the Federal Reference Method for $PM_{2.5}$ in Pittsburgh, Pennsylvania, *Atmos. Environ., 38,* 3305-3318, 2004.

Rivera-Carpio C. A., C. E. Corrigan, T. Novakov, J. E. Penner, C. F. Rogers, and J. C. Chow, Derivation of contributions of sulfate and carbonaceous aerosols to cloud condensation nuclei from mass size distributions, *J. Geophys. Res., 101(D14),* 19483-19493, 1996.

Rogge, W. F., M. Mazurek, L. M. Hildemann, and G. R. Cass, Quantification of urban organic aerosols at a molecular level: Indentification, abundance and seasonal variation, *Atmos. Environ., 27,* 1309-1330, 1993.

Russell, L. M., Aerosol organic-mass-to-organic-carbon ratio measurements, *Environ. Sci. Technol., 37,* 2982-2987, 2003.

Santarpia, J. L., R. Li, and D. R. Collins, Direct measurement of the hydration state of ambient aerosol populations, *J. Geophys. Res., 109(D18),* Art. No. D18209, September 29, 2004.

Santarpia, J. L., R. Gasparini, R. Li, and D. R. Collins, Diurnal variations in the hygroscopic growth cycles of ambient aerosol populations, *J. Geophys. Res., 110,* doi:10.1029/2004JD005279, 2005.

Saxena, P., L. M. Hildemann, P. H. McMurry, and J. H. Seinfeld, Organics alter hygroscopic behavior of atmospheric particles, *J. Geophys. Res., 100(D9),* 18755-18770, 1995.

Schwab, J. J., H. D. Felton, and K. L. Demerjian, Aerosol chemical composition in New York state from integrated filter samples: Urban/rural and seasonal contrasts, *J. Geophys. Res., 109(D16),* doi:10.1029/2003JD004078, 2004.

Seinfeld, J. H., and S. N. Pandis, *Atmospheric Chemistry and Physics: From Air Pollution to Climate Change,* John Wiley, New York, pp 444, 1998.

Sheridan, P. J., D. J. Delene, and J. A. Ogren, Four years of continuous surface aerosol measurements from the Department of Energy's Atmospheric Radiation Measurement Program Southern Great Plains Cloud and Radiation Testbed site, *J. Geophys. Res., 106(D18),* 20735-20747, 2001.

Siefert, R. L., A. M. Johansen, and M. R. Hoffman, Chemical characterization of ambient aerosol collected during the southwest monsoon and intermonsoon seasons over the Arabian Sea: Labile-Fe(II) and other trace metals, *J. Geophys. Res., 104(D3),* 3511-3526, 1999.

Sisler, J. F. and W. C. Malm, The relative importance of soluble aerosols to spatial and seasonal trends of impared visibility in the United States, *Atmos. Environ., 28(5),* 851-862, 1994.

Sloane, C. S., Optical properties of aerosols- comparisons of measurements with model calculations, *Atmos. Environ., 17,* 409-416, 1983.

Sloane, C. S., Effect of composition on aerosol light scattering efficiencies, *Atmos. Environ., 20(5),* 1025-1037, 1986.

Sloane, C. S., J. Watson, J. Chow, L. Pritchett, L. W. Richards, Size segregated fine particle measurements by chemical species and their impact on the visibility impairment in Denver, *Atmos. Environ., 25A(5/6),* 1013-1024, 1991.

Stanier, C. O., A. Y. Khlystov, and S. N. Pandis, Ambient aerosol size distributions and number concentrations during the Pittsburgh Air Quality Study (PAQS), *Atmos. Environ., 38,* 3275-3284, 2004.

Stith, J. L., L. F. Radke, and P. V. Hobbs, Particulate emission and the production of ozone and nitrogen oxides from the burning of forest slash, *Atmos. Environ., 15,* 73-82, 1981.

Subramanian, R., A. Y. Khlystov, J. C. Cabda, and A. L. Robinson, Evaluation of measurement methods, *Aerosol Sci. and Technol., 38(S1),* 27-48, 2004.

Tang, I. N., Chemical and size effects of hygroscopic aerosols on light scattering coefficients, *J. Geophys. Res.,101(D14),* 19245-19250, 1996.

Tang, I. N., Thermodynamic and optical properties of mixed-salt aerosols of atmospheric importance, *J. Geophys. Res.,102(D2),* 1883-1893, 1997.

Tang, I. N., and H. R. Munkelwitz, Water activities, densities, and refractive indices of aqueous sulfates and sodium nitrate droplets of atmospheric importance, *J. Geophys. Res., 99(D9),* 18801-18808, 1994.

Tanner, R. L., W. J. Parkhurst, M. L. Valente, and W. D. Phillips, Regional composition of $PM_{2.5}$ aerosols measured at urban, rural, and "background" sites in the Tennessee valley, *Atmos. Environ., 38,* 3143-3153, 2004.

ten Brink, H. M., J. P. Veefkind, A. Waijers-Ijpelaan, and J. C. Van der Hage, Aerosol light scattering in the Netherlands, *Atmos. Environ., 30(24),* 4251-4261, 1996.

Turpin, B. J., and H.-J. Lim, Species contributions to $PM_{2.5}$ mass concentrations: Revisiting common assumptions for estimating organic mass, *Aerosol Sci. Technol., 35,* 602-610, 2001.

Turpin, B. J., P. Saxena, G. Allen, P. Koutrakis, P. McMurry, and L. Hildemann, Characterization of the southwestern desert aerosol, Meadview, AZ, *J. Air Waste Manage., 47(3),* 344-356, March 1997.

Turpin, B. J., P. Saxena, and E. Andrews, Measuring and simulating particulate organics in the atmosphere: Problems and prospects, *Atmos. Environ., 34,* 2983-3013, 2000.

VanCuren, R. A., Asian aerosols in North America: Extracting the chemical composition and mass concentration of the Asian continental aerosol plume from long-term aerosol records in the western United States, *J. Geophys. Res.,108(D20),* 4623, doi:10.1029/2003JD003459, 2003.

VanCuren, R. A., and T. A. Cahill, Asian aerosols in North America: Frequency and concentration of fine dust, *J. Geophys. Res., 107(D24),* 4804, doi:10.1029/2002JD002204, 2002.

van de Hulst, H. C., *Light Scattering by Small Particles*, New York, Dover, 1981.

Van Vaeck, L., and K. Van Cauwenberghe, Cascade impactor measurements of the size distribution of the major classes of organic pollutants in atmospheric particulate matter, *Atmos. Environ., 12,* 2239, 1978.

Virkkula A., R. Van Dingenen, F. Raes, J. Hjorth, Hygroscopic properties of aerosol formed by oxidation of limonene, alpha-pinene, and beta-pinene, *J. Geophys. Res., 104,* 3569-3579, 1999.

Wang, J., R. C. Flagan, J. H. Seinfeld, H. H. Jonsson, D. R. Collins, P. B. Russell, B. Schmid, J. Redemann, J. M. Livingston, S. Gao, D. A. Hegg, E. J. Welton, and D. Bates, Clear-column

radiative closure during ACE-Asia: Comparison of multiwavelength extinction derived from particle size and composition with results from Sun photometry, *J. Geophys. Res., 107(D23)*, 4688, doi:10.1029/2002JD002465, 2002.

White, W. H., On the theoretical and empirical basis for apportioning extinction by aerosols: A critical review, *Atmos. Environ., 20,* 1659-1672, 1986.

White, W. H., The components of atmospheric light extinction: A survey of ground-level budgets, *Atmos. Environ., 24A(10),* 2673-2679, 1990.

White, W. H., Contributions to light extinction, In *National Acid Precipitation Assessment Program (NAPAP) Report 24 on Visibility*, pp 24-85–24-102, 1991.

White, W. H., and P. T. Roberts, On the nature and origins of visibility-reducing aerosols in the Los Angels Air Basin, *Atmos. Environ., 11,* 803-812, 1977.

White, W. H., R. A. Eldred, P. J. Feeney, C. E. McDade, B. P. Perley, D. J. Shadoan, and P. H. Wakabayashi, Behavior of fine-particle elemental data near the detection limit, Paper # 24, A&WMA Specialty conference: Regional and Global Perspectives on Haze: Causes, Consequences and Controversies, Asheville, NC, October 25-29, 2004.

Xu, J., M. H. Bergin, X. Yu, G. Liu, J. Zhao, C. M. Carrico, and K. Baumann, Measurement of aerosol chemical, physical and radiative properties in the Yangtze delta region of China, *Atmos. Environ., 36,* 161-173, 2002.

Yu, X.-Y., T. Lee, B. Ayres, S. M. Kreidenweis, W. C. Malm, and J. L. Collett, Jr., Particular nitrate measurement using nylon filters, *Submitted to Atmos. Environ.,* 2005a.

Yu X.-Y., T. Lee, B. Ayres, S. M. Kreidenweis, W. C. Malm, and J. L. Collett, Jr., Negative bias of ammonium nitrate determination using nylon filters, *Submitted to Atmos. Environ.,* 2005b.

Zhang, X. Q., P. H. McMurry, S. V. Hering, and G. S. Casuccio, Mixing characteristics and water content of submicron aerosols measured in Los Angeles and at the Grand Canyon, *Atmos. Environ., 27A,* 1593-1607, 1993.

Zhang X., B. J. Turpin, P. H. McMurry, S. V. Hering, and M. R. Stolzenburg, Mie theory evaluation of species contributions to 1990 wintertime visibility reduction in the Grand Canyon, *J. Air Waste Manage., 44,* 153-162, February 1994.

Zhang, Q., M. R. Canagaratna, J. T. Jayne, D. R. Worsnop, and J.-L. Jimenez, Time- and size-resolved chemical composition of submicron particles in Pittsburgh: Implications for aerosol sources and processes, *J. Geophys. Res., 110(D07),* doi:10.1029/2004JD004649, 2005.

Zhuang, H., C. K. Chan, M. Fang, and A. S. Wexler, Size distributions of particulate sulfate, nitrate, and ammonium at a coastal site in Hong Kong, *Atmos. Environ., 33,* 843-853, 1999.